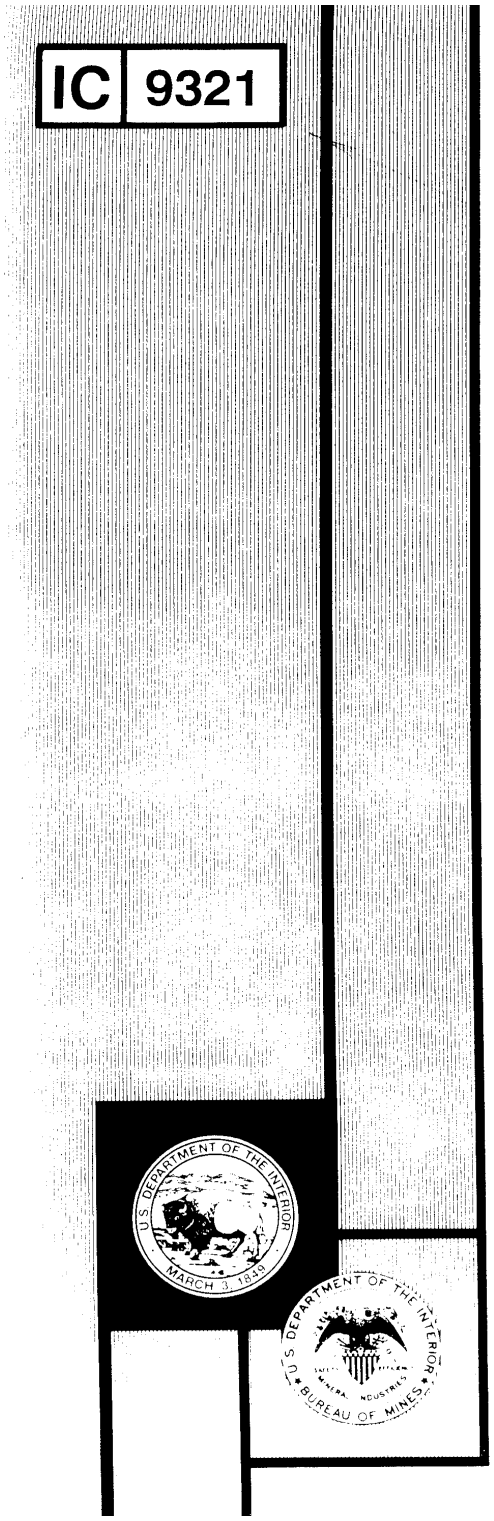


BUREAU OF MINES
INFORMATION CIRCULAR/1992

# MULSIM/NL Theoretical and Programmer's Manual

By R. Karl Zipf, Jr.

UNITED STATES DEPARTMENT OF THE INTERIOR

Information Circular 9321

# MULSIM/NL Theoretical and Programmer's Manual

By R. Karl Zipf, Jr.

UNITED STATES DEPARTMENT OF THE INTERIOR
Manuel Lujan, Jr., Secretary

BUREAU OF MINES
T S Ary, Director

**Library of Congress Cataloging in Publication Data:**

**Zipf, R. Karl.**
MULSIM/NL theoretical and programmer's manual / by R. Karl Zipf, Jr.

p. cm. — (Information circular; 9321)

Includes bibliographical references (p. 40).

Supt. of Docs. no.: I 28.27:9321.

1. MULSIM/NL. I. Title. II. Series: Information circular (United States. Bureau of Mines); 9321.

TN295.U4 [TN288] 622 s—dc20 [622'.28'0285369] 91-47152 CIP

## CONTENTS

## CONTENTS—Continued



## ILLUSTRATIONS

## ILLUSTRATIONS—Continued



## TABLES

## UNIT OF MEASURE ABBREVIATIONS USED IN THIS REPORT

| | | | |
|---|---|---|---|
| cm | centimeter | $MJ/m^2$ | megajoule per square meter |
| ft | foot | m/m | meter per meter |
| lb | pound | MPa | megapascal |
| m | meter | psi | pound per square inch |

## Disclaimer of Liability

The U.S. Bureau of Mines expressly declares that there are no warranties expressed or implied that apply to the software contained (or described) herein. By acceptance and use of said software, which is conveyed to the user without consideration by the Bureau of Mines, the user hereof expressly waives any and all claims for damage and/or suits including special, consequential, or other similar damages arising out of or in any way connected with the use of the software contained (or described) herein.

# MULSIM/NL THEORETICAL AND PROGRAMMER'S MANUAL

By R. Karl Zipf, Jr.[1]

## ABSTRACT

MULSIM/NL (multiple seams, nonlinear) is a three-dimensional boundary-element method (BEM) program developed at the U.S. Bureau of Mines for stress and displacement analysis of coal mines and thin metalliferous veins. It can analyze one to four parallel seams that can have any orientation with respect to the Earth's surface. Three main new features distinguish MULSIM/NL from its predecessors: (1) nonlinear material models, (2) multiple mining steps, and (3) energy release and strain energy computations. MULSIM/NL has six material models for the in-seam material: (1) linear elastic for coal, (2) strain softening, (3) elastic plastic, (4) bilinear hardening, (5) strain hardening, and (6) linear elastic for gob. Detailed checks show that numerical stress and displacement calculations compare well to known analytic solutions for simple problems. The total energy release calculated by MULSIM/NL is comprised of three basic terms: (1) strain energy release from the mined-out material, (2) linear kinetic energy release due to change in gravitational potential over the mined-out area, and (3) nonlinear kinetic energy release due to nonlinear materials in the total backfill and gob area. The strain energy release term is modified to account for nonlinear stress-strain behavior in the unmined materials. Comparisons of these numerical energy release rate calculations with known analytic solutions show excellent agreement.

[1]Structural engineer, Denver Research Center, U.S. Bureau of Mines, Denver, CO.

# INTRODUCTION

## PURPOSE AND OBJECTIVE

The program described in this U.S. Bureau of Mines report is part of the MULSIM/NL package, which features the actual BEM program described herein, as well as a preprocessor program called MULPRE/NL and a plotting postprocessor program called MULPLT/NL. The preprocessor helps the user generate the requisite input file for the main program MULSIM/NL, whereas the postprocessor assists the user in studying the calculated stresses and displacements in a very rapid graphical manner.

Documentation and instructions for the MULSIM/NL package are divided into two related reports with each providing essential elements toward an understanding of the whole. The objective of this report, "MULSIM/NL - Theoretical and Programmer's Manual," is to provide certain mathematical and programming details to those engineers and programmers who need to fully understand the FORTRAN program or desire to alter and enhance it. A related report, "MULSIM/NL - Application and Practitioner's Manual," provides users with detailed operating instructions for MULSIM/NL along with several practical examples to better illustrate the capabilities of the program.

Development of MULSIM/NL stems from a need to reduce mine accidents due to bumps in U.S. coal mines. A bump (very similar to a rock burst in many respects) is the violent failure of highly stressed in-place coal. They can range in size from small face bumps, which violently eject several pounds of coal across an entry, to massive longwall panel bumps, which violently eject hundreds of tons of coal and damage or destroy millions of dollars worth of longwall mining equipment. Naturally, coal mine bumps pose a severe hazard to the miners. The smaller bump events may severely injure a miner unlucky enough to be in its path, whereas the larger events may result in multiple fatalities (*1*).[2] Even if a bump does not result in costly lost-time accidents or fatalities, recovery of production may take days to complete while damaged mining equipment is repaired. Furthermore, sterilization of large coal reserves may occur if the bump risk becomes too great and sections of the mine are abandoned. MULSIM/NL is an important tool for bump control because it provides a means to calculate stress, displacement, and energy changes for various mining configurations in bump-prone conditions. Through judicious use of numerical models such as MULSIM/NL, engineers can choose alternate mine designs that may decrease the bump risk.

In addition, MULSIM/NL has many practical uses beyond coal mine bump research. Stresses and displacements calculated by MULSIM/NL can help an engineer design pillar sizes and understand multiple-seam mining interactions.

## MULSIM/NL ENHANCEMENTS

Three significant enhancements to earlier versions of MULSIM resulted in MULSIM/NL, namely (1) nonlinear material models, (2) multiple mining steps, and (3) comprehensive energy release and strain energy computations. These enhancements stem from the needs of current Bureau research on coal mine bumps. Field measurements made on this and numerous other coal pillar research projects clearly indicate that coal follows highly nonlinear stress-strain paths of various forms. In addition, the gob or backfill material left in the wake of coal extraction follows yet other nonlinear stress-strain paths as it consolidates and closure occurs. Prior versions of MULSIM (*2-3*) only permitted linear stress-strain relations for in-seam materials such as coal or gob. MULSIM/NL now has six material models from which to choose including (1) linear elastic for coal, (2) strain softening, (3) elastic plastic, (4) bilinear hardening, (5) strain hardening, and (6) linear elastic for gob.

MULSIM/NL also calculates detailed energy changes due to mining. The basis for these calculations is the energy release rate (ERR) concept advanced by Cook (*4*), later by Walsh (*5*), and most recently by Salamon (*6*) and Brady and Brown (*7*). Early South African research on rock bursts in deep gold mines found that the ERR, i.e., the energy dissipation per unit area mined, correlated well to the incidence and severity of devastating rock bursts (*8-9*). Based on the South African experience with ERR and rock bursts, the hypothesis is put forth that ERR also correlates with the incidence and severity of coal bumps. MULSIM/NL implements the theoretical developments of Salamon (*6*) into its ERR computations. The implementation is also complete in that it correctly considers the nonlinear component of the energy release arising from nonlinear backfill or gob material. In addition, MULSIM/NL also computes various useful strain energy quantities for the unmined, nonlinear material in the BEM mesh. These energy quantities include the total strain energy delivered to an element, the recoverable elastic strain energy available from an element, and the dissipated strain energy from an element. Examination of these quantities

[2]Italic numbers in parentheses refer to items in the list of references preceding the appendixes at the end of this report.

may provide some indication of the burst-bump potential of specific regions in the BEM model.

Last, MULSIM/NL features multiple mining steps to simulate various stages of mine development. This feature enables the user to examine stress and displacement changes as the mine development advances. Such changes are generally much more readily comparable to field measurement programs that tend to measure stress and displacement (convergence) changes as opposed to total or absolute stresses and displacements. The energy computations also need the multiple mining step feature since they require stress and displacement changes.

These extensive enhancements necessitated complete restructuring and reprogramming to create MULSIM/NL. Earlier versions of MULSIM used complicated indexing and one-dimensional arrays throughout the program. The new MULSIM/NL takes advantage of today's larger memory computers and uses numerous multidimensional arrays and vectors that better reflect the underlying mathematical foundations of MULSIM/NL. The reprogramming resulted in a much more understandable, reliable, and modifiable program that should serve users well in the foreseeable future.

### SCOPE

The remainder of this manual discusses theoretical and programming details of these enhancements that form the MULSIM/NL program. The enhancements are largely based on Sinha's (*2*) original program MULSIM; hence, many details on vast portions of the BEM program are best addressed in that Ph.D. dissertation.

Discussion first focuses on certain BEM developments leading up to this Bureau version. Next, sections are devoted to the material nonlinearities and the energy calculations. Subsequent sections document checks on the nonlinear BEM and energy computations. Finally, recommendations are suggested for future development of MULSIM/NL.

## ORIGINS AND PREVIOUS VERSIONS OF MULSIM/NL

### HISTORICAL REVIEW

BEM applied to solid mechanics and geomechanics emerged into a mature engineering discipline during the 1970's and 1980's. Numerous text books now exist on the subject (*10-12*), as well as a steady stream of specialty conferences (*13*). Very basically, BEM evolved as a numerical method for solving the integral equations of elasticity theory, at first in two dimensions, and later in three. Two fundamentally different formulations of BEM exist: namely, a direct method and an indirect method. According to Wardle (*14*), no one formulation is clearly superior for all problems, rather each method may have mathematical and numerical advantages depending on the problem geometry and boundary conditions. Research and development work have resulted in various schemes to improve accuracy through better element formulations (*15*) and in methods to include anisotropy in the media (*16*). Other significant developments have occurred in elastoplasticity of the continuum as reviewed by Telles (*17*) and in coupling with other methods, such as finite elements (*18-19*).

Much of the initial practical development work in BEM stemmed from mining applications and the study of the tabular orebodies, like coal seams and gold-bearing reefs. The key notion for analysis of planar excavations was to treat the excavation plane as a discontinuity in displacement within an infinite elastic medium. Berry (*20*) and Berry and Sales (*21-22*) used this displacement-discontinuity approach to derive solutions for subsidence profiles over tabular excavations. Salamon (*23-25*) formulated the "face element method" for arbitrary tabular excavation geometries in which the displacement discontinuity at one element was the sum of the contributions from every other element. Lacking a computer, he used a graphical method to evaluate the summations and compute closures across complicated excavation shapes. Eventually, Salamon's face element approach served as the basis for the first computer program using an indirect (the displacement discontinuity) formulation of the BEM (*26*).

The early BEM formulations only considered the closure distribution across the displacement-discontinuity plane that is subject to a normal stress field. Later developments by Starfield and Crouch (*27*) permitted an inclined excavation plane relative to the primitive stress directions. Further work by Crouch and Fairhurst (*28*) included certain nonlinear material models as boundary conditions across the plane of the displacement discontinuity.

In a sense, the initial indirect BEM formulations only considered a one-component displacement discontinuity (that is, one normal to the excavation plane). Research to develop more general displacement discontinuities that included shear components began in two dimensions. Crouch (*29*) developed a two-dimensional BEM analysis of a tabular seam near the Earth's surface by making use of elementary displacement-discontinuity solutions within an

isotropic infinite half-space. Further two-dimensional generalizations by Crouch (*30*) enabled analysis of nontabular and multiple seams arbitrarily close to the Earth's surface. Finally, Sinha (*2*) developed general three-dimensional solutions for stresses and displacements both normal and parallel to the displacement-discontinuity plane. He presented programs for (1) tabular seams near the Earth's surface, (2) multiple seams at great depth, and (3) a nontabular seam at depth. It is the second program that formed the essence of MULSIM/BM (*3*) and MULSIM/NL.

## SINHA'S MULSIM

The original MULSIM was intended for stress and displacement analysis of multiple seams at great depth below the Earth's surface. It could accommodate up to four parallel seams where each seam is modeled by a 12 by 12 array of coarse mesh blocks. A 5 by 5 grid of fine-mesh elements can subdivide each block if requested. Figure 1, taken from Sinha, shows the general modeling-grid scheme. The seams are parallel to each other and share a common Z axis. The local X and Y axes in each seam also remain parallel (i.e., there is no rotation about the Z axis), and there is no origin offset.

The surrounding rock mass is a linear elastic medium. The in-seam material is also linear elastic; however, certain anelastic behavior is also considered. For example, one of the seams can be considered a bedding or fault plane parallel to the other seams. MULSIM models any gouge material in a seam plane with a Mohr-Coulomb failure criterion that allows the element to yield and deform in response to normal and shear stresses.

The general structure of the original program MULSIM is shown in figure 2. In principle, program flow is straightforward and simple, although the details are complex. Input consists of a file defining the problem and its geometry. After calculating primitive stresses and influence coefficients, the program enters an iterative equation-solving loop to calculate the unknown displacement components. When it has found all the elemental displacements, the program then calculates induced and total stresses and outputs the results. All output is simply printed as tables in a rather lengthy line printer file.

In his dissertation, Sinha (*2*) derives all the three-dimensional displacement-discontinuity influence coefficients from potential theory, and he presents the basic programs for analyzing common mining situations in seam deposits. He also conducts rigorous tests of the program to ensure its accuracy.

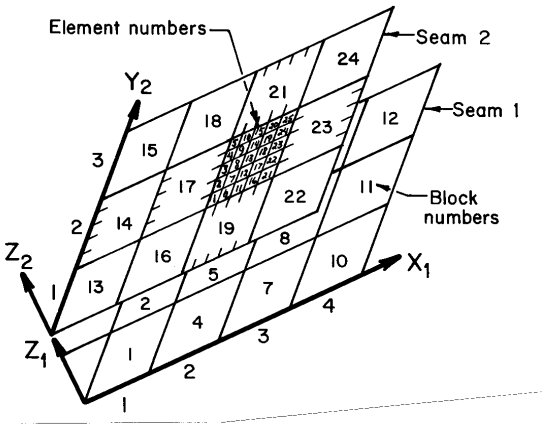


**Figure 1.—Multiple-seam grids for program MULSIM (*2*).**

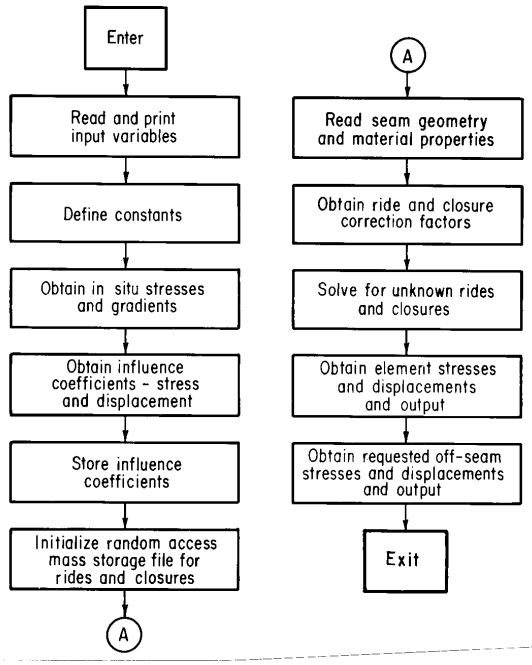


**Figure 2.—Programming structure of MULSIM (*2*).**

## MULSIM/BM

During the period 1984-85, the Bureau upgraded and restructured Sinha's original program to create MULSIM/BM (*3*). All the original capabilities of the program remain in the enhancement since MULSIM/BM still calculates stresses and displacements in single or multiple parallel seams (up to four) that are inclined at any angle to the Earth's surface and oriented at any angle to the principal stress field. The program neglects the effect of the Earth's surface and assumes that the seam planes are at great depth (i.e., depth greater than opening width).

MULSIM/BM includes these major new features:

(1) *Additional Linear In-Seam Material Properties* - The original program permits only one linear property set for the in-seam material, whereas the new version permits up to 26 different linear elastic materials.

(2) *Inserted Material or Gob Model* - Since the original program permits only one material, no method exists to have a different lower modulus material remain in the wake of mining. In addition to allowing numerous linear elastic materials, the new version features an inserted material or gob model to represent the layer of broken rock, such as gob left behind in coal mining, or other artificial supports such as backfill, packwalls, or cribs. Certain in-seam materials can be identified as inserted materials, in which case, the model uses a linear stress-strain relationship with zero stress at zero seam closure (*3*).

(3) *Increased Coarse- and Fine-Mesh Size* - The original MULSIM allows up to four seams each with a 12 by 12 array of coarse-mesh blocks, each of which can be subdivided into a 5 by 5 array of fine-mesh elements. MULSIM/BM expands the permissible coarse-mesh array size up to 40 by 40. The allowable number of parallel seams remains at four. The number of coarse-mesh blocks divisible into fine-mesh elements also increased slightly from a 12 by 12 coarse-mesh block array to a 20 by 20 array, thereby permitting a 100 by 100 array of fine-mesh elements.

(4) *Coarse-Mesh Block Stress and Displacement Calculations* - In the original version, MULSIM only prints stress and displacement calculations within the array of fine-mesh elements. Usually, only the fine-mesh calculations are of interest; however, for certain applications, having the coarse-mesh stress and displacement calculations available is desirable. MULSIM/BM now displays those calculations in the print file. Data files retain block and element locations and stress and displacement calculations separately for the coarse-mesh blocks and fine-mesh elements.

(5) *Addition of Extraction Ratios in Coarse Mesh* - The new version, MULSIM/BM, allows the user to specify the extraction ratio of each coarse-mesh block. This feature enables the user to include effects of prior mining in the coarse-mesh area without having to specify all the details of the mine layout. The program then decreases the stiffness of a partially extracted block as a function of the extraction ratio.

MULSIM/BM has seen considerable use in various Bureau projects. Beckett and Madrid (*3*) describe its utility in general coal mine modeling. Kripakov (*31*) also presents examples of its utility in coal mine modeling and discusses a coupling procedure between MULSIM/BM and a finite-element analysis. Recently, Kripakov and Rockwell (*32*) used MULSIM/BM to study various coal mine gate road pillar configurations under bump-prone conditions. Among other conclusions, they recommended further developments of Bureau BEM programs to include nonlinear in-seam material properties and various energy calculations. These developments have been included in the Bureau's latest BEM development, MULSIM/NL.

## ITASCA ADDITIONS

During 1988, the Itasca Consulting Group, Minneapolis, MN, provided certain upgrades to MULSIM/BM while under contract to the Bureau. These modifications, namely multiple mining steps and basic linear energy release computations satisfied portions of the Bureau's goals for a BEM-based numerical model with (1) nonlinear material properties, (2) multiple mining steps, and (3) comprehensive nonlinear energy release and strain energy computations.

Implementing multiple mining steps is an essential prerequisite for implementing energy computations. By itself though, the multiple mining step feature provides a useful tool for the analyst and/or engineer. With it, the user can simulate a continuous mining process by several discrete steps. For example, a mining-cut sequence might split a barrier pillar with 20 10-ft-deep continuous miner cuts. Each cut might be one step in a detailed BEM analysis. To simulate progression of a longwall face, each mining step in the BEM analysis might remove an entire row of elements along the longwall face. Then in a sequence of about 10 mining steps, the BEM analysis might simulate the mine-by cycle of a tailgate pillar. With the multiple mining step option, the analyst and/or engineer can examine progressive changes in stress and displacement. Load transfers can be observed numerically as they occur during mine development.

Figure 3 shows the necessary program structure modifications to implement multiple mining steps. After initial data are read and influence coefficients are computed and stored, the program enters a FORTRAN "Do loop," where it reads the seam geometry and seam materials and proceeds with stress, displacement, and finally energy computations. Then, it re-reads the seam geometry and seam materials and proceeds with calculations for the next mining step. This procedure is repeated for all mining steps.

As an aside, the multiple mining step option has considerable computational advantages over running a series of separate single-step problems. MULSIM uses a simple Gauss-Seidel iteration procedure to solve the system of equations for unknown elemental displacements. For the first iteration of the first mining step, the unknown displacements are customarily set to zero. Once convergence is achieved and the elemental displacements are known for the current mining step, then these displacements serve as the initial guess for the solution at the next step. If the mining steps are small and the change in mining geometry is not too radical, then using the displacements of the prior step as the initial guess ensures rapid convergence to the solution of the next step.

As shown in figure 3, calculation of linear energy changes follows immediately the stress and displacement calculations. The energy release for an element mined-out this step is

$$W_R = \frac{1}{2}\sigma_{i-1}\left(D_i - D_{i-1}\right), \qquad (1)$$

where $W_R$ = total energy release going from state 1 to state 2,

$\sigma_{i-1}$ = element stress during prior mining step,

$D_i$ = element displacement in current mining step,

and $D_{i-1}$ = element displacement in prior mining step.

Graphically, this energy quantity is shown in figure 4 (top). Total energy release is simply the sum of all the elemental energy releases. ERR is just the total energy release divided by the total elemental area mined this step, i.e., the

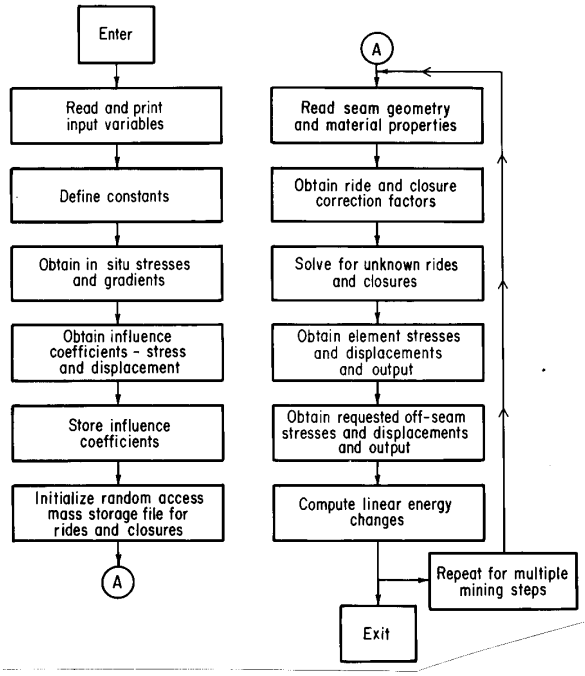


**Figure 3.—Modified program structure of MULSIM with multiple mining steps and linear energy calculations.**

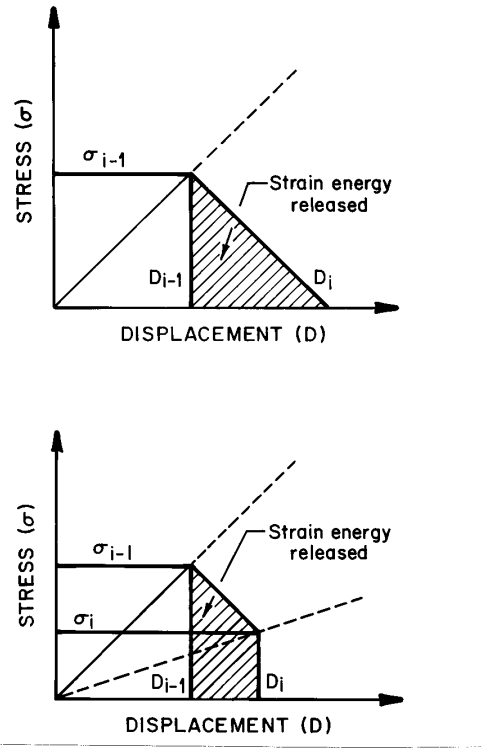


**Figure 4.—Stress-displacement curves showing strain energy release. Top, From element extraction; bottom, from element softening.**

energy release per unit area mined. (As will be discussed later, the previous ERR relation corresponds to the dominant term in an ERR expression derived and discussed by Salamon (*6*).)

In addition to ERR, Itasca also provided calculations for the energy release due to element modulus softening given by

$$W_{RMS} = \frac{1}{2}\left(\sigma_{i-1} + \sigma_i\right)\left(D_i - D_{i-1}\right), \qquad (2)$$

where $W_{RMS}$ = energy release due to modulus softening

and $\sigma_i$ = element stress in current mining step.

With the multiple mining step feature, the user can approximate a yielding or softening behavior in the seam materials by reducing the linear elastic modulus from a high value in the (i-1) step to a low value in the i step. Such a modulus reduction causes the energy release given by equation 2 and shown in figure 4 (bottom). The theoretical basis of this procedure seems problematic. Furthermore, $W_{RMS}$ is also step size and path dependent. All theoretical problems aside, the energy release due to modulus softening does provide a useful approximation to a nonviolent component of the energy dissipation occurring due to mining.

## NONLINEAR MATERIAL PROPERTIES IN MULSIM/NL

### GENERAL MECHANICS OF BOUNDARY-ELEMENT METHOD

This section provides a simplistic discussion on the basics of how BEM work, beginning with certain mathematical concepts and analytic solutions central to the BEM. These fundamental analytic solutions lead to the formation of a large system of algebraic equations. Boundary conditions applied to this system of equations then fully define the particular problem at hand. Finally, the equations are solved for stresses and displacements at each element.

Numerical methods to solve complex problems in elasticity fall into two broad categories: differential methods, such as finite-element and finite-difference methods, and integral methods, such as BEM. With differential methods, the entire problem domain (i.e., the rock mass) is divided into elements or node points, and certain boundary conditions are specified on the edges of the problem domain. Stresses and displacements are then calculated at each element or node point in the subdivided rock mass. In contrast, integral methods only require subdivision of the problem boundary into elements; therefore, the integral methods require much less computational effort than the equivalent differential methods. Stress and displacement calculations occur along the boundary and at requested points in the interior. In many practical rock mechanics problems, boundary stresses and displacements are the only ones of interest; therefore, integral methods are well suited.

The BEM applies quite well to the stress analysis of thin tabular deposits such as coal seams, deep gold reefs, and narrow veins. Sinha (*2*), and later Wardle (*14*), discuss that the key abstraction underlying BEM is visualizing the tabular deposit as a crack or discontinuity in an otherwise homogeneous, isotropic, linear elastic rock mass. Figure 5 shows this crack or seam plane in the surrounding rock mass or host media. The top and bottom surfaces of the crack plane form the problem boundary (i.e., the roof and floor in coal mining or the hanging wall and footwall in metal mining). The rock mass is the internal region for this problem, whereas the coal seam or vein material is an external region for the problem.

The next critical step in the BEM is dividing the crack or seam plane into several square boundary elements. Figure 6 shows the seam plane subdivided into elements. The actual mine plan within this seam plane may have a very complex geometry. The individual elements are then

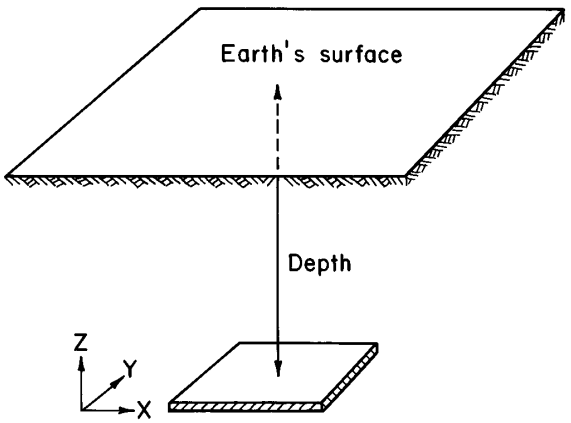


**Figure 5.—Boundary-element-method seam plane in surrounding rock mass.**

assigned material properties (or boundary conditions) to approximate this geometry. Figure 7 shows an actual mine plan and the modeling approximation where individual elements are considered either mined out or unmined with assigned material properties.

The central foundations to BEM rest on certain analytic solutions from basic elasticity theory. In two dimensions, one of these solutions is for a crack of width 2a subjected to uniform pressure components $P_x$ and $P_z$. Figure 8 shows this pressurized crack problem. By integrating analytic solutions to the Kelvin problem, expressions are obined for the stress and displacement components of the pressurized crack in terms of the crack pressure components $P_x$ and $P_z$ and the spatial coordinates x and z.

Another even more important solution is that of a "displacement discontinuity" in an infinite solid as shown in figure 9. Instead of applying constant pressure components to the crack walls, constant displacement components are applied resulting in a so-called "displacement discontinuity." Again, it is possible to find analytic expressions for the stress and displacement components in terms of the displacement discontinuity components $D_x$ and $D_z$ and the spatial coordinates x and z.

## Basic Equations of Boundary-Element Method

Figure 9 shows a two-dimensional displacement discontinuity; however, it is also possible to extend the concept and solutions to three dimensions. The solution forms, following Sinha's (*2*) notation, are

$$\tau_x = b D_x + c D_y ,$$

$$\tau_y = d D_x + e D_y ,$$

$$\sigma_z = a D_z , \qquad (3)$$

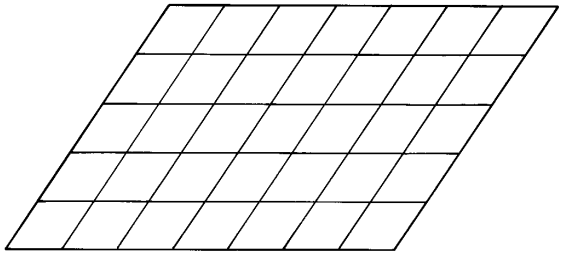

Figure 6.—Boundary-element-method seam plane subdivided by elements.

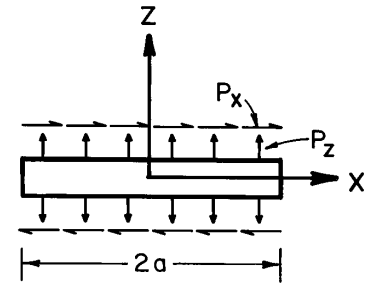


Figure 8.—Pressurized crack problem in two dimensions. 2a is crack width, and $P_x$ and $P_z$ are pressure components.

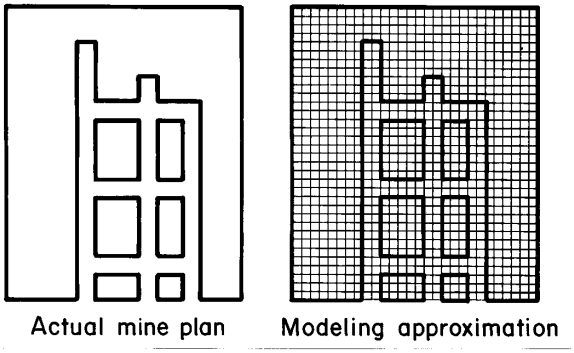


Figure 7.—Actual mine plan in-seam plane and gridded modeling approximation.

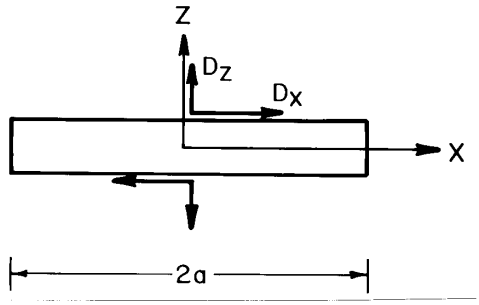


Figure 9.—Displacement-discontinuity problem in two dimensions. 2a is crack width, and $D_x$ and $D_z$ are displacement components.

where $\tau_x$ = shear stress in local x direction of element,

$D_x$ = displacement discontinuity in x direction,

$D_y$ = displacement discontinuity in y direction,

$\tau_y$ = shear stress in local y direction of element,

$\sigma_z$ = normal stress in local z direction of element,

$D_z$ = displacement discontinuity in z direction,

and a, b, c, d, and e are influence functions depending on the material properties (E,$\nu$) of the host medium and the spatial coordinates (x, y, z). Equation 3 relates an applied displacement discontinuity at the origin to the induced stresses at a point (x, y, z) due to that applied displacement discontinuity. While equation 3 applies to a point displacement discontinuity, it also applies approximately over an element as shown in figure 10. Here, constant displacement discontinuities $D_x$, $D_y$, and $D_z$ over the source element (k, l) induce stresses $\tau_x$, $\tau_y$, and $\sigma_z$ at the field element (i, j). Equation 4 reflects the change from point stresses and displacement discontinuities to elemental stresses and displacement discontinuities.

$$\tau_x^{i,j} = {}_{k,l}^{i,j}b\, D_x + {}_{k,l}^{i,j}c\, D_y$$

$$\tau_y^{i,j} = {}_{k,l}^{i,j}d\, D_x + {}_{k,l}^{i,j}e\, D_y$$

$$\sigma_z^{i,j} = {}_{k,l}^{i,j}a\, D_z \qquad (4)$$

Again, equation 4 gives induced stress components at element (i, j) due to displacement discontinuities at (k, l). Therefore, the total induced stress at element (i, j) is the sum of the induced stresses from all the displacement discontinuities at all the elements (k, l). Taking this summation on equation 4 results in

$$\tau_x^{i,j} = \sum_{k,l}\left[{}_{k,l}^{i,j}b\, D_x + {}_{k,l}^{i,j}c\, D_y\right]$$

$$\tau_y^{i,j} = \sum_{k,l}\left[{}_{k,l}^{i,j}d\, D_x + {}_{k,l}^{i,j}e\, D_y\right]$$

$$\sigma_z^{i,j} = \sum_{k,l}\left[{}_{k,l}^{i,j}a\, D_x\right]. \qquad (5)$$

If N represents the number of elements, then equation 5 represents a system of 3N equations with 6N unknowns, 3N stress components $\tau_x$, $\tau_y$, and $\sigma_z$, and 3N displacement discontinuities $D_x$, $D_y$, and $D_z$.

## Application of Boundary Conditions

Obviously, a unique solution for the unknowns requires 3N additional independent equations which are generated from the boundary conditions. Figure 11 shows an elemental displacement discontinuity and the nature of the applied boundary conditions. For unmined elastic elements (i.e., those containing coal, vein material, gob, or backfill), the elemental stresses and displacements are related through the elemental material properties. For simple linear elastic materials, the boundary conditions are

$$\tau_x = G\, D_x/t,$$

$$\tau_y = G\, D_y/t,$$

$$\sigma_z = E\, D_z/t, \qquad (6)$$

where G is a shear modulus, E is Young's modulus, and t is the element thickness. It is straightforward to extend these boundary conditions to more complex nonlinear material properties.

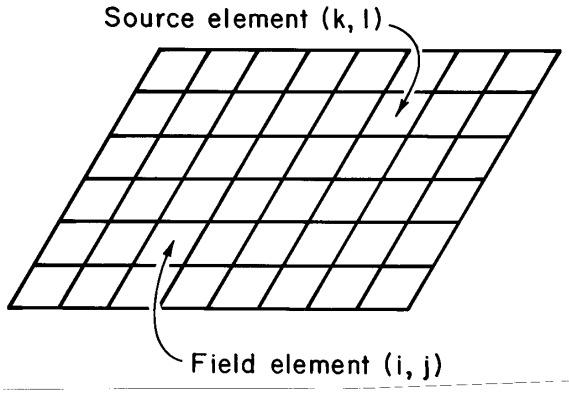


**Figure 10.—Source element (k, l) and field element (i, j) within seam plane.**

For the mined-out or open elements, the elemental stresses are zero, and the boundary conditions are

$$\tau_x = 0,$$

$$\tau_y = 0,$$

$$\sigma_z = 0. \qquad (7)$$

Thus, the boundary conditions given by equations 6 and 7 provide the additional 3N relations, which together with the boundary-element equations 5, enable computation of the remaining unknown elemental stresses and displacement discontinuities. Numerical solution of this system of linear algebraic equations is normally accomplished with a Gauss-Seidel iteration procedure. See Dahlquist and Bjork (*33*) for details of this method.

### Some Notes on BEM Boundary Conditions

The three boundary conditions on an element must act independently of one another. Thus, the normal and shear components of stress and displacement applied to an element are uncoupled. Coupling the normal and shear components with some complex constitutive relation may result in an overdetermined system of equations with unknown consequences on the solution. Also note (fig. 11) that horizontal components of stress do not exist in the in-seam elements. Therefore, the engineer and/or analyst using BEM must find artificial means to account for the effects of horizontal stress or confinement on the behavior of an element. One common procedure involves the use of a family of stress-strain curves ranging from highly strain softening through elastic plastic to represent materials under increasing confinement. The highly strain-softening material is used near an opening where the confinement is low, and the elastic-plastic material is used in the interior of a model where the confinement is high.

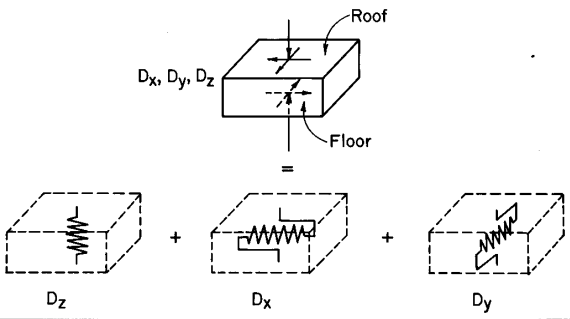


**Figure 11.—Three boundary conditions applied to elemental displacement discontinuity. $D_x$, $D_y$, and $D_z$ are elemental displacement discontinuity components.**

## SIX MATERIAL MODELS FOR MULSIM/NL

As alluded to in the previous discussions on the formulation of BEM nonlinear in-seam material properties are incorporated into the model via the boundary conditions on the system of boundary-element equations. This section discusses theoretical and programming details of the nonlinear material models added to MULSIM/NL. Initial discussions focus on the derivation and formulation of the six material models now available in MULSIM/NL. Additional mathematical details provide the essence of total-stress versus induced-stress BEM formulations. Implementing the material nonlinearities required a shift from the induced-stress approach used in MULSIM to the total-stress approach used in MULSIM/NL. Subsequent discussions then focus on the logic, algorithms, and convergence schemes necessary to actually program the models. Finally, the section closes with certain programming details of the material property subroutines and the total-stress BEM formulation.

Figure 12 shows the stress-strain models for MULSIM/NL that include (1) linear elastic coal, (2) strain-softening coal, (3) elastic-plastic coal, (4) bilinear hardening gob, (5) strain-hardening gob, and (6) linear elastic gob. The first three models are for the unmined in-seam coal material, while the latter are for the broken gob material left in the wake of mining. As will be discussed later, the distinction between coal material models and gob material models becomes crucial in the subsequent energy calculations.

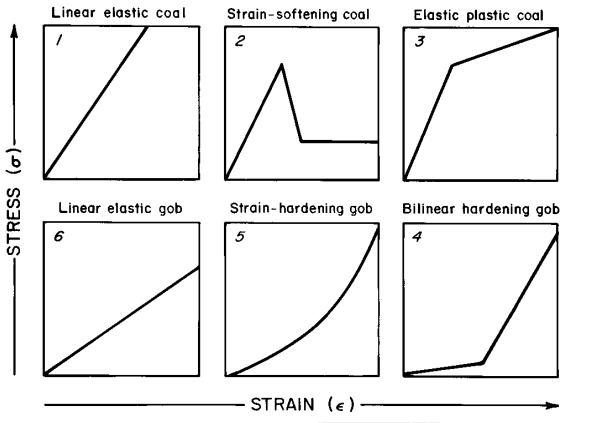


**Figure 12.—Six different stress-strain models available in MULSIM/NL.**

### Linear Elastic for Coal (Model 1)

This basic model requires little discussion since it is the basis for MULSIM (*2*) and MULSIM/BM (*3*). The required parameters for the model are E (Young's modulus) and G (shear modulus) which may or may not be related by

$$G = \frac{E}{2(1+\nu)}. \tag{8}$$

In the BEM calculations, E relates the normal stress to the normal displacement (closure) across an element, whereas G relates the associated shear stresses to the corresponding shear displacements (rides). As discussed earlier, the three boundary conditions applied to each element behave independently of one another.

With the linear elastic model, MULSIM/NL works internally with a stiffness K given by

$$K = \frac{E}{t} \tag{9}$$

where E is the modulus and t is the seam thickness.

As will be discussed later, the linear elastic model works equally well in either induced-stress or total-stress approaches to the BEM.

### Linear Elastic for Gob (Model 6)

This model is the counterpart to model 1 and is intended for the gob material left in wake of the mining. Required parameters are again E and G plus a "gob height factor," n. The factor n is the ratio between the height of broken, rotated gob fragments and the unmined seam height. The factor n typically ranges from 2 to 6 and averages about 4. Beyond a range of 2 to 6 seam thicknesses, the rock mass surrounding mined-out gob areas remains linear elastic. With linear elastic gob elements, MULSIM/NL uses a stiffness given by

$$K = \frac{E}{nt}. \tag{10}$$

In principle, the factor n accounts for the larger effective seam thickness present in extracted areas that are now filled with gob material. Another way to consider n is as a modulus reduction factor as done by Beckett and Madrid (*3*). For further details on the meaning of n, the gob height factor, see appendix E of this report.

### Strain-Softening for Coal (Model 2)

This model, after Crouch and Fairhurst (*28*), approximates the complete stress-strain curve observed during laboratory strength tests on coal conducted under true displacement control. In principle, it also describes the yielding behavior of moderately sized pillars or the perimeters of large pillars. Field observations by Wang (*34*) and Iannacchione (*35*) strongly support the use of a strain-softening model to simulate the behavior of full-size pillars in many mines.

Required input parameters for this stress-strain model are a peak stress and peak strain plus a residual stress and residual strain. In addition, the model requires a Poisson's ratio, $\nu$. For the normal components of stress and displacement, the strain-softening model uses the peak and residual stress-strain points. However, for the two shear components, MULSIM/NL scales the specified peak and residual stresses by a factor of $1/[2(1+\nu)]$. In the linear elastic portion of the strain-softening model, MULSIM/NL relates normal stress and displacement with an elastic modulus computed as $E = \sigma_p/\epsilon_p$, where $\sigma_p$ is peak stress and $\epsilon_p$ is peak strain. The shear stresses and displacements satisfy a similar relation in the initial linear portion where shear modulus is computed as $G = (\sigma_p/E_p)/[2(1+\nu)]$. Recall that E and G are related via equation 8.

One restriction on the strain-softening model is that residual strain must exceed peak strain and peak stress must exceed residual stress. For strains greater than residual, stress remains constant at the residual level. As a final point, implementation of the model requires a total-stress approach to the BEM since the model is defined in terms of absolute or total, stresses and strains.

### Elastic-Plastic for Coal (Model 3)

This stress-strain model, closely akin to the strain-softening model, approximates a "pseudo-ductile" behavior believed to occur in pillar cores (*36*). Required input for the model is again a peak stress and peak strain, the slope of the postyield portion (in degrees), and a Poisson's ratio, $\nu$. As with the previous model, the factor $1/[2(1+\nu)]$ scales the amplitude of the normal stress-strain curve to obtain the shear stress-strain relations. E and G satisfy equation 8 in the initial linear portion. Since the material model is specified in terms of <u>total</u> stress and strain, as opposed to induced stress and strain, implementation again requires a total-stress formulation of the BEM.

### Bilinear Hardening for Gob (Model 4)

This stress-strain model, analogous to the elastic-plastic model in certain respects, permits a certain amount of deformation to occur prior to introducing significant element stiffness. Input requirements for the model are stress and strain at the hinge point, modulus in the hardening region past the hinge point, and Poisson's ratio, $\nu$. Again, the

stress-strain relation for the normal direction of the element is scaled by $1/2[(1+\nu)]$ to obtain the stress-strain relation for the tangential directions of the element.

This gob model also requires the gob height factor n. This factor increases the effective seam thickness for those elements employing the various material models for gob. An alternative way to view n is as a modulus reduction factor to account for effective seam thickness in the gob areas that exceeds seam thickness in the coal areas.

### Strain-Hardening for Gob (Model 5)

This model allows the gob material to increase in stiffness as it consolidates under increasing load. Appendix E provides the complete derivation of this model. The model assumes that the gob formation occurs via a two-step mechanism: first, the overburden rock behind the active face fractures, collapses, and swells to fill the newly created void, and second, the gob consolidates and follows a nonlinear, strain-hardening constitutive relationship vertical stress on the gob increases. As shown in figure 13, derivation of the model begins by assuming that the tangent modulus of the gob increases linearly from an initial modulus value $E_I$ to a final modulus value $E_F$ over the stress range 0 to $\sigma_v$, where $\sigma_v$ is the final stress. Beyond a stress level of $\sigma_v$, the tangent modulus of the gob may continue to increase, but for practical purposes, stress levels beyond $\sigma_v$ are unlikely except in rare multilevel mining cases. The relation describing the linear increase in tangent modulus is

$$E = \left[\frac{E_F - E_I}{\sigma_v}\right]\sigma + E_I . \qquad (11)$$

The differential relation between stress ($\sigma$) and strain ($\epsilon$) is

$$d\sigma = E\, d\epsilon . \qquad (12)$$

Combining these relations and integrating produces the following stress-strain relation for gob:

$$\sigma = \frac{E_I}{n}\left[\frac{n\sigma_v}{E_F - E_I}\right]\left[\exp\left[\frac{E_F - E_I}{n\sigma_v}\right]\left[\frac{D}{t}\right] - 1\right] \qquad (13)$$

where $E_I$ = initial modulus,

$E_F$ = final modulus,

$\sigma_v$ = virgin vertical stress,

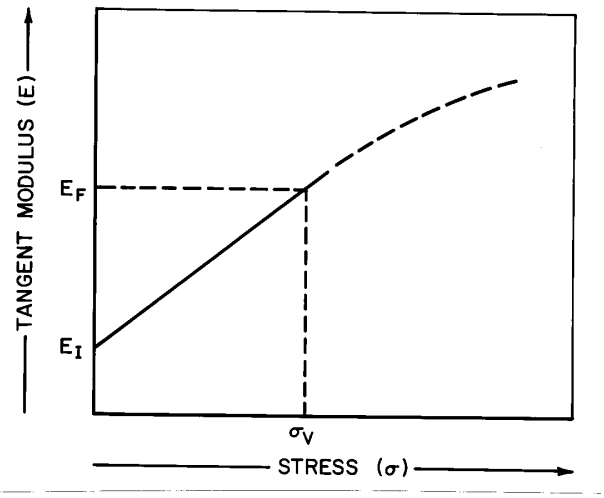


**Figure 13.—Assumed linear relationship between tangent modulus (E) and stress ($\sigma$) over range 0 to $\sigma_v$. $E_I$ is initial modulus at zero vertical stress, and $E_F$ is final modulus at vertical stress $\sigma_v$.**

D = seam closure,

t = seam thickness,

and n = gob height factor.

The parameter $(E_F - E_I)/(n\ \sigma_v)$ controls the degree of nonlinearity in the model. Input parameters are $E_I$, $E_F$, $\sigma_v$, n, and $\nu$. As with the prior models, scaling the above stress-strain relation for the normal direction of the element by a factor $1/[2(1+\nu)]$ provides an appropriate stress-strain relation for the tangential directions of the element. Again, a total-stress formulation of the BEM is required.

## TOTAL-STRESS FORMULATION FOR MULSIM/NL

In making the change from strictly linear elastic material properties, it becomes necessary to shift the basic boundary-element formulation from an induced-stress approach to a total-stress approach. The original MULSIM and MULSIM/BM programs conduct computations strictly with the induced stresses. After the equations are solved, the induced stresses are added to the primitive stresses to obtain the total stresses for output. With linear elastic materials, the elastic modulus serves as the proportionality constant between the induced stress and displacement - a proportionality unaffected by the magnitude of total stress. With nonlinear materials, however, the absolute magnitude

of the stresses does become important, and it is essential to work with total stresses during the equation-solving process.

Following the notation used by Sinha (*2*), the fundamental boundary-element equation relating elemental stress components (T) to elemental displacement discontinuities (D) is

$$T = \sum_{m \in y} \left[ \overline{TC} + \overline{TC}^{*} \right] D \qquad (14)$$

where $[\overline{TC}]$ and $[\overline{TC}^{*}]$ are m × n matrices of displacement coefficients for the infinite body and half-space solutions, respectively, and T and D are n dimensional vectors. In principle, equation 14 is identical to equation 5 given in the prior simplified explanation of BEM workings.

### Induced-Stress Boundary Conditions

For an induced-stress formulation, the boundary conditions for the mined-out areas are

$$[T] + [P] = [0] \qquad (15)$$

and for the elastic areas are

$$[T] + [K]^{T}[D] = [0] \qquad (16)$$

where P is the far field primitive stress and K is the element stiffness. For linear elastic elements, the stiffnesses K are constants and do not depend on the elemental displacements D or the induced-elemental stresses T in any respect. Combining equations 14, 15, and 16 results in a linear system of equations of the form

$$Ax = b. \qquad (17)$$

Direct solution of this system is not feasible since the unknown elemental displacements D must satisfy the additional restriction

$$[D] \leq [t] \qquad (18)$$

where t is a constant vector of elemental thicknesses. This restriction necessitates use of an indirect method like the Gauss-Seidel scheme provided by Dahlquist and Bjork (*33*) for n = 1,2,... N:

$$x_n^{(k+1)} = x_n^{(k)} + \omega \frac{- \sum_{m=1}^{n-1} a_{mn} x_m^{(k+1)} - a_{nn} x_n^{(k)} - \sum_{m=n+1}^{N} a_{mn} x_m^{(k)} + b_n}{a_{nn}} \qquad (19)$$

where n is the current unknown index, N is the maximum number of unknowns, k is the iteration number, m is a summation index, and $\omega$ is the overrelaxation factor. $\omega$ is defined by the user and typically ranges from 1.0 to 1.5. A new variable for summation of element stress influences, $\Gamma$, is defined as

$$\Gamma_n = - \sum_{m=1}^{n-1} \left[ \overline{TC}_{mn} + \overline{TC}^{*}_{mn} \right] D_m^{(k+1)} - \left[ \overline{TC}_{nn} + \overline{TC}^{*}_{nn} \right] D_n^{(k)} - \sum_{m=n+1}^{N} \left[ \overline{TC}_{mn} + \overline{TC}^{*}_{mn} \right] D_m^{(k)}. \qquad (20)$$

For the mined-out areas, combining equations 14 and 15 and then forming a recursive relationship after 19 results in

$$D_n^{(k+1)} = D_n^{(k)} + \omega \left[ \frac{- \Gamma_n - P_n}{\overline{TC}_{nn} + \overline{TC}^{*}_{nn}} \right]. \qquad (21)$$

Similarly, in the elastic areas, combining equations 14 and 16 results in

$$D_n^{(k+1)} = D_n^{(k)} + \omega \left[ \frac{- \Gamma_n - K_n D_n^{(k)}}{\overline{TC}_{nn} + \overline{TC}^{*}_{nn} + K_n} \right]. \qquad (22)$$

Basically, Sinha's original MULSIM, and its enhancement MULSIM/BM, implement and solve equations 20, 21, and 22 for a linear elastic induced-stress approach. Figure 14, modified from Sinha (*2*), provides a flowchart for this critical area of the program - namely, the equation solver. These three equations are noted in this flowchart.

### Total-Stress Boundary Conditions

With nonlinear materials, however, the elemental stiffness K depends on the absolute magnitude of the elemental displacements and stresses. (In fact, K becomes a function of D.) It is therefore no longer sufficient to

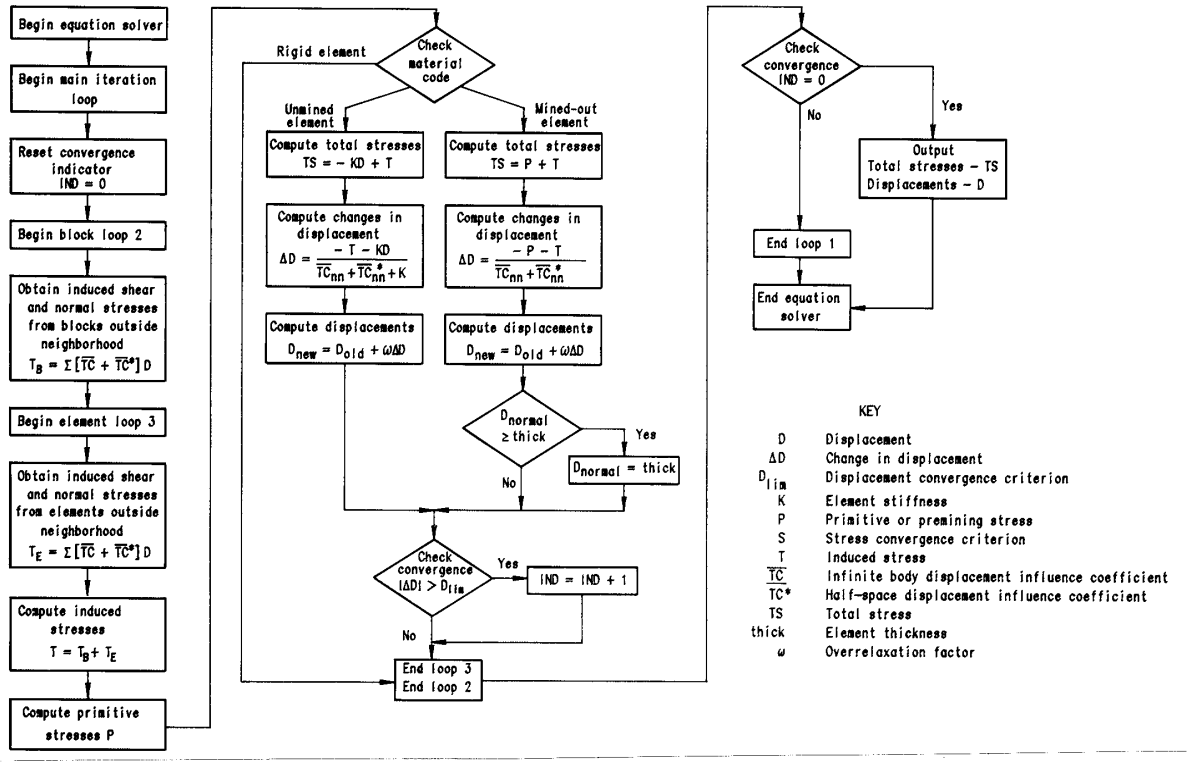


**Figure 14.—Flowchart of iteration scheme using induced-stress approach to solve for unknown stresses and displacements.**

consider just the induced stresses in the elastic areas; hence, total stresses are required. For a total-stress formulation, the boundary conditions for the mined-out areas are

$$[T] + [P] = [0] \tag{23}$$

and for the elastic areas are

$$[T] + [P] + [K]^T[D] = [0]. \tag{24}$$

As noted earlier, for nonlinear materials, K is a function of D. Therefore, combining equations 14, 23, and 24, now results in a nonlinear system of equations of the form:

$$[A]x = b(x) \tag{25}$$

where the right-hand side is now some nonconstant function of x. In addition, the restriction given by equation 18, limiting D to less than or equal to the element thickness, still applies. Fortunately, however, the Gauss-Seidel iteration procedure given by equation 19 also applies to nonlinear systems after appropriate modifications.

For the mined-out areas, combining equation 14 with 23 and then forming a recursive relation after 19 results in

$$D_n^{(k+1)} = D_n^{(k)} + \omega \left[ \frac{-\Gamma_n - P_n}{\overline{TC}_{nn} + \overline{TC}^*_{nn}} \right] \tag{26}$$

which is, of course, identical to equation 21. Similarly, in the elastic areas, combining equations 14 and 24 results in

$$D_n^{(k+1)} = D_n^{(k)} + \omega \left[ \frac{-\Gamma_n - K_n D_n^{(k)} - P_n}{\overline{TC}_{nn} + \overline{TC}^*_{nn} + K_n} \right]. \tag{27}$$

As stated earlier, with the nonlinear material models for the elements, K is no longer constant, but depends on D.

The solution procedure must continuously update the values of K according to the latest estimates of D until stable, final values of D are achieved.

The new nonlinear equation solver in MULSIM/NL invokes equations 26 and 27 and continuously updates K as a function of D. Figure 15 presents the new flowchart and provides key details of the new solver.

### Illustration of Convergence Schemes

Each iteration step for the nonlinear system proceeds in two stages. The first stage executes the summation given by equation 20 and provides total stress at that block or element. Based on the new total-stress estimate and the displacement estimate from the prior iteration, the second stage of the iteration process computes a new estimate of the stiffness K at that block or element following the specified material model and its material properties. Using this updated stiffness value K, MULSIM/NL then computes a new displacement estimate based on either equation 26 or 27. Repeating this two-stage iteration process for total stress then stiffness and displacement results in rather rapid convergence to stable final values for the unknown stresses and displacements at each block and element.

Figure 16 shows this two-stage iteration process for two kinds of material models. In both cases, total stress and displacement (or strain) lie at the point 1A for the current iteration. For the strain-softening or elastic-plastic material models, MULSIM/NL uses the current displacement estimate to determine the intercept labeled 1B on the stress-strain curve. It then determines a new stiffness estimate for use in the next iteration from that intercept. In contrast, with the strain-hardening or bilinear hardening material models, MULSIM/NL uses the current total stress estimate to determine the intercept labeled 1B on the stress-strain curve. In both cases, the iterative equation-solving process repeats itself until the calculated stresses and displacements (strains) converge to the prescribed stress-strain model within acceptable limits. The number of iterations required can range from 10 to 200 depending on the size and complexity of the model. A typical problem may need 20 to 50 iterations.

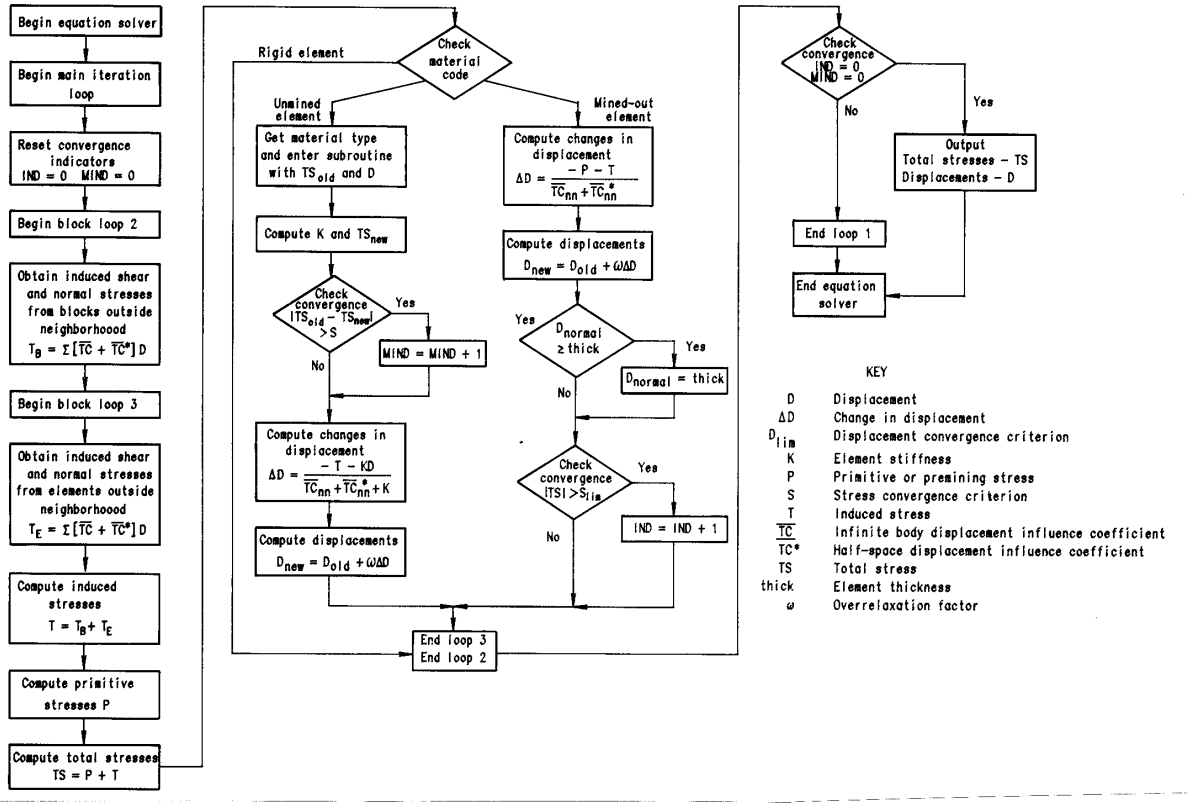


**Figure 15.—Flowchart of iteration scheme using total-stress approach to solve for unknown stresses and displacements.**

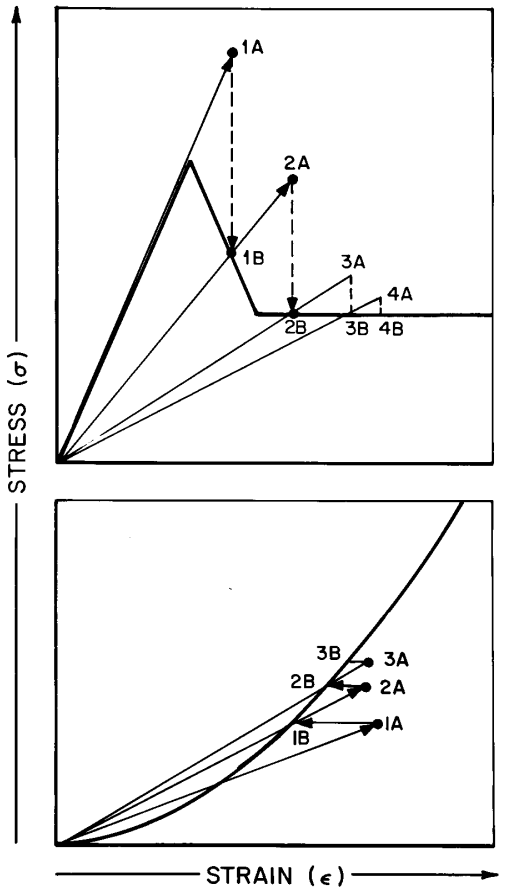


**Figure 16.—Two-stage iteration process for nonlinear material models in MULSIM/NL. Top, Strain-softening and elastic-plastic materials; bottom, strain-hardening and bilinear hardening materials. Alphanumeric labels indicate two-stage iteration progress toward final solution for stress and displacement.**

## FORTRAN IMPLEMENTATION OF MATERIAL NONLINEARITIES

### Equation-Solver Logic

Figure 15 shows the flowchart-logic diagram for the MULSIM/NL equation solver that incorporates material nonlinearities. Much of the FORTRAN code appears in the MULSIM/NL subroutine called SOLVER. This solver uses three sets of nested DO loops for this process. The first set (outermost) is the main iteration loop for the Gauss-Seidel scheme. The iterative calculations in the loop repeat themselves until satisfactory convergence occurs, or the user-specified maximum number of iterations is exceeded. The second set of DO loops increments through each block in the mesh, while the optional third set of DO loops (innermost) increments through all 25 elements in a fine-mesh block. The second and third sets of DO loops evaluate equation 20 which provides the induced and total stress components for the block or element.

After evaluation of the induced and total stress components for an element or block, the program branches three ways according to the applied boundary conditions. In the special case of rigid blocks or elements (i.e., infinite stiffness), the displacement discontinuity components are identically zero as are the induced stresses. The total stresses remain identically equal to the primitive stresses.

For the mined-out areas, the program first calculates displacement discontinuity components for the element according to equation 26 and then applies a series of convergence tests. By definition, total stresses in the open elements are zero, and the induced stresses are equal and opposite to the primitive stresses. Acceptable convergence occurs when these total stresses are approximately zero. An exception can occur in the normal direction of the element if the calculated normal displacement or closure exceeds the thickness of the element. In this case, the normal displacement is set equal to the thickness, and the total stresses are allowed to have positive or compressive values. With complete normal closure, the stresses begin to increase, and ultimately, the total normal stress component may approach the primitive normal stress component. If an element fails either a displacement or a stress convergence criterion, then the equation solver automatically proceeds with another iteration up to a user-set limit.

For the elastic areas, the program first calculates displacement-discontinuity components according to equation 27. It then retrieves the most recent total stress and displacement values for the element or block and enters the appropriate material property subroutine to obtain a new, updated modulus (or stiffness) estimate. Obtaining updated values for total stress is the first stage of the iteration process. Once inside the proper material subroutine (from a current choice of six material models), the second stage of the iteration process begins. As discussed earlier, and shown in figure 16, the strain-softening and elastic-plastic models start from the current displacement to find the intercept on the stress-strain curve of the material, whereas the strain-hardening and bilinear hardening models start from the current total stress to find this intercept.

In both cases, locating this intercept on the prescribed stress-strain curve provides an updated modulus (or stiffness) value for use in the next iteration of the equation solver. Upon returning to the solver with this secant modulus, the program continues the current iteration using equation 27 to calculate updated displacements.

### Material Property Subroutine Structure

MULSIM/NL uses a 26 by 10 array called EPROP to store parameters used by the six nonlinear stress-strain material models. The program permits up to 26 different materials labeled A through Z which in turn can follow any one of the six material models shown in figure 12. EPROP allows each material model to have up to 10 descriptive parameters. The value of the first parameter directs the program to the proper stress-strain model for each material defined. These are the assignments for the six models currently permitted: 1 - linear elastic coal, 2 - strain-softening coal, 3 - elastic-plastic coal, 4 - bilinear gob, 5 - strain-hardening gob, and 6 - linear elastic gob. Table 1 shows the required parameters and their location in EPROP for the six material models. Quite naturally, when defining materials for a given model and reading the input file, MULSIM/NL expects the material descriptors in a compatible format.

The six material property subroutines have very similar structures. Associated with each element or block is a material code, A through Z, which corresponds to positions 1 to 26 in EPROP. When MULSIM/NL requires updated material properties, it reads the first parameter in EPROP for that material which, in turn, directs MULSIM/NL to the proper material property subroutine. Each subroutine can then read the remaining parameters in EPROP for that material and interpret those parameters accordingly. As discussed earlier, each subroutine returns updated secant moduli for the normal direction of the element and the two tangential directions.

Finally, each nonlinear material property subroutine incorporates a convergence check. The old total stress values from the initial stage of the iteration step must equal (or nearly equal) the new total stress value computed by the material model subroutine. If the old and new total stresses agree within an acceptable user-defined limit, then the solution has converged. Otherwise, the iteration steps continue up to a user-defined maximum.

**Table 1.—Material model parameters and material property array EPROP structure**

| Model | 1 | 2 | 3 | 4 | 5 | 6 |
|---|---|---|---|---|---|---|
| 1 . . . | Linear elastic coal-(1). | Young's modulus (E). | Shear modulus (G). | NAp . . . . . | NAp . . . . . | NAp. |
| 2 . . . | Strain softening coal (2). | Peak stress | Peak strain . . . | Residual stress | Residual strain | Poisson's ratio ($\nu$). |
| 3 . . . | Elastic-plastic coal-(3). | . . do . . . . | . . do . . . . . | Plastic modulus | Poisson's ratio ($\nu$). | NAp. |
| 4 . . . | Bilinear hardening gob-(4). | Offset stress. | Offset strain . . | Hardening modulus. | . . do . . . . . | Gob height factor (n). |
| 5 . . . | Strain-hardening gob-(5). | Initial modulus ($E_I$). | Final modulus ($E_F$). | Final stress ($\sigma_v$). | Gob height factor (n). | Poisson's ratio ($\nu$). |
| 6 . . . | Linear elastic gob-(6). | Young's modulus (E). | Shear modulus (G). | Gob height factor (n). | NAp . . . . . | NAp. |

NAp Not applicable.

NOTE.—For these 6 material models, there are no parameters 7 through 10.

# NONLINEAR ENERGY CALCULATIONS IN MULSIM/NL

This section begins by briefly tracing the origins of energy release rate (ERR) concepts applied to rock burst control in the mines. Salamon (*6*) re-examined the theoretical basis of the ERR concept. The analytic results of his work provide the basis for the nonlinear ERR calculations in MULSIM/NL. The discussions summarize Salamon's (*6*) derivations and provide key details of the FORTRAN implementation in MULSIM/NL.

## EVOLUTION OF ENERGY RELEASE RATE CONCEPTS

Cook (*37*) first noted the enormous energy changes that result from underground mining and postulated "excess potential energy causes the damage noticed as rock bursts." Subsequent papers by Cook (*4, 38*) provided complete derivations and discussions of what became the ERR concept.

When an excavation is created underground, an enormous gravitational potential energy, $W_{GP}$, source becomes available and is given approximately by

$$W_{GP} = \sigma_z V_{ex}, \tag{28}$$

where $\sigma_z$ is the in situ vertical stress and $V_{ex}$ is the total excavation volume. Immediately after excavation creation, the excavation walls converge to some extent and a portion of the available gravitational potential energy given by equation 28 is transformed into work. This change in gravitational potential energy, $W_G$, is

$$W_G = \sigma_z V_c, \tag{29}$$

where $V_c$ is the excavation closure volume. Part of the gravitational potential energy change given by equation 29 transforms into an increase in the strain energy storage, $W_S$, of the rock mass surrounding the excavation. Cook (*4*) showed that this strain energy storage necessarily has the following bounds:

$$0 < W_S \leq \tfrac{1}{2} W_G. \tag{30}$$

Thus, creation and subsequent partial closure of an excavation results in a certain positive strain energy storage increase in the rock mass that never exceeds one-half the gravitational potential energy change.

Energy conservation requires that

$$W_G = W_S + W_R, \tag{31}$$

where $W_R$ is the energy release due to mining. Note, that the energy release, $W_R$, is introduced to preserve conservation. Considering equations 30 and 31, the following additional inequality must also apply:

$$W_S \leq W_R < W_G. \tag{32}$$

In the special case of a linear elastic rock mass, then equations 30 and 32 become:

$$W_R = W_S = \tfrac{1}{2} W_G. \tag{33}$$

Stated semantically, upon creation of an underground excavation, the increase in strain energy storage in the surrounding rock mass must equal the energy release identically, which in turn, equals exactly one-half the change in gravitational potential energy. Cook (*4*) concluded

> "the energy release must either be in the form of nonviolent dissipation in the course of crushing of rock or supports, or in the form of violent events. In the former case, the released energy is transformed mainly into heat through friction, and in the latter case, into kinetic energy. A portion of the violent events is manifested as rock bursts."

Thus, the energy release may provide a quantitative measure of the damage potential from rock bursts.

Associated with the energy release is the ERR defined as the energy release per unit area mined. (Note that the use of rate in ERR is unfortunate since there is no relation to time involved.) The energy release is fixed by the depth and size of excavation, and engineers have relatively little control over its magnitude. However, the ERR depends on the layout and extraction sequence for an excavation, and engineers can exert considerable influence over its magnitude. Researchers in South Africa have demonstrated a clear correlation between the number and incidence of damaging rock bursts and the ERR (*8-9, 39*). Thus, the ERR provides an indicator to assess rockburst potential. By analogy, a similar correlation may exist between ERR and the risk of coal mine bumps. When evaluating mine layouts and extraction sequences with ERR, the objective is to minimize the peak ERR. This objective is achieved by keeping the ERR relatively constant over an extraction sequence. In general, the most uniform ERR results when extraction begins at the most highly stressed areas and proceeds toward the low stress areas.

Subsequent researchers continued to develop understanding of the energy changes due to mining. Walsh (*5*) presented general theoretical relations describing mining-induced energy changes. These included terms to

account for energy dissipation due to cracking in the rock mass. Brady and Brown (*39*) provided practical mine design applications of BEM incorporating energy change calculations. Finally, energy release concepts have been included in rock mechanics text books (*7*).

## RECENT ENERGY RELEASE RATE CONCEPTS

Recent theoretical work by Salamon (*6*) demonstrated that certain ERR concepts require serious revision. In the 1960's, Cook (*4, 37-38*) recognized that when an excavation is created, half of the change in gravitational potential energy (i.e., half the work done by the external body forces) is stored as elastic strain energy in the rock mass. Therefore, as seen in the prior derivations, to preserve energy conservation, the other half of the gravitational potential energy change is necessarily released.

These early researchers hypothesized that the released energy was either dissipated nonviolently as fracturing and other inelastic behavior in the rock mass, or it was transformed into kinetic energy (i.e., seismic energy). Some of these kinetic or seismic events might, in turn, manifest themselves as damaging rock bursts. The early derivations of energy release assumed, erroneously, that opening creation occurs suddenly or in one large step.

Salamon's recent theoretical findings dispel the notion that the energy release serves as the source for kinetic, seismic, and/or rock burst energy—it is not. Other sources for seismic and rock burst energies are required. This major revision in thinking concerning energy release, however, does not necessarily diminish its practical utility as an indicator of rock burst and/or coal mine bump potential.

Salamon (*6, 40*) reconsidered the basic energy balance for mining and, most important, considered the step-wise nature of mining. Retaining Salamon's notation, the following derivation captures the essence of his work. As shown in figure 17, mining progresses from state I to state II in small steps. The small mined-out volume of rock this mining step is $V_M$, and the surface area of the new mined-out area is $S_M$. Work, W, is done on the system, as shown by external forces acting on the system surface, and by internal body forces acting within the system. Basic energy conservation requires that this energy supply W is immediately transformed into three energy sinks: strain energy in the rock mass, strain energy in the opening supports and backfill, and energy dissipation. Stated symbolically, energy conservation in going from state I to state II is

$$W = \Delta U + W_{SP} + W_R, \qquad (34)$$

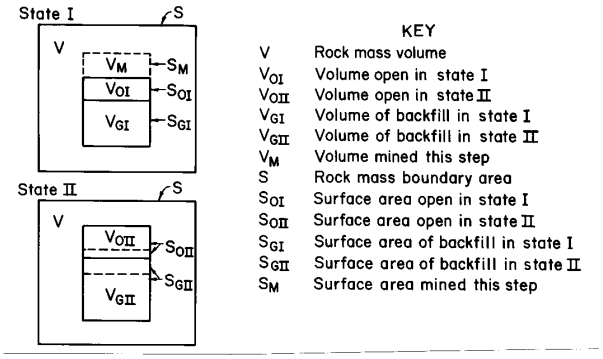


**Figure 17.—Basic notation for energy calculations as mining progresses from state I to state II.**

where $W$ = total work done on system,

$\Delta U$ = change in strain energy in rock mass volume V,

$W_{SP}$ = change in backfill and support strain energy,

and $W_R$ = total energy release going from state I to state II.

The total strain energy in the rock mass in state I, $U_I$, is

$$U_I = U + U_M, \qquad (35)$$

where $U$ = total strain energy in rock mass volume V outside the mined-out volume $V_M$

and $U_M$ = total strain energy in rock mass volume $V_M$ mined-out this step.

The total strain energy in the rock mass in state II, $U_{II}$ is

$$U_{II} = U + U_C, \qquad (36)$$

where $U_C$ = induced strain energy in rock mass volume V for this step.

The change in strain energy for this step is thus

$$\Delta U = U_{II} - U_I = U + U_C - (U + U_M) = U_C - U_M. \qquad (37)$$

Substituting into equation 34, the energy balance becomes

$$W = U_C - U_M + W_{SP} + W_R. \quad (38)$$

Solving for the energy release, this step yields

$$W_R = U_M + (W - U_C - W_{SP}). \quad (39)$$

The energy release this step is comprised of the strain energy released from the mined-out rock, $U_M$, and the kinetic energy release, $W_K$, where

$$W_K = W - U_C - W_{SP}. \quad (40)$$

Considering the stresses in the rock mass T, body forces in the rock mass X, stresses in the backfill (gob) and supports R, and the associated displacements u, Salamon (*6*) derived the following general expression for the energy release at this step based on equation 39:

$$W_R = \left[\frac{1}{2}\int_{S_M} T_I u_I ds - \frac{1}{2}\int_{V_M} X_I u_I dv\right] + \left[\frac{1}{2}\int_{S_M} T_I \Delta u ds + \frac{1}{2}\int_{S_{GII}} (1-\alpha)\Delta R \Delta u ds\right] \quad (41)$$

where $T_I$ = rock mass stress in state I,

$u_I$ = displacement in state I,

$\Delta u$ = change in displacement from state I to state II,

$\Delta R$ = change in gob (backfill) stress from state I to state II,

$X_I$ = body force in state I,

$S_M$ = surface area mined this step,

$V_M$ = volume mined this step,

$S_{GII}$ = surface area of gob (backfill) in state II,

and $\alpha$ = nonlinearity factor for the gob or backfill where $0 \leq \alpha$.

Specifically, for linear materials, $\alpha = 1$, and for strain-hardening materials, $\alpha < 1$.

An abbreviated derivation of this relation is presented in appendix A. As with the more generic energy conservation relation given by equation 39, the first bracketed term is the strain energy release from the mined-out rock, or $U_M$, and the second bracketed term is called the kinetic energy release, or $W_K$. Two basic parts makeup the kinetic part of the energy release namely, a linear part and a nonlinear part. The linear part (i.e., the first term) represents a change in gravitational potential from the newly mined-out area. The nonlinear term accounts for an energy release in the total gob and/or backfill area due to the nonlinear stress-strain behavior of this material.

Figure 18 illustrates the significance of the nonlinearity parameter $\alpha$. Introduction of this parameter accounts for material nonlinearity when calculating strain energy at the point (R, u). For linear gob and/or backfill materials, $\alpha$ equals 1 and the nonlinear part of the kinetic energy release is zero. For materials with $\alpha$ less than 1, a certain positive kinetic energy release occurs in the gob and/or backfill. For materials with $\alpha$ between 1 and 2, a negative kinetic energy release occurs in the gob and/or backfill; however, such materials do not seem to occur in nature.

Again, Salamon (*6*) derived equation 41 on the basis of a small mining step that excavates a certain volume of rock (or coal) $V_M$ over a mining area $S_M$. If the final excavation geometry such as that shown in figure 17 state II, is achieved in a single large mining step, then the concepts advanced by Cook (*4*) apply and an energy release equal to one-half the change in gravitational potential occurs as per equation 33. Considering equation 41, Salamon (*6*) proves analytically that for large mining steps, the first term (the strain energy release from the mined-out rock) is negligible compared with the second term (the kinetic energy release). Therefore, for large mining steps with linear elastic backfill and/or gob, equation 41 reduces to

$$W_R \approx \frac{1}{2}\int_{S_M} T_I \Delta u ds \quad (42)$$

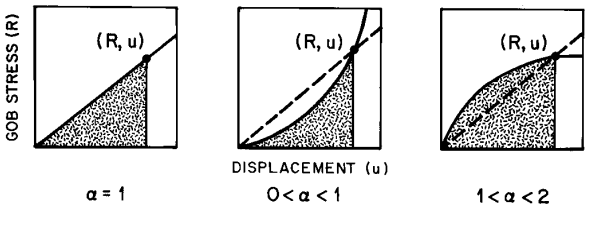


**Figure 18.—Strain energy calculations for various linear and nonlinear material behaviors showing how parameter $\alpha$ accounts for degree of nonlinearity.**

i.e., the total energy release equals half the change in gravitational potential again, in concurrence with Cook (*4*).

However, mining does not occur in giant steps, rather it occurs in small steps that approach zero size at the limit. In this case, Salamon (*6*) proves that the kinetic energy release tends to zero, and, therefore, the total energy release is nothing more than the strain energy release from the mined-out rock! This result is plainly visible if one considers a weightless rock mass ($X_I = 0$) and a linear elastic gob and/or backfill ($\alpha = 1$) in which case equation 41 reduces to

$$W_R = \frac{1}{2}\int_{S_M} T_I u_I ds + \frac{1}{2}\int_{S_M} T_I \Delta u ds. \qquad (43)$$

At the limit, as the mining step size approaches zero, $\Delta u$ tends to zero, and equation 43 can be approximated by

$$W_R \approx \frac{1}{2}\int_{S_M} T_I u_I ds. \qquad (44)$$

Figure 19, modified from Salamon (*40*), illustrates the step-size dependence of the energy release components, namely strain energy release $U_M$ and kinetic energy release $W_K$, that are normalized by the total energy release. For this example, Figure 19 shows that the kinetic energy term decays rapidly as the mining step sizes become smaller. As the mining step size becomes small, the kinetic energy release tends to zero, and the total energy release becomes equal to the strain energy release from the mined-out material. Thus, the kinetic energy release component of the total energy release cannot serve as an energy source for devastating rock bursts or coal bumps since that term disappears with small step sizes. Note, however, that the total energy release, $W_R$ which is the sum of $U_M$ and $W_K$, remains constant and independent of mining step size! In the limiting case of small step sizes, the energy release is nothing more than the strain energy release from the rock excavated during the current step. That strain energy is dissipated completely as heat during the excavation process and is, therefore, totally unavailable to drive rock bursts or coal mine bumps as was originally postulated by Cook (*4*).

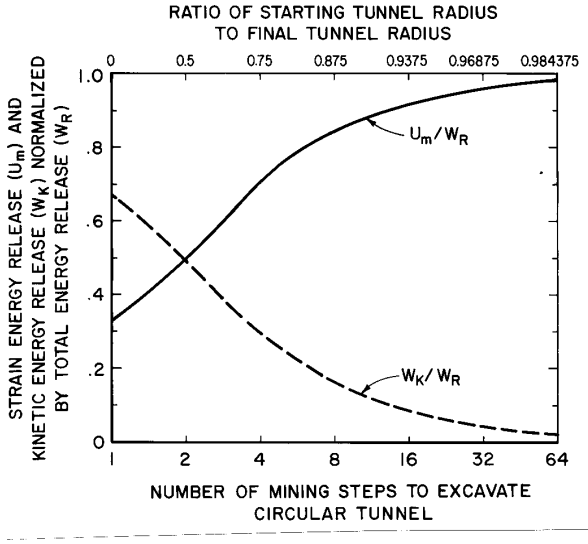


**Figure 19.—Step-size dependence of energy release components for radial expansion of circular tunnel.**

These insights into total energy release and the associated ERR do not diminish its utility as a practical indicator of rock burst or coal mine bump potential. The old interpretation of energy release made the supposition that high total energy releases corresponded to high kinetic energy releases which, in turn, might drive rock bursts. As was shown by Salamon (*6*), this is not true since in the limit, the total energy release approaches the strain energy release from the mined-out material. The correlation between energy release and rock bursts arises because rock bursts are most frequently associated with highly stressed rock. Mining out highly stressed rock must result in a high strain energy release which, in turn, must equal a high total energy release. Thus, the total energy release merely serves as an indicator of the stress level in the rocks mined-out this step. Higher energy releases correlate to higher rock stress states which in turn correlate to greater rock burst hazards.

## PROGRAMMING ENERGY RELEASE CALCULATIONS IN MULSIM/NL

The step-wise energy release equation (41 or A-17) derived by Salamon (*6*) provides the basis for energy calculations in MULSIM/NL. This section discusses the programming of this relationship into a practical boundary-element program. The discussion begins with an overview of the intermediate stress-displacement files written by MULSIM/NL. These files serve as the essential input to subroutine ENERGY which performs all MULSIM/NL energy calculations. These energy calculations proceed on two different levels—local (i.e., for each element) and global (i.e., for the entire BEM). Subroutine ENERGY then generates final output files from MULSIM/NL that contain calculated stresses, displacements, and the local energy quantities on an element-by-element basis. Last, ENERGY reports global energy changes for the entire model in accordance with equation 41 (i.e., total energy release, strain energy release, and kinetic energy release for each mining step).

Implementation of equation 41 is not as straightforward as it seems. Three different cases can arise that complicate the programming logic. These cases are discussed

in relation to a flowchart diagramming the energy calculations in MULSIM/NL.

Equation 41 is repeated below as 45 for more direct reference.

$$W_R = \left[\frac{1}{2}\int_{S_M} T_I u_I ds - \frac{1}{2}\int_{V_M} X_I u_I dv\right] + \left[\frac{1}{2}\int_{S_M} T_I \Delta u ds + \frac{1}{2}\int_{S_{GII}} (1-\alpha)\Delta R \Delta u ds\right] \quad (45)$$

where $T_I$ = rock mass stress in state I,

$u_I$ = displacement in state I,

$\Delta u$ = change in displacement from state I to state II,

$\Delta R$ = change in gob (backfill) stress from state I to state II,

$X_I$ = body force in state I,

$S_M$ = surface area mined this step,

$V_M$ = volume mined this step,

$S_{GII}$ = surface area of gob (backfill) in state II,

and $\alpha$ = a nonlinearity factor for the gob and/or backfill (for linear materials, $\alpha = 1$, and for strain-hardening materials, $\alpha < 1$).

The first two terms comprise the strain energy release from the mined-out material. The second term, reflecting the body forces, is always small relative to the first and is neglected in all subsequent calculations. As discussed earlier, the third and fourth terms are called the linear and nonlinear components of the kinetic energy release. Together, the strain energy release and the kinetic energy release form the total energy release.

### Intermediate Stress-Displacement Files

To evaluate equation 45, stresses and displacements are required from MULSIM/NL for each coarse-mesh block and fine-mesh element, and for every mining step in the sequence. As developed in the previous section, MULSIM/NL calculates each prescribed mining step using a variety of nonlinear stress-strain models for the in-place coal and/or vein material and the gob and/or backfill material left in the wake of mining. Upon completion of each mining step, MULSIM/NL writes the stress-displacement results to intermediate files. Each seam requires a coarse-mesh and a fine-mesh data file; thus, two stress-displacement data files are written for each seam. These files contain the block and/or element centroidal coordinates, the material property code, three components of calculated stresses, and three displacement components. These files provide a convenient way to access stresses and displacements for the current mining step and the previous mining step.

### Local Energy Calculations

Subroutine ENERGY enters its main loops and considers each block and element in the model. For each block and/or element, six local energy quantities are computed as follows:

(1) Strain energy release.
(2) Kinetic energy release.
    Linear part (gravitational).
    Nonlinear part (backfill and/or gob).
(3) Total energy release.
(4) Total strain energy.
(5) Recoverable strain energy.
(6) Dissipated strain energy.

The first three quantities are found by applying equation 45 on an elemental basis. For those elements within the mined-out area this step, $S_M$, ENERGY calculates ½ $T_I$ $u_I$ (the strain energy release from the mined-out material for a linear element) and ½ $T_I$ $\Delta u$ (the linear part of the kinetic energy release for that element). For those elements within the area $S_{GII}$, i.e., the current backfill and/or gob area, ENERGY evaluates ½ (1-$\alpha$) $\Delta R$ $\Delta u$ (the nonlinear part of the kinetic energy release). Next, the total energy release for that element is computed. Normally, this quantity is, either the sum of ½ $T_I$ $u_I$ plus ½ $T_I$ $\Delta u$ if the element is within $S_M$, or just ½ (1-$\alpha$) $\Delta R$ $\Delta \mu$ if the element is within $S_{GII}$. Sometimes the total energy release for that element is the sum of all three of these quantities for the special case of an element within both $S_M$ and $S_{GII}$.

The last three strain energy quantities are calculated over each unmined (nongob and/or backfill) element in the model. These energy quantities, especially the recoverable strain energy, may provide a very useful indicator of potentially dangerous highly stressed areas. Moreover, the procedure for calculating recoverable strain energy provides a basis for modifying equation 45 to account for strain energy release from nonlinear materials in the mined-out area $S_M$.

As shown in appendix A, which summarizes Salamon's work (*6*), the strain energy release for the mined-out material (equation A-6) assumes linear stress-strain behavior. The modified strain energy release calculations in subroutine ENERGY account for certain nonlinear stress-strain behaviors. Figure 20 shows the linear and nonlinear material models available in MULSIM/NL for the unmined seam material (coal or rock) and the assumed strain energy relationships. On loading to a point (T,u), each material requires a total strain energy input equal to the total area under the given stress-strain curve up to that point. Upon unloading, the modified strain energy release calculations assume that the unloading modulus equals the initial loading modulus. Thus, for nonlinear materials, the strain energy release from the mined-out material must equal the "recoverable strain energy" depicted in figure 20. The difference between the total and recoverable strain energy is the "dissipated strain energy" which is energy presumed to dissipate nonviolently through cracking and pseudoplastic flow of the material. As can be seen in figure 20, the dissipated strain energy is zero for the linear material model, and the total strain energy equals the recoverable strain energy; hence, the strain energy release.

In summary, the strain energy release component of equation 45 is modified as shown in figure 20 to account for nonlinear (dissipative) behavior in the material mined-out this step over the area $S_M$. In MULSIM/NL energy calculations, the recoverable strain energy calculated as shown in figure 20 replaces the strain energy release term of equation 45.

Finally, subroutine energy writes the final output files for MULSIM/NL. For each block and/or element, these files contain block and/or element centroidal coordinates, the material property code, three stress components, three displacement components, and the following six energy quantities for the block and/or element: total strain energy, recoverable strain energy, dissipated strain energy,

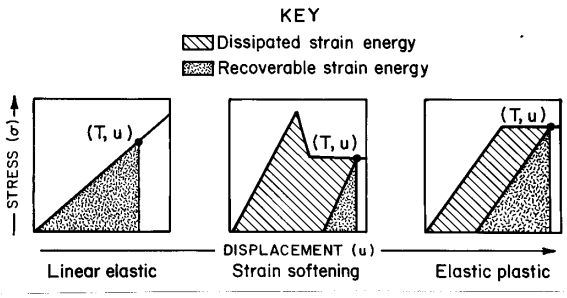


**Figure 20.—Basic strain energy relationships for linear and nonlinear material models in MULSIM/NL that apply to unmined seam material (either coal or rock). (T, u) is stress-displacement state of element.**

strain energy release, kinetic energy release, and total energy release. The three energy release quantities for the block and/or element may be nonzero over the area mined this step ($S_M$) and the total backfill and/or gob area ($S_{GII}$); whereas, the strain energy quantities may be nonzero only in areas outside of $S_M$ and $S_{GII}$.

## Global Energy Calculations

As subroutine ENERGY proceeds through the local elemental energy calculations, it also performs summations of the elemental energy releases that, in effect, approximate the integrations prescribed in equation 45. The strain energy release is the summation over the mined-out area this step ($S_M$) of the elemental recoverable strain energy. The prior section discusses this minor modification from strict adherence to equation 45. The linear component of the kinetic energy release is the summation over $S_M$ of the elemental change in gravitational potential energy. The nonlinear component of the kinetic energy release is the summation over the total backfill and/or gob area ($S_{GII}$) of energy dissipation due to material nonlinearity. The total kinetic energy release is simply the sum of the linear and nonlinear components, and finally, the total energy release is the sum of the strain energy and kinetic energy releases. Upon exiting ENERGY, the aforementioned energy release summations are written to a print file. For each mining step, this file contains the different energy release components for the coarse-mesh blocks, the fine-mesh elements, and their total. Finally, these energy release quantities are normalized by the area mined this step (area $S_M$) to obtain the corresponding energy release rates.

## Three Special Cases

Earlier discussions alluded to certain special cases that can arise which complicate the programming of equation 45. Figure 21 shows the three possible cases as mining progresses from state I to state II. In case A, the newly mined-out area $S_M$ exactly balances the newly backfilled area $\Delta S_G$, and the open area in state I equals the open area in state II. In case B, the backfilling lags the mining and the open area increases, whereas in case C, the backfilling exceeds the mining and the open area decreases. Also, as shown in figure 21, individual elements can undergo several types of changes as mining progresses in a step from state I to state II.

In the simplest case A, four types of change exist. Those elements in region 1 are unmined in state I and remain unmined in state II. Total strain energy, recoverable strain energy, and dissipated strain energy are computed

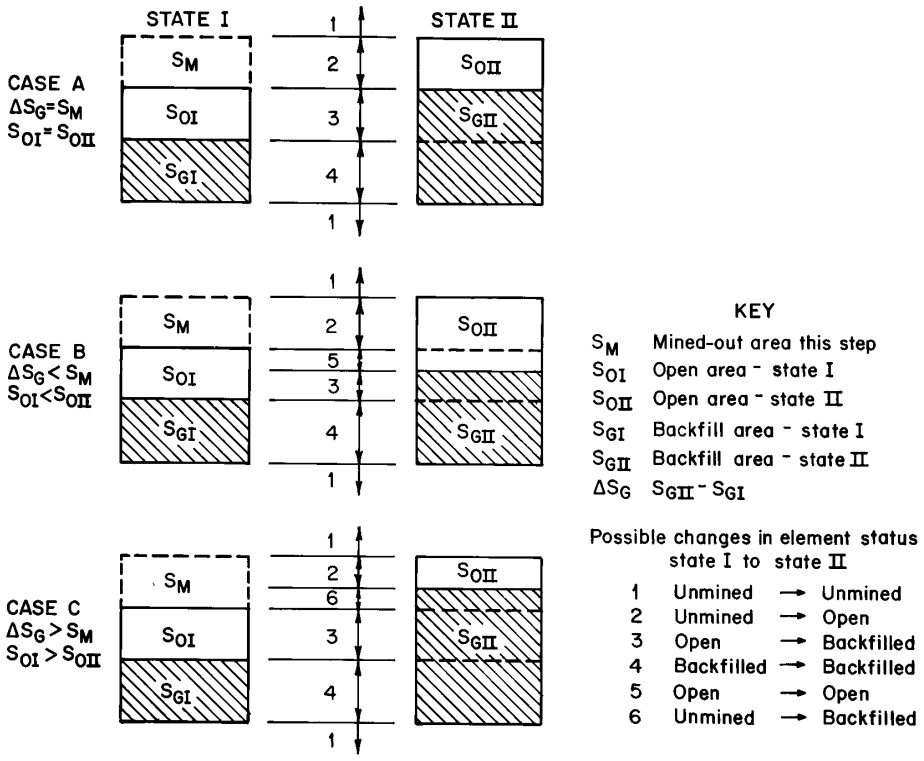


**Figure 21.—Three special cases of mining progress from state I to state II showing how elements can undergo six different status changes between state I and state II.**

and recorded for type 1 elements with the methods shown in figure 20. Elements in region 2 are mined out in going from state I to state II. As discussed earlier, strain energy release for these elements is computed as the recoverable strain energy shown in figure 20. This method for nonlinear materials replaces the first term in equation 45 where the strain energy release from a linear element is computed as $\frac{1}{2} T_I u_I$. In addition, elements in region 2 also contribute a linear component of the kinetic energy release given as $\frac{1}{2} T_I \Delta u$. Together, the strain energy release and linear kinetic energy release comprise the total energy release for the element. These three energy releases are recorded for the element, and the energy release summations for this model step are updated. Elements in regions 3 and 4 begin as open or backfilled, respectively, in state I and change to, or remain, backfilled in state II. For these elements, a nonlinear component of the kinetic energy release is calculated as $\frac{1}{2} (1-\alpha) \Delta R \Delta u$. (The only difference between regions 3 and 4 is the state I stress, which is zero in region 3 and nonzero in 4.) In these elements, the nonlinear kinetic energy release makes up the whole of the total energy release. These two energy releases are recorded for the element, and the energy release summations for the model are updated.

Case B in figure 21 illustrates the first exception. As before, case B has elements in regions 1 through 4; however, when the backfilling lags the mining, a region (5) exists with elements that were mined-out and open in state I and remained so in state II. Such elements contribute zero energy to the energy release and contain no strain energy. Therefore, such elements require no computations that is easily accommodated in the program!

Finally, case C in figure 21 shows the other exception, which arises when backfilling exceeds the mining. In this

case, elements in region 6 exist which have gone from unmined coal to backfill (gob) in one step without remaining open during an intermediate step. Such elements belong to both the set $S_M$ and $S_{GII}$. For these elements, the strain energy release is computed as the recoverable strain energy; the linear component of the kinetic energy release is computed as ½ $T_I$ $\Delta u$, and the nonlinear component of the kinetic energy release is computed ½ $\Delta R$ $\Delta u$. The total energy release for these special elements is the sum of these three parts. The strain energy release, total kinetic energy release, and total energy release are recorded for the element, and all energy release summations are updated.

## Subroutine Energy Logic Diagram

The three special cases just discussed give rise to six element classes or types which require separate consideration during the energy calculations. The logic diagram shown in figure 22 reflects these six logic paths and provides the essence of subroutine ENERGY.

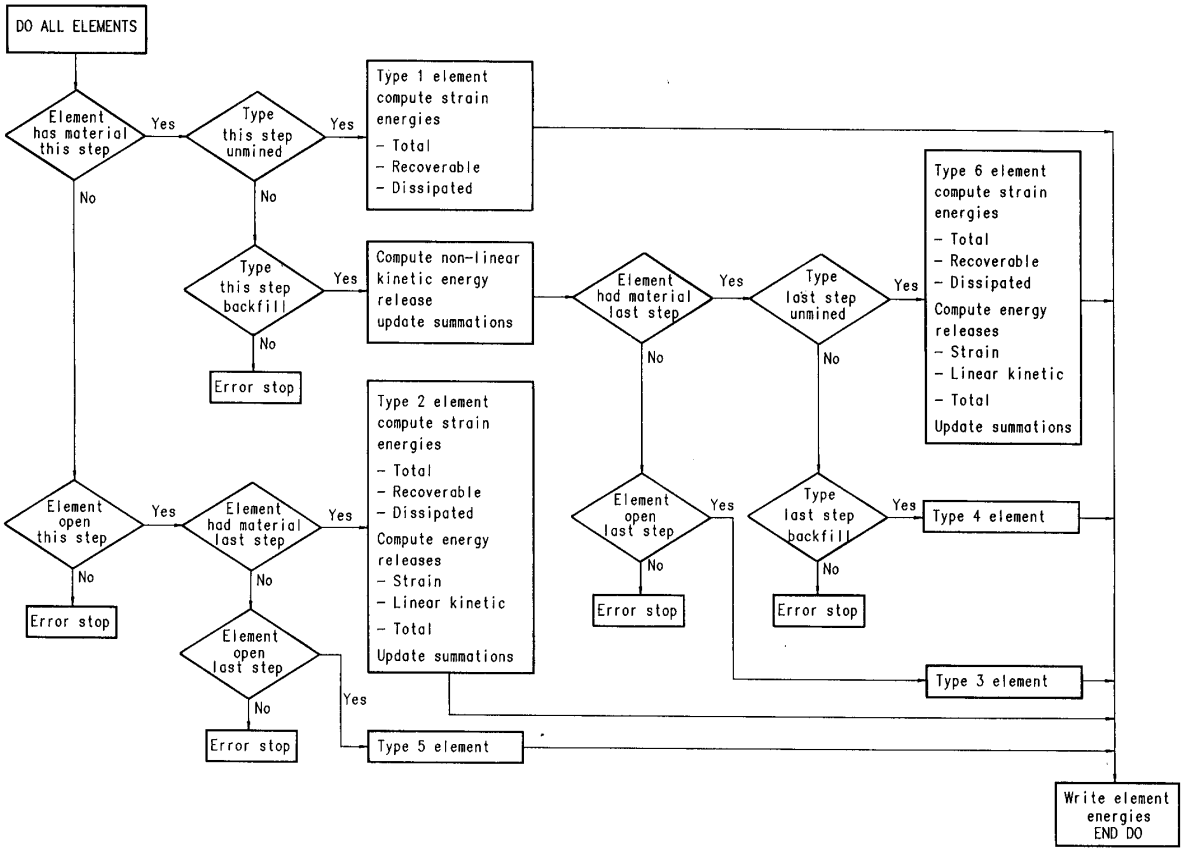


**Figure 22.—Simplified flowchart for subroutine ENERGY showing six possible logic paths.**

## MULSIM/NL PROGRAM CHECKS AND BEHAVIOR

This section provides checks on the accuracy of the stress and displacement calculations conducted by MULSIM/NL and illustrates certain behavioral aspects of the model. The first check compares the linear stress-displacement calculations of MULSIM/NL with known analytic solutions. Simultaneously, these calculations also examine rigid boundary effects. The presence of completely rigid material outside the problem grid can have a severe impact on the quality of numerical results. Another series of MULSIM/NL models examines element size effects on the numerical reliability of the stress-displacement calculations. Finally, the last study examines the new nonlinear material models in MULSIM/NL. While it is not possible to check the accuracy of the nonlinear models against an exact solution, certain qualitative behavioral checks are feasible. The intent of all these checks is to provide some essential quality control on this complicated numerical model.

### SOME SIMPLE ANALYTIC SOLUTIONS

Jaeger and Cook (*41*) provide certain analytic solutions essential for checking BEM programs. The solutions are for an elliptic crack of width 2c subject to a stress P perpendicular to this crack plane. Figure 23 shows this two-dimensional crack problem. In more practical terms, this problem corresponds to an infinitely long slot of width 2c in an infinite medium, i.e., a longwall panel of width 2c and infinite length. The vertical stress distribution along the edge of this opening is given by

$$\sigma_y = P \coth(\epsilon), \qquad (46)$$

where $\epsilon = \cosh^{-1}(x/c)$.

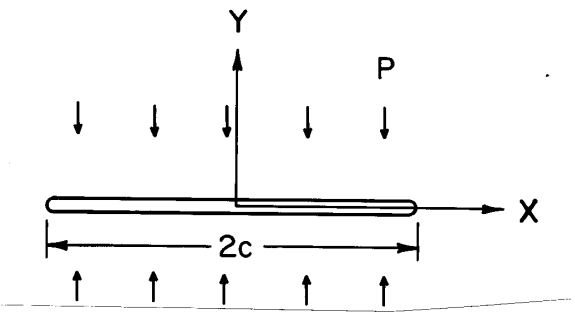


**Figure 23.—Elliptic crack of width 2c subject to stress P perpendicular to crack plane.**

This equation applies along the x axis for $x/c > 1$. Normal convergence across this opening is given by

$$V = \frac{4(1-\nu^2)}{E} P (c^2-x^2)^{1/2}, \qquad (47)$$

which applies across the region $-1 < x/c < +1$. These relationships provide important checks on the accuracy of MULSIM/NL. The need for this checking arises because of the radical changes to the equation solver in MULSIM/NL brought about by the addition of nonlinear material models.

### RIGID BOUNDARY EFFECTS

Figure 24 shows the first simple problem geometry studied with MULSIM/NL which is an infinitely long planar opening of width 2c. The objective of these initial studies is to compare the accuracy of MULSIM/NL with known linear elastic solutions and to illustrate rigid boundary effects on the computed stresses and displacements. Analytic solutions presented in the previous section give computed stresses and displacements along the symmetry line of the meshes shown in figure 24.

Rigid boundary effects arise in BEM because the inseam material outside the defined mesh is infinitely stiff or rigid. The presence of rigid material just outside the defined mesh can affect stress and displacement calculations in elements near the mesh boundary. Sinha (*2*) considered this rigid boundary when designing the original linear MULSIM program. In MULSIM, a coarse-mesh surrounds a central fine mesh which is the area where accurate stress and displacement calculations are desired. The coarse mesh improves the accuracy of numerical calculations within the fine mesh by pushing the rigid boundary far away from it. The following studies will illustrate these rigid boundary effects on the BEM calculations and suggest some guidelines for minimizing their effects in practical modeling.

The numerical model used has a central fine-mesh area 4 blocks by 12 (i.e., 20 fine-mesh elements by 60). As shown in figure 24, three different coarse-mesh sizes are considered: a small coarse mesh 20 by 10; a middle mesh 20 by 20, and a large mesh 20 by 30. In addition, three different block sizes are used in the model; namely, 6.25, 25, and 100 m that have corresponding element sizes of 1.25, 5.0, and 20 m. Varying the block and/or element size also changes the opening width 2c from 25 to 100 m

and then to 400 m. All models are subject to a vertical stress of 7 MPa and use a Young's modulus of 3,450 MPa and a Poisson's ratio of 0.25.

Figure 25 shows computed and analytic displacements (i.e., convergence) across an opening width 2c of 100 m. Going from the small coarse-mesh (20 by 10 blocks) to the middle-size coarse-mesh (20 by 20) gives a marked improvement to the accuracy of the numerical computations. Going from the middle mesh size to the large size (20 by 30 blocks) does not result in significant improvement. As shown in figure 25, numerical displacement calculations agree with the analytic to within 5%. The discrepancies are attributed to normal discretization and truncation errors and do not suggest any programming error.

Figure 26 shows computed and analytic stresses away from the edge of the 100-m opening. For all different coarse-mesh sizes, the agreement with analytic appears acceptable. Coarse-mesh size does have a marked effect on the peak edge stress which increases from 22.5 to 25 MPa (or 10%) as coarse mesh size increases.

Figures 25 and 26 illustrate numerical accuracy and rigid boundary effects for a simple MULSIM/NL analysis

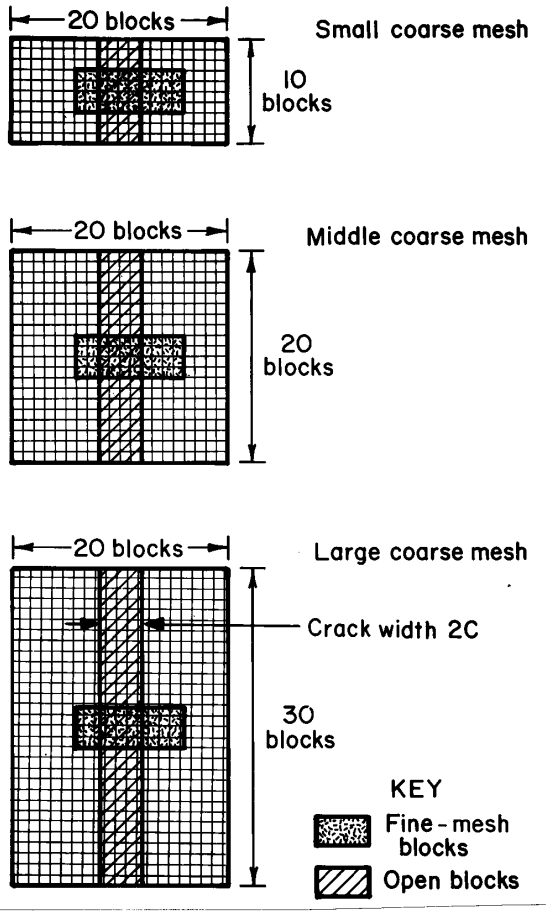


**Figure 24.—MULSIM/NL models for rigid boundary effect studies of infinitely long planar crack of width 2c.**

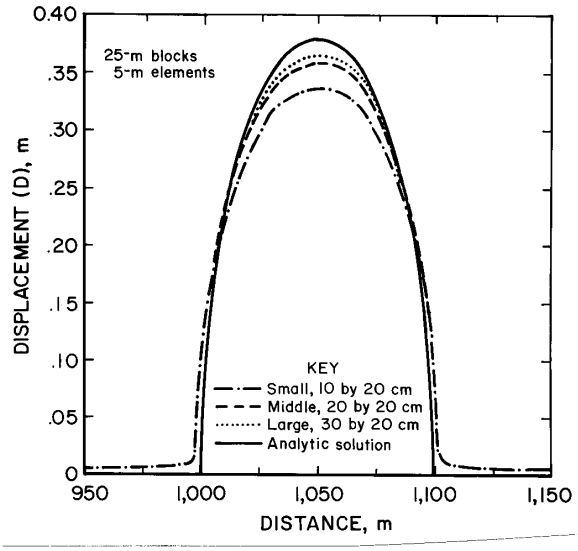


**Figure 25.—Computed and analytic displacements across 100-m opening with different coarse-mesh sizes.**

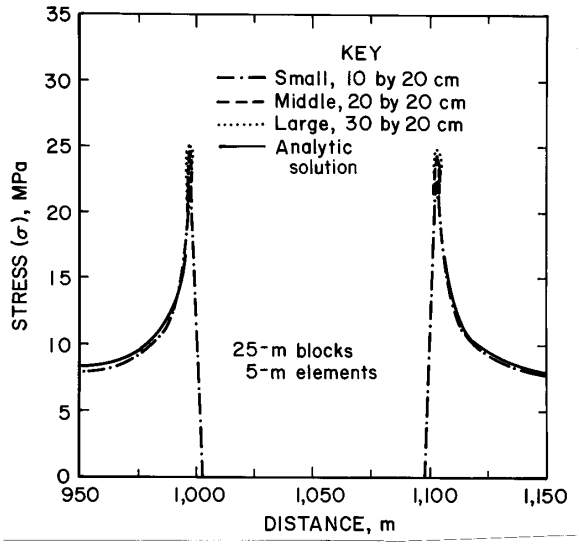


**Figure 26.—Computed and analytic stresses at edge of 100-m opening with different coarse-mesh sizes.**

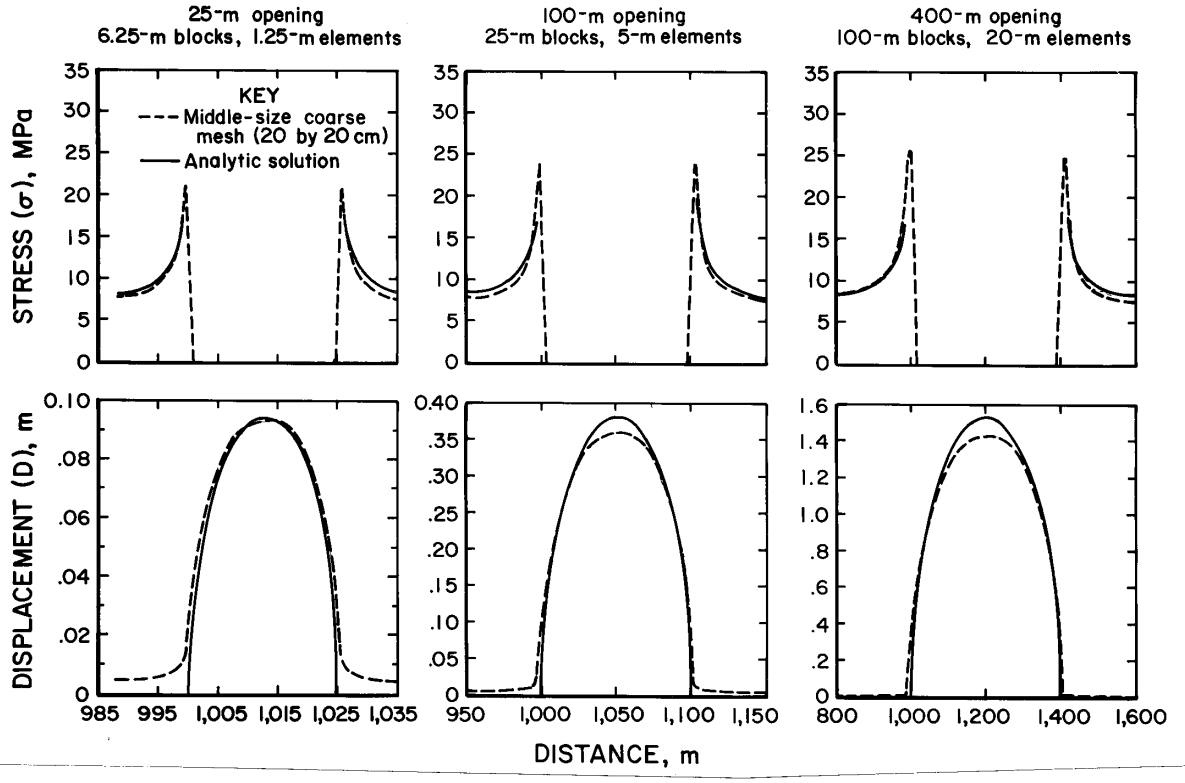


**Figure 27.—Comparison of computed and analytic stresses and displacements illustrating rigid boundary effects.**

of a 100-m-wide opening. Appendix B shows similar figures for the 25- and 400-m openings. Again, numerical computations agree with analytic solutions, and the computations show similar rigid boundary effects.

Finally, figure 27 compares numerical calculations with a middle-size coarse mesh to the analytic solutions for the 25-, 100-, and 400-m openings. With the displacement calculations, the magnitude of the peak displacement and the shape of the displacement profile scales with increased opening width. However, with the stress calculations, the magnitude of the peak stress increases slightly and only the shape of the stress profile scales with opening width. In all cases, agreement with the analytic solution appears adequate.

Several interacting factors affect the peak stress magnitudes shown in figure 27. Intuitively, the peak stress and the stress profile should increase with opening width, and indeed consideration of the analytic solution given by equation 46 shows that it does. Block and element size can also have a significant effect on peak stress computation. Smaller blocks and elements approximate actual stress profiles more accurately, and, therefore, models with smaller blocks and elements should have higher peak stresses at opening edges. However, figure 27 exhibits just the opposite trend, with peak stresses increasing slightly as block and/or element and opening size increase. The seeming discrepancy is a rigid boundary effect. The models made with smaller block and/or element and opening widths are also smaller in overall dimensions; hence, the rigid boundary is physically closer to the region of interest. Again, presence of the rigid boundary tends to decrease the magnitude of peak stresses and displacements in elements too close to that boundary.

There are no strict guidelines that one can apply to eliminate rigid boundary effects from BEM computations. The magnitude of these effects depends on the specific problem geometry under consideration. The simple problem shown here, coupled with experience, suggests that the

model edge must be about 10 block widths away from a region of interest. Alternatively, the coarse mesh should extend for 10 blocks beyond the fine mesh to minimize rigid boundary effects everywhere within the fine mesh.

## ELEMENT SIZE EFFECTS

As alluded to in the prior section, element size impacts the numerical accuracy of BEM programs, particularly near openings where stresses tend to become large at a very fast rate. This section will examine element size effects systematically and show the effect element size can have on the accuracy of stress and displacement calculations with MULSIM/NL. Figure 28 shows the model geometries used in these studies. As in the rigid boundary effects studies, this section considers an infinitely long planar opening of width 2c. The coarse-mesh size is 20 by 20 blocks with a central fine-mesh 4 blocks by 12 (i.e., 20 elements by 60). The models examine three different opening widths (25, 100, and 400 m) with block (element) sizes of 6.25 (1.25), 12.5 (2.5), 25 (5), 50 (10), and 100 (20) m.

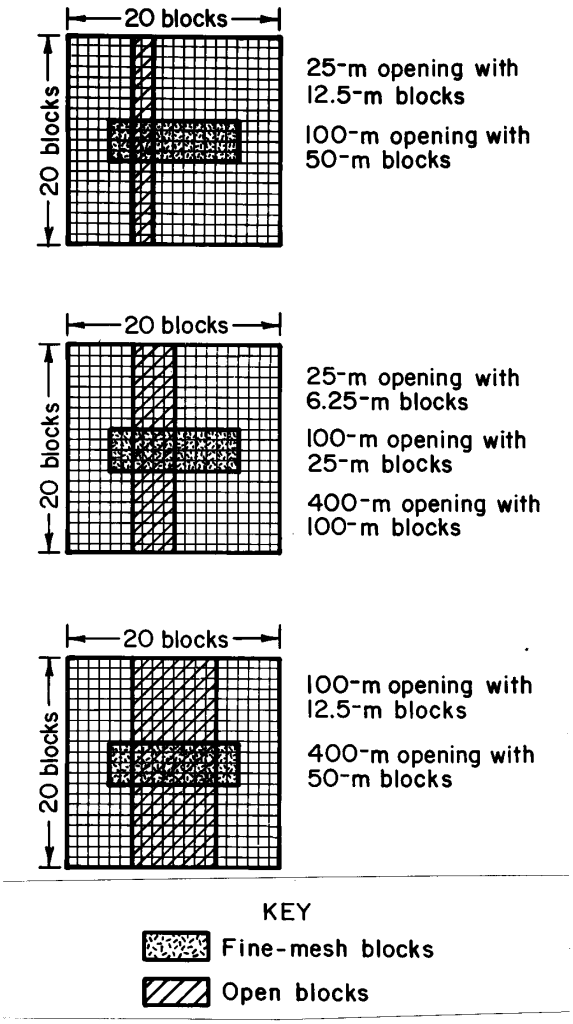


**Figure 28.—MULSIM/NL models for element size effect studies.**

Figure 29 shows displacement profiles across a 100-m opening modeled with 12.5-, 25-, and 50-m blocks (2.5-, 5-, and 10-m elements). Normally, accuracy improves with decreasing block size; however, once again, rigid boundary effects enter the problem and produce the opposite effect. Close examination of the 100-m-opening model geometries in figure 28 shows why rigid boundary effects will impact the 12.5-m-block model more than the 50-m-block model. The latter case approximates a two-dimensional problem more closely with the analytic displacement solution given by equation 47, whereas the former requires a true three-dimensional solution.

The stress profiles away from the opening edge do show the expected trend, that is smaller block sizes capture high peak edge stresses more accurately. Indeed, figure 30 shows that the peak edge stress increases dramatically as block size decreases. (Appendix C shows additional stress and displacement comparisons for 25- and 400-m- opening widths. Similar observations are noted for those numerical experiments.)

Figure 31 compares stress and displacement calculations made with different element sizes for different opening

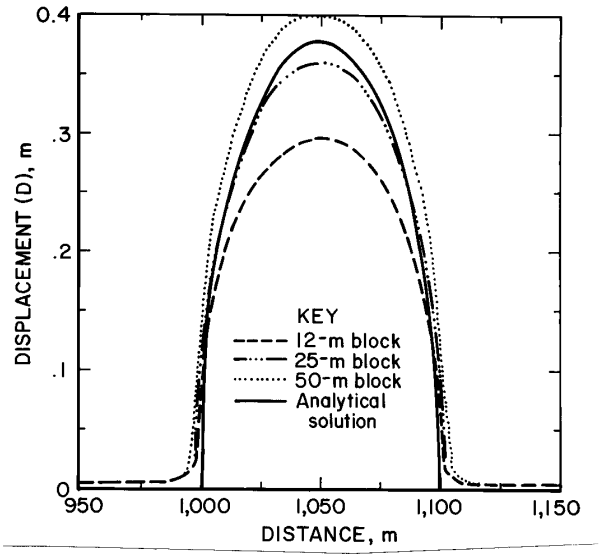


**Figure 29.—Computed and analytic displacements across 100-m opening with different block and element sizes.**

widths. For these models, stresses agree to within about 5% of analytic. Displacements can also show reasonable agreement with analytic (within 5%) depending on how well the two-dimensional solution approximates the model.

The important point of this exercise is that the choice of element size can have a profound effect on stress displacement calculations. Figures 29 and 30 show that near an opening boundary, the element size can affect displacement calculations by over 30%, stress calculations by almost 50%. The choice of element size also impacts the rigid boundary effect. In fact, the two are inseparable. Smaller element sizes which tend to improve the accuracy of stress and displacement calculations also tend to show deleterious rigid boundary effects because of the smaller model size. In summary, because of these somewhat fickle element size and rigid boundary effects on stresses and displacements computed with MULSIM/NL, caution is required in all comparisons especially when different element sizes and different model geometries are involved. Again, as shown in figures 29 and 30, large differences can arise that may be artificial.

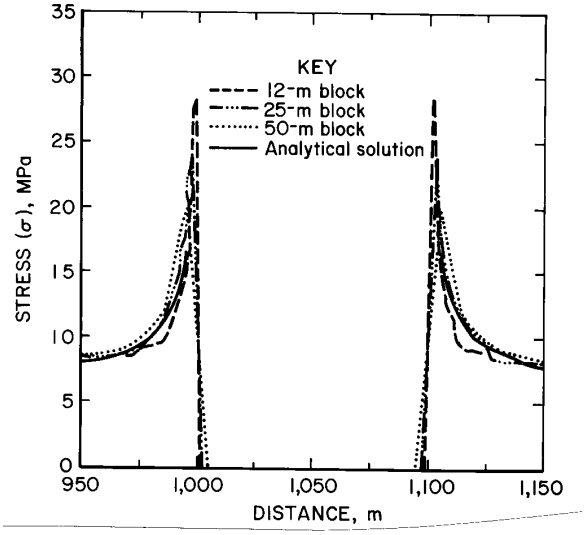


**Figure 30.—Computed and analytic stresses at edge of 100-m opening with different block and element sizes.**

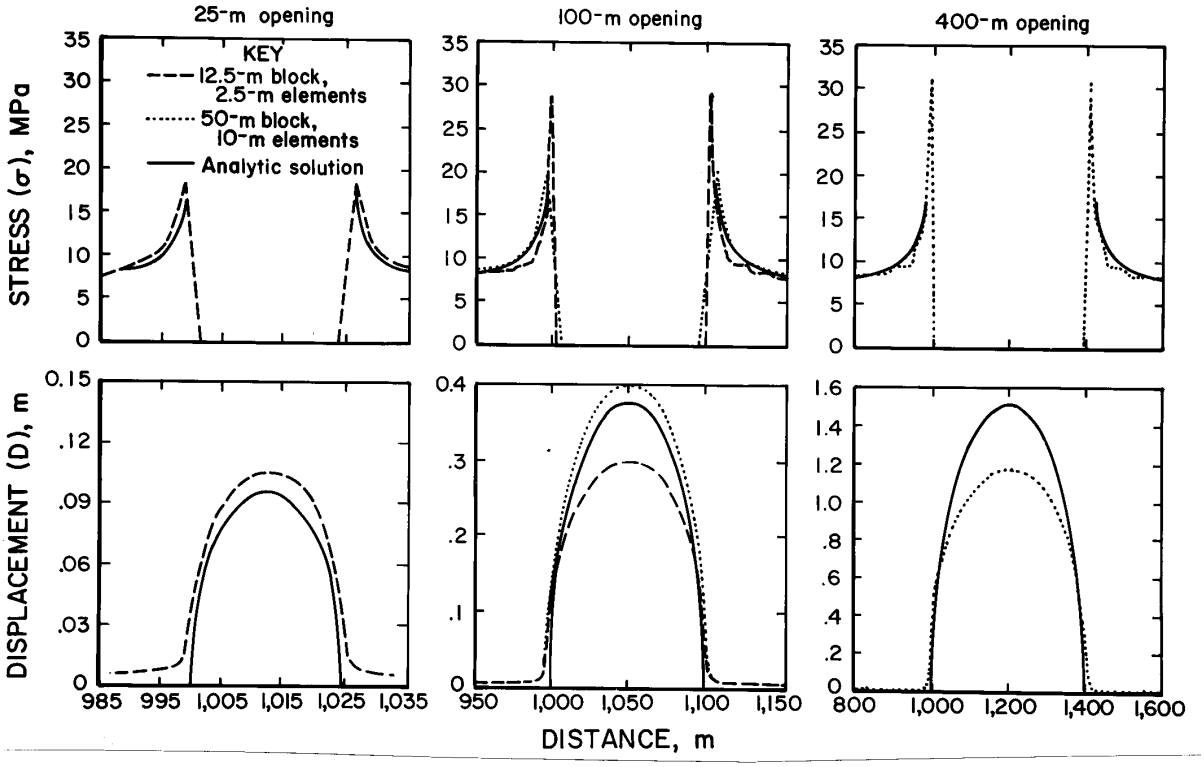


**Figure 31.—Comparison of computed and analytic stresses and displacements illustrating element size effects.**

## NONLINEAR EFFECTS

Figure 32 shows the model geometry used to illustrate the qualitative behavior of the nonlinear material models in MULSIM/NL. Again, the problem considered is an infinitely long, planar opening of width 2c. The model uses a 30- by 40-block coarse-mesh with a central fine mesh measuring 4 by 20 blocks (20 by 100 elements). Opening width increases from 50 to 100 m and then to 200 m. Two different material property sets are compared. The first set is completely linear. Young's modulus for the rock mass and the seam is set to 3,450 MPa. The second set includes the linear elastic properties of the first and also introduces strain-hardening and strain-softening elements. For the hardening elements placed in the mined-out area, initial modulus is 28 MPa and final modulus is 140 MPa at a stress of 7 MPa. Table 2 gives the four types of softening elements used by the second set. The first type is used in the first row of elements adjacent to the opening; the second type in the second row and so forth.

**Table 2.—Strain-softening properties used in nonlinear models**

| Type | Peak | | Residual | |
|---|---|---|---|---|
| | Stress, MPa | Strain | Stress, MPa | Strain |
| 1 ..... | 6.90 | 0.0020 | 2.75 | 0.0033 |
| 2 ..... | 13.80 | .0040 | 6.90 | .0080 |
| 3 ..... | 24.15 | .0070 | 20.70 | .0120 |
| 4 ..... | 34.50 | .0100 | 34.50 | .1000 |

Finally, figure 33 compares calculated stresses and displacements using the strictly linear material property set with the nonlinear set. Using strain-softening elements along the opening edge decreases the peak edge stress dramatically. The magnitude of the peak stress tends to increase with opening width as expected. The increase is

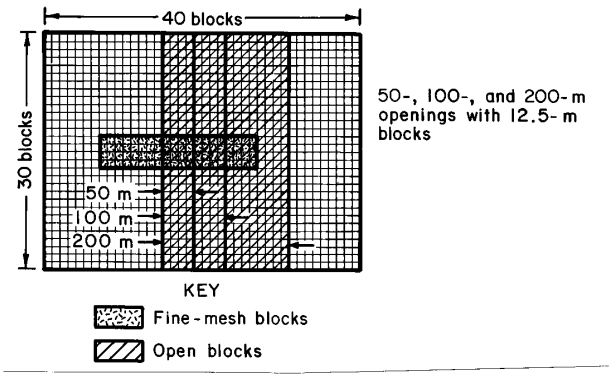


**Figure 32.—MULSIM/NL models for nonlinear effect studies.**

significant (about 40%) for the linear model and somewhat less (about 25%) for the nonlinear model. Presence of the hardening elements causes the mined-out area to increase its stress level; however in this case, the stress levels are still much less than the in situ vertical stress of 7 MPa. Hardening elements also cause the vertical displacement to decrease (up to 25%) in the mined-out area as expected.

In summary, while exact checks are not readily possible on the nonlinear capabilities of MULSIM/NL, the model does behave as expected when these nonlinearities are utilized. Stress profiles in the strain-softening areas reflect the strain-softening material input parameters. Calculated stresses and displacements for an element always lie on or near the prescribed nonlinear stress-strain curve of that element. These validation checks, while far from exhaustive, lend strong credibility to the correctness of MULSIM/NL, both in concept and in programming.

## SUBROUTINE ENERGY CHECKS AND BEHAVIOR

This section examines the energy subroutine in MULSIM/NL with three different test sets. The purpose of these tests is to validate the energy calculations and to examine the many factors affecting them. The first tests enable a rigorous comparison between MULSIM/NL energy calculations and the known analytic solution to a very simple problem. The second tests study the influence of mining step size on the relative proportion of energy components comprising the total energy release. Finally, the last tests examine quantitatively the effect of certain key geometric and material property values on the total energy release and its components. These final tests are a simple parametric study of the energy release.

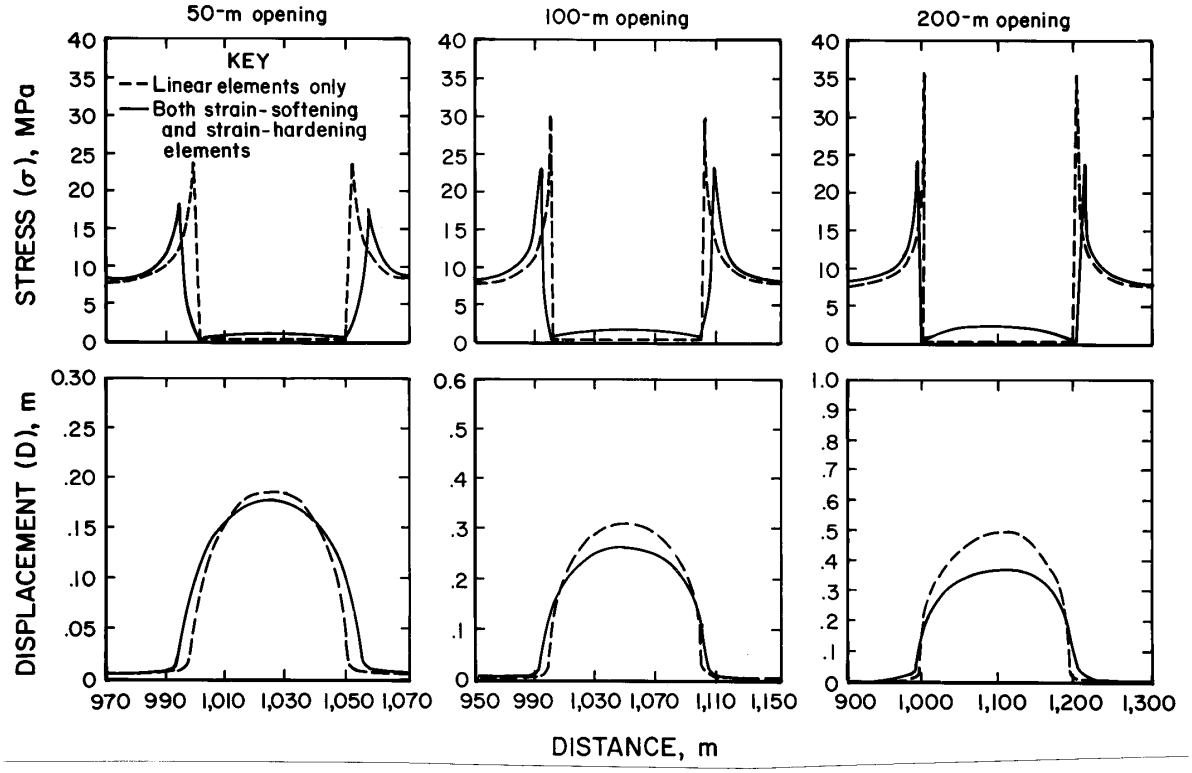


**Figure 33.—Comparison of computed stresses and displacements using linear and nonlinear material properties.**

## ANALYTIC CHECKS ON ENERGY RELEASE CALCULATIONS

The same problem shown in figure 23 also provides analytic checks on the accuracy and reliability of the energy release rate implementation in MULSIM/NL. Analytic energy release rate expressions exist for a thin, two-dimensional crack of width 2c subject to a farfield stress P perpendicular to the crack plane. For the two-dimensional crack plane shown in figure 23, equation 47 gives the convergence across the opening as a function of position, modulus, and farfield stress. As the opening width (W=2c) increases, a critical width $W_{cr}$ is attained at which the convergence just equals the opening thickness. Solving equation 47 for this critical width gives:

$$W_{cr} = \frac{HE}{2(1-\nu^2)P}, \qquad (48)$$

where H = crack or seam thickness,

E = Young's modulus,

$\nu$ = Poisson's ratio,

and P = farfield stress perpendicular to plane.

Brady and Brown (*7*) provide the required energy release rate expressions for the two-dimensional crack shown in figure 23 which approximates thin tabular excavations such as longwall panels. For a panel width less than critical ($W \leq W_{cr}$), the energy release rate is

$$W_R = \pi \frac{(1-\nu^2)}{2E} P^2 W. \qquad (49)$$

For a panel width greater than critical ($W > W_{cr}$), the energy release rate approaches the following value asymptotically:

$$W_R = H P. \qquad (50)$$

Equation 50 shows that, well beyond a certain critical width, this mining geometry can approach steady-state conditions and achieve a uniform energy release rate.

Figure 34 shows the coarse-mesh grid used to simulate extension of a two-dimensional crack plane with MULSIM/NL. In this model, the crack width extends from 50 to 500 m in 10 equal 50-m steps. Figure 34 shows just a few of these steps for clarity. Since the crack length always exceeds the crack width by a factor of 3 or more, the three-dimensional numerical model approximates the two-dimensional analytic solution for the energy release rate. Both the analytic solutions and the numerical model use the following input parameters:

Young's modulus - 3,750 MPa

Poisson's ratio - 0.25

Farfield stress - 10 MPa

Thickness - 1 m.

Figure 35 compares the ERR calculated numerically with MULSIM/NL to those determined analytically. Equation 48 gives a critical opening width of 200 m. For widths less than critical, the ERR calculated with equation 49 increases linearly to about 8 MJ/m². For widths greater than 200 m, the ERR approaches an asymptote of 10 MJ/m². As shown in figure 35, the 10-step numerical ERR agree reasonably well with the analytic values. The numerical values fall short of the analytic by about 10%. These discrepancies are attributed to end effects. The two-dimensional analytic solutions apply to an opening of width W and infinite length, whereas the three-dimensional numerical models have a finite length. Calculated displacement profiles at the ends of the opening are somewhat lower than those in the middle; hence, ERR are also somewhat low. The agreement between the numerical and analytic results provides good evidence that the energy calculations in MULSIM/NL function properly. In addition, this test also serves to confirm the accuracy of the stress and displacement calculations within MULSIM/ NL, since these calculations must be correct in order for the subsequent energy calculations to be correct.

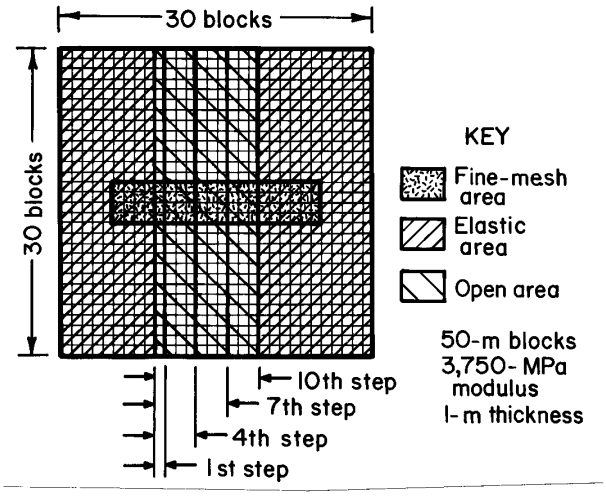


Figure 34.—MULSIM/NL grid for widening-crack problem.

## STEP-SIZE EFFECT TESTS

As discussed in a prior section, the total energy release is composed of a kinetic energy release component and a strain energy release component. Salamon (*6, 40*) showed theoretically that the relative proportion between these two components depends on the mining step size. When using smaller mining areas per step to achieve a given state (i.e., using more mining steps to reach a given excavation geometry), the relative proportion between kinetic and strain energy release changes, although the total energy release remains constant. In the limit, as the mined areas per step

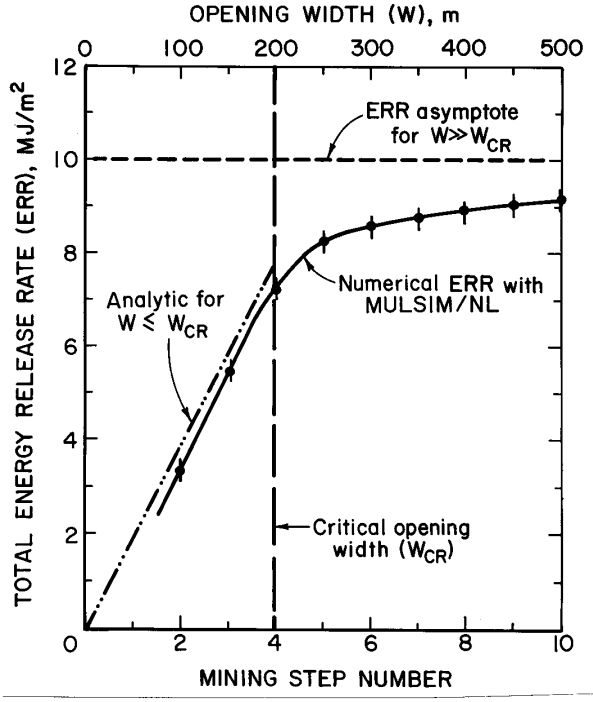


Figure 35.—Comparison of analytic and numerical energy release rates for widening-crack problem.

approaches zero (i.e., the number of mining steps used to create an excavation becomes a continuum), the kinetic energy release component becomes zero, while the strain energy release component approaches the total energy release.

The step-size effect tests seek to observe the theoretical energy release relationships with numerical experiments using MULSIM/NL. Figure 36 shows the four meshes used for the experiments. In each of these tests, an 800-m-wide opening is created with an increasing number of effective mining steps; since, in each case, the number of actual mining steps is always just two. The size of this second step decreases such that its size is the same size as the last step of an actual 4-, 8-, then 16-step model.

Figure 37 plots the kinetic and strain ERR normalized to the total energy release rate versus the number of steps used to excavate the opening. The figure shows analytic derivations by Salamon (*40*) for the excavation of a spherical cavity. When that cavity is created in a single step, half the total energy release rate comes from the kinetic component and the other half derives from the strain energy component. Increasing the number of steps used to create the spherical cavity causes the strain ERR to dominate the total ERR, while the kinetic ERR tends to zero. Again, the total ERR remains constant.

Figure 37 also shows the numerical calculations with MULSIM/NL for the excavation of an 800-m-wide tabular opening. In this example, the kinetic ERR dominates the total ERR. For practical purposes, the strain ERR is negligible. However, the same underlying trend still exists such that increasing the number of mining steps used to create an excavation causes the kinetic ERR component to decrease relative to the strain ERR component, while the total ERR remains constant.

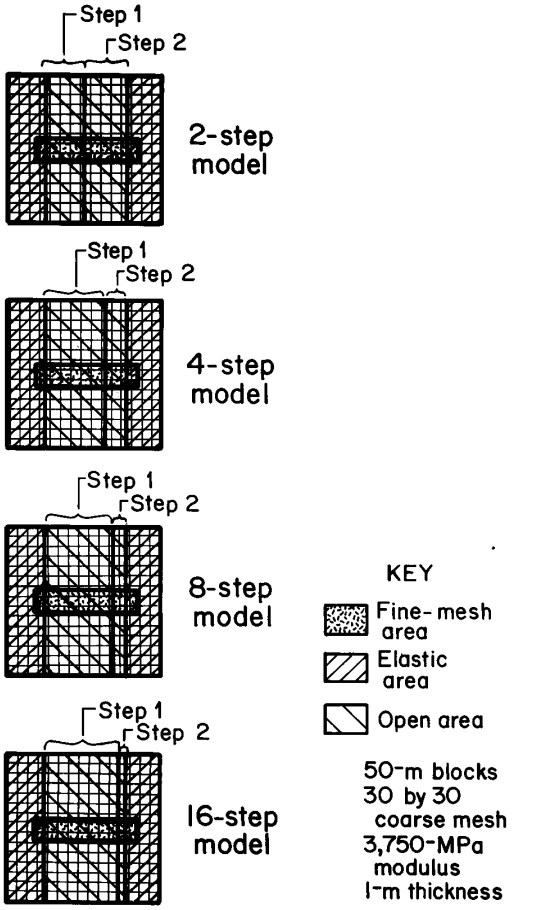


**Figure 36.—Four MULSIM/NL grids for step-size effect tests.**

## NONLINEAR EFFECTS ON ENERGY CALCULATIONS

The ERR derivations showed that total ERR is comprised of a strain ERR component and a kinetic ERR component, which, in turn, is composed of a linear and a nonlinear part. The following studies examine these three components to discern what factors affect their relative magnitude, hence, relative importance in the total ERR. These parametric studies examine, systematically, the following important factors using several different small MULSIM/NL models:

(1) The size of the open area relative to the total backfill area in the model.

(2) The amount of open area in the whole model which must either increase, decrease, or remain constant between mining steps.

(3) The average stiffness of the backfill material.

(4) The degree of nonlinearity of the backfill material.

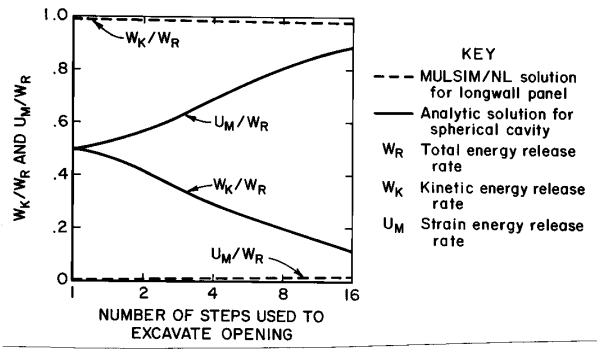


**Figure 37.—Normalized energy release rate components versus number of excavation steps for analytic case and numerical case.**

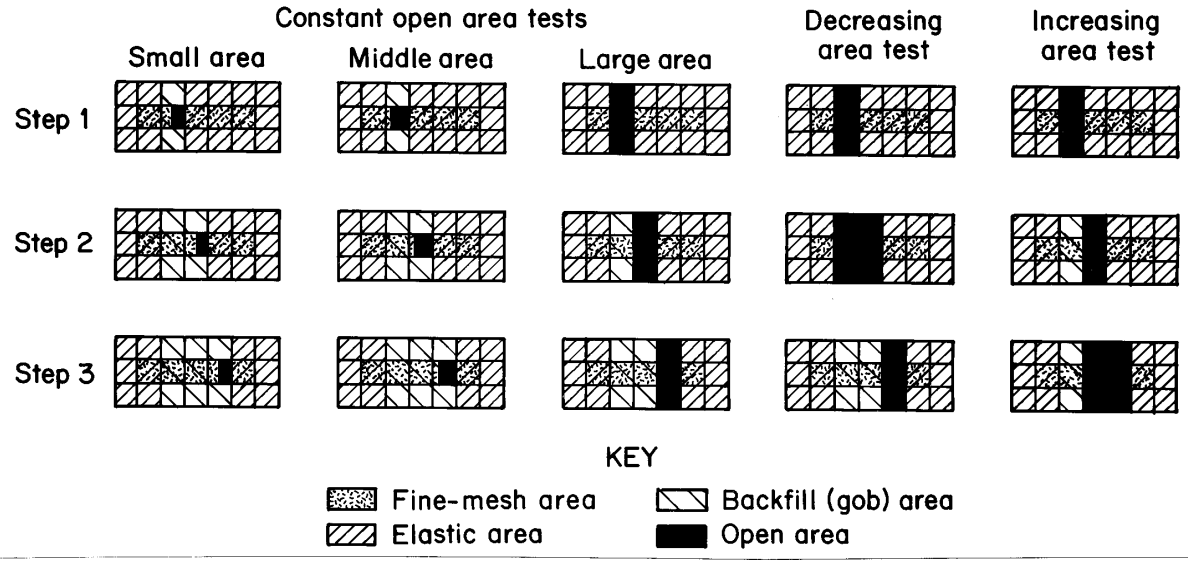


**Figure 38.—Five different three-step MULSIM/NL models used to study constant, decreasing, and increasing area effects on total energy release and its components.**

Figure 38 shows the five, three-step MULSIM/NL grids used for these studies. The first three meshes have a constant open area that moves in steps across the grid. These three meshes examine final ratios between open area and backfill (gob) area of 0.05 (small), 0.10 (middle) and 0.33 (large). The last three meshes vary the amount of open area between steps two and three. In the large, constant area test, of course, that open area amount remains constant. In one mesh, that area decreases, and in the other, it increases.

These models compare two basic materials for the backfill. The first is simple linear elastic, with a 70-MPa modulus. The second is strain hardening with a 7-MPa initial modulus and a 560-MPa final modulus at 7 MPa stress. Figure 39 shows the stress-strain curves for the linear and nonlinear backfill materials used in these models. The figure shows typical values only; however, during these studies, numerous other linear and nonlinear material parameters received consideration.

Figures 40 and 41 show the computed total ERR and its three components (linear kinetic, nonlinear kinetic, and strain energy release rate) for the five models shown in figure 38. The calculations in figure 40 use the linear backfill properties whereas those in figure 41 use the nonlinear strain-hardening model.

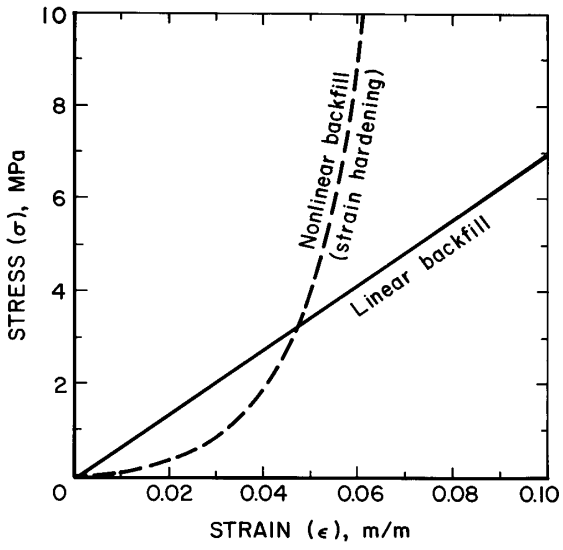


**Figure 39.—Linear and nonlinear stress-strain curves for backfill material used in model studies.**

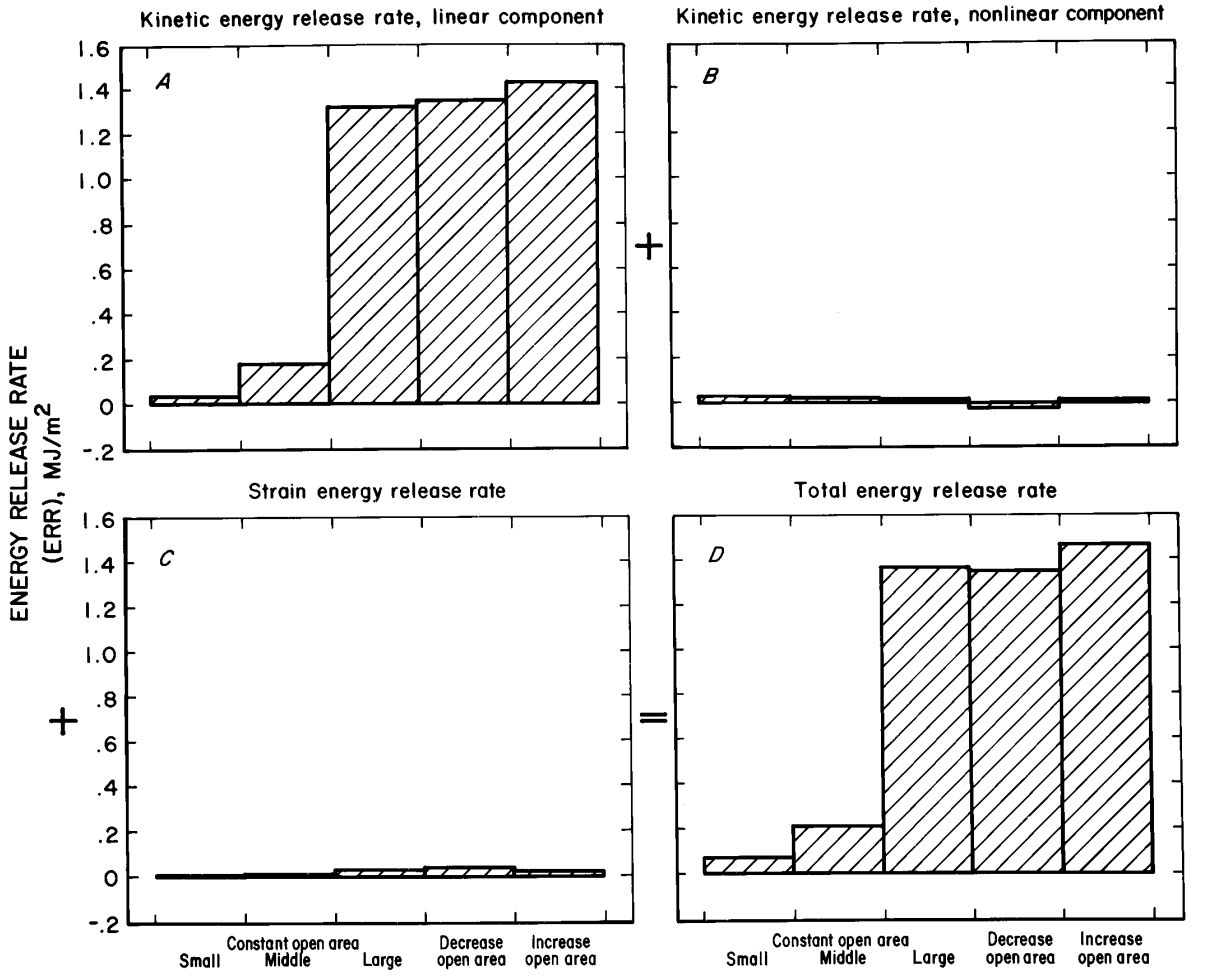


**Figure 40.—Total energy release from mining step 2 to 3 and its components for five different test models with linear backfill material. Note: graph *A* + graph *B* + graph *C* = graph *D*.**

The constant open area numerical experiments (i.e., the first three models in figure 38) suggest the following observations:

(1) The linear kinetic ERR and the strain ERR appear to vary approximately as the square of the open area to backfill area ratio for both the linear and nonlinear backfill models.

(2) The linear kinetic ERR dominates the strain ERR by an order of magnitude or more. However, neglecting the strain ERR is not recommended, since it can become significant with low open-area-to-backfill and/or gob-area ratios. Such low ratios are perhaps more typical of practical MULSIM/NL modeling.

(3) The nonlinear kinetic ERR may vary inversely as the area ratio. Large backfill or gob areas may contribute a nonlinear kinetic ERR component that actually exceeds the linear kinetic ERR. Again, small open-area-to-backfill-area ratios (i.e., large backfill and/or gob areas relative to the open area) probably characterize practical mining situations better than the large area ratios. Thus, until further studies dictate otherwise, the nonlinear kinetic

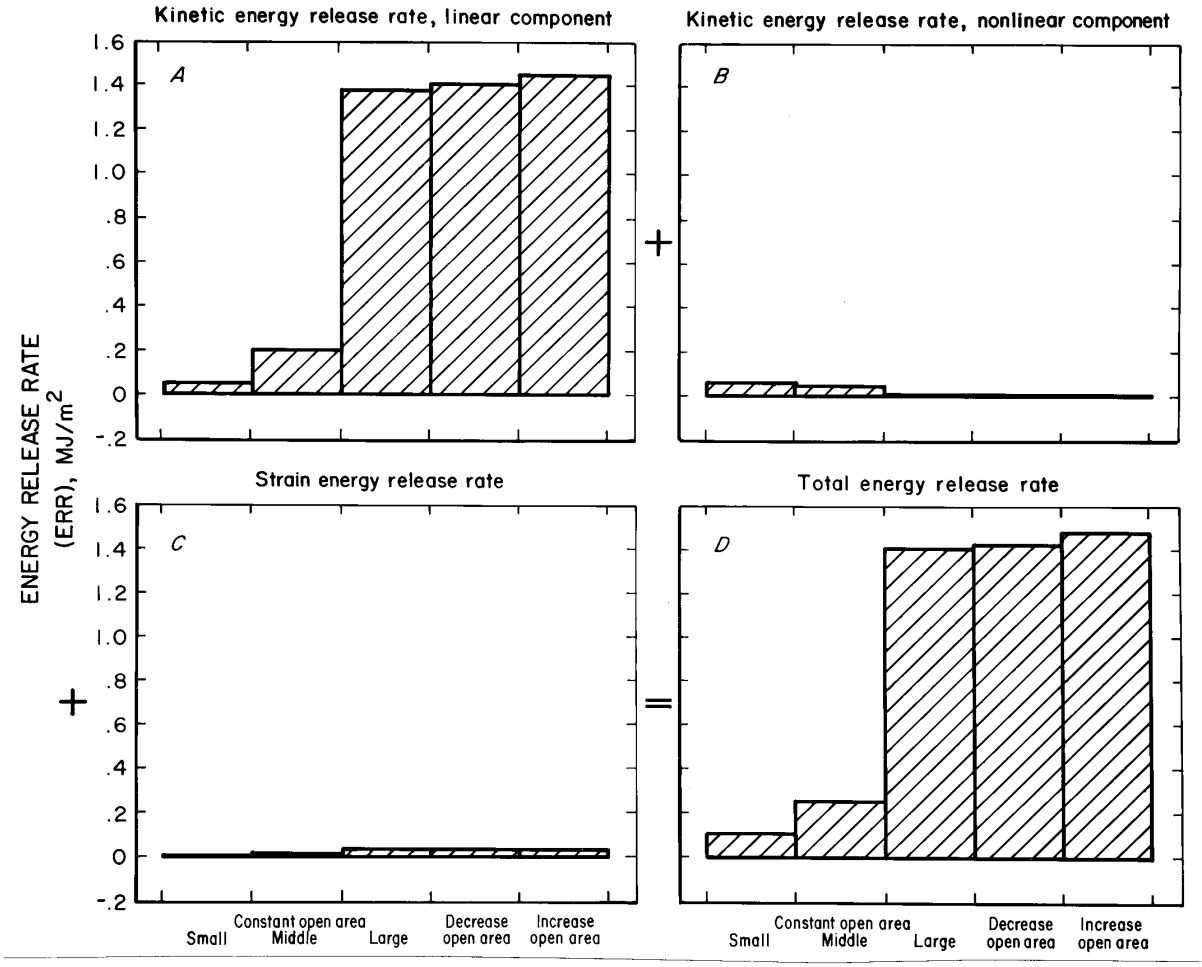


**Figure 41.—Total energy release from mining step 2 to 3 and its components for five different test models with nonlinear backfill material. Note: graph *A* + graph *B* + graph *C* = graph *D*.**

ERR and the strain ERR should be retained in total ERR calculations.

(4) Alternatively, there is a possibility that the above trends which are credited to the open-area-to-backfill-area ratio may be due to a larger overall backfill area. This possibility requires further study.

(5) Additional MULSIM/NL tests not supported by tables and figures suggested that increasing the modulus of the backfill (final modulus for the nonlinear tests with the strain-hardening backfill model), causes the linear kinetic ERR and the total ERR to decrease. The relative magnitude of the ERR decrease depends on the open-area-to-backfill-area ratio. The small ratio models had larger relative decreases in ERR. In these example problems, varying the modulus in the linear backfill from 50 to 150 MPa caused a 25% decrease in ERR for the small area ratio model and a 10% decrease from the large area ratio model. Varying the final modulus in the nonlinear strain-hardening backfill from 140 to 560 MPa caused 15% and 10% ERR decreases for the small and large area ratios. Present measurements of the stress-strain behavior of gob limit the reliability of gob modulus estimates to an order of magnitude only. Such poor reliability in gob modulus estimates adversely impacts ERR estimates. Thus, research studies on the stress-strain behavior of gob material may substantially improve the quality of ERR calculations.

(6) Changing the modulus of the backfill and/or gob, whether linear or nonlinear, had no perceptible effect on the strain ERR values. In all cases considered, the strain ERR component of the total ERR remained negligible.

The changing open area tests (i.e., the last three models in figure 38) led to many observations similar to those of the constant area tests. However, the strain ERR and the nonlinear kinetic ERR are negligible in the total ERR due to the large open area to backfill and/or gob area ratio in these models. Increasing the modulus of the backfill (gob) always tends to decrease the total ERR and its dominant component, the linear kinetic ERR. Also, changes in backfill modulus or its degree of nonlinearity has an almost negligible effect on the calculated strain ERR.

In addition to the prior observations, the changing area tests suggest that decreasing the open area between mining steps (causing the backfilling or gob formation activities to accelerate) has little effect on the total ERR. Conversely, increasing the open area between steps (allowing the backfilling or gob formation activities to lag) causes the total ERR to increase. In this example, that increase is on the order of 10%. Such an increase may suggest greater burst and/or bump potential.

## SUMMARY AND RECOMMENDATIONS

### SUMMARY

MULSIM/NL is a new Bureau boundary-element-method program for stress analysis of coal mines and thin metalliferous veins. This Information Circular provides certain theoretical documentation on that program. Accordingly, its intended audience is those engineers and programmers who need to understand the FORTRAN program fully, or who need to alter and enhance it.

MULSIM/NL is a three-dimensional boundary-element-method (BEM) program capable of performing stress analyses of planar structures in coal seams or thin veins. It can analyze one to four parallel seams that can have any orientation with respect to the Earth's surface. Topographic or free surface effects are neglected; therefore, the seam depth should exceed the modeling block width by a factor of 3 or more. MULSIM/NL utilizes a coarse-mesh grid of blocks to approximate the larger model bounds and a fine-mesh grid of elements embedded within the coarse mesh to provide greater numerical detail within a region of interest. The allowable coarse-mesh block array size is 40 by 40. Up to a 20 by 20 array of these blocks may be subdivided into a 100 by 100 array of fine-mesh elements.

Three main new features distinguish MULSIM/NL from its predecessors MULSIM (*2*) and MULSIM/BM (*3*), namely: (1) nonlinear material models, (2) multiple mining steps, and (3) comprehensive energy release and strain energy computations. MULSIM/NL now has six material models for the in-seam material from which to choose: (1) linear elastic for coal, (2) strain softening, (3) elastic plastic, (4) bilinear hardening, (5) strain hardening, and (6) linear elastic for gob. The first three models are intended for the in-place coal or vein material prior to mining, whereas the latter three models are intended for the gob or backfill material left in the wake of full extraction mining. The strain-hardening model for gob and/or backfill material derived and implemented as part of this research may be a unique addition to the variety of material models available in mining-oriented BEM programs.

Unlike its predecessors, MULSIM/NL uses a total stress approach when solving the basic BEM system of equations. Such radical changes in the equation-solving procedure, plus the addition of the six nonlinear material models, necessitated detailed checks on the MULSIM/NL stress and displacement calculations. Numerical stress and displacement calculations compare reasonably well to known analytic solutions for simple problems. MULSIM/NL models exhibit rigid boundary and element size effects. Until studies with a particular model dictate otherwise, having at least 10 coarse-mesh blocks beyond the fine-mesh boundary will usually keep the rigid boundary outside the model far enough away and lead to good quality calculations in the fine mesh. Smaller element sizes tend to improve the accuracy of stress and displacement calculations; however, they can also lead to deleterious rigid boundary effects because of the smaller model size. Exact checks on the nonlinear material models are not feasible; however, stresses and displacements calculated with these models behave qualitatively as expected.

The second distinguishing feature of MULSIM/NL is the multiple mining step capability which enables simulation of the various stages of mine development. This feature allows the user to calculate stress and displacement changes as the mine development advances. These changes are much more directly comparable with field measurement programs that typically measure stress and

displacement (convergence) changes as opposed to total or absolute stresses and displacements.

The energy calculations constitute the last unique feature of MULSIM/NL. Salamon (*6*) provides the theoretical basis for the comprehensive energy release rate (ERR) computations performed by MULSIM/NL. The total energy release is comprised of three basic terms: (1) a strain energy release from the mined-out material, (2) a linear kinetic energy release due to the change in gravitational potential over the mined-out area, and (3) a nonlinear kinetic energy release due to nonlinear materials in the total backfill and/or gob area. All terms are included in the implementation; however, the strain energy release term is modified slightly to account for nonlinear stress-strain behavior in the unmined materials. MULSIM/NL also computes various useful strain energy quantities for each unmined element throughout the BEM model.

Comparisons of numerical ERR calculations from MULSIM/NL with known analytic solutions show excellent agreement. The ratio between open-area-to-backfill or gob area influences the relative magnitude and importance of the three energy release components. With large open-area-to-gob-area ratios, the kinetic energy release component (change in gravitational potential) dominates the total energy release. With the small ratios that are more typical of most practical BEM models of mines, then all three components of the energy release (strain, linear kinetic, and nonlinear kinetic) have importance.

These extensive enhancements necessitated complete restructuring and reprogramming to create MULSIM/NL. Earlier versions of MULSIM used complicated indexing and one-dimensional arrays throughout the program. The new MULSIM/NL takes advantage of today's larger memory computers and uses numerous multidimensional arrays and vectors that better reflect the underlying mathematical foundations of MULSIM/NL. The reprogramming resulted in a much more understandable, reliable, and modifiable program that should serve users well in the foreseeable future.

Development of MULSIM/NL stems from a need to alleviate safety hazards in certain U.S. coal mines plagued with coal mine bumps. With its six nonlinear in-seam material models, multiple mining step capabilities, and comprehensive energy release and strain energy calculations, MULSIM/NL provides a means to calculate stress, displacement, and energy changes for various mining configurations in bump-prone or rock burst conditions. In addition, MULSIM/NL has many practical uses beyond coal mine bump research. Stresses and displacements calculated by MULSIM/NL can help an engineer design pillar sizes and understand multiple-seam mining interactions. This program is one tool out of many that engineers can use in the fight to alleviate coal mine bumps and rock bursts. Through judicious use of numerical models such as MULSIM/NL, engineers can choose mining methods that decrease the risk of these violent failures.

## RECOMMENDATIONS

Many avenues exist to improve MULSIM/NL. The three possibilities suggested here may be especially useful in the near term.

First, MULSIM/NL could benefit from further restructuring and reprogramming to take advantage of modern vectorizing compilers and future parallel computers. One way to render MULSIM/NL highly vectorizable is to eliminate use of the coarse mesh.

The second suggestion is to calculate a condition number for the system of equations solved by MULSIM/NL. Operating experience with MULSIM/NL shows that certain models lead to an ill-conditioned system of equations with slow solution convergence and an unreliable final solution. It is very easy to create such misbehaved models. A condition number for the system of equations provides a simple, quantitative measure of the solution reliability.

The third suggestion is to include topographic influence in the boundary-element calculations. One approach to these calculations would define an upper displacement discontinuity at the topographic surface. Each element of this surface would require elevation data. The solution procedure would then require calculation of semi-infinite body influence coefficients between the topographic surface and the main seam plane. Unfortunately, the computed topographic influence coefficients would require a lot of memory, and the computational effort may prove very costly.

Another, less rigorous, approach would define in situ stresses at all elements in the seam plane. The existing boundary-element calculations can include these element-specific, in situ stresses very easily. The problem then becomes one of estimating the seam plane in situ stresses that include the topographic influence. Horizontal seam planes only require an estimate of the vertical stress component, which considerably simplifies the problem.

## REFERENCES


1. Campoli, A. A., C. A. Kertis, and C. A. Goode. Coal Mine Bumps: Five Case Studies in the Eastern United States. BuMines IC 9149, 1987, 34 pp.

2. Sinha, K. P. Displacement Discontinuity Technique for Analyzing Stresses and Displacements Due to Mining in Seam Deposits. Ph.D. Thesis, Univ. MN, Ann Arbor, MI, 1979, 311 pp.

3. Beckett, L. A., and R. S. Madrid. MULSIM/BM - A Structural Analysis Computer Program for Mine Design. BuMines IC 9168, 1988, 302 pp.

4. Cook, N. G. W., E. Hoek, J. P. G. Pretorius, W. D. Ortlepp, and M. D. G. Salamon. Rock Mechanics Applied to the Study of Rock Bursts. J. S. Afr. Inst. Min. Metall., v. 66, No. 10, 1966, pp. 435-528.

5. Walsh, J. B. Energy Changes Due to Mining. Int. J. Rock Mech. Min. Sci., v. 14, 1977, pp. 25-33.

6. Salamon, M. D. G. Energy Considerations in Rock Mechanics: Fundamental Results. J. S. Afr. Inst. Min. Metall., v. 84, No. 8, 1984, pp. 233-246.

7. Brady, B. H. G., and E. T. Brown. Rock Mechanics for Underground Mining. George Allen and Unwin (London), 1985, 527 pp.

8. Hodgson, K., and N. C. Joughin. The Relationship Between Energy Release Rate, Damage, and Seismicity in Deep Mines. Paper in Proceedings of 8th Symposium on Rock Mechanics, Univ. MN, ed. by C. Fairhurst. AIME, 1967, pp. 194-203.

9. Cook, N. G. W. Rockburst and Rockfalls. Chamber of Mines of S. Afr., Johannesburg, SA, Publ. No. 216, 1978.

10. Crouch, S. L., and A. M. Starfield. Boundary Element Methods in Solid Mechanics. George Allen and Unwin (London), 1983, 322 pp.

11. Banerjee, P. K., and R. Butterfield. Boundary Element Methods in Engineering Science. McGraw-Hill (New York), 1982, 452 pp.

12. Brebbia, C. A., and S. Walker. Boundary Element Techniques in Engineering. Newnes-Butterworth (London), 1980, 323 pp.

13. Brebbia, C. A., and J. J. Connor. BEM-11. Proceedings of 11th International Conference on Boundary Element Methods in Engineering, Springer-Verlag (Berlin FRG), 3 volumes, 1989, 1,217 pp.

14. Wardle, L. J. Boundary Element Methods for Stress Analysis of Tabular Excavations. Ph.D. Thesis, Univ. Queensland, Australia, 1986, 141 pp.

15. Lachat, J. C., and J. O. Watson. Effective Numerical Treatment of Boundary Integral Equations: A Formulation for Three-Dimensional Elastostatics. Int. J. Numer. Meth. Eng., v. 10, 1976, pp. 991-1005.

16. Vogel, S. M., and F. J. Rizzo. An Integral Equation Formulation of Three-Dimensional Anisotropic Boundary Value Problems. J. Elast., v. 3, 1973, pp. 203-216.

17. Telles, J. C. F. The Boundary Element Method Applied to Inelastic Problems. Lecture Notes in Engineering, v. 1, Springer-Verlag (Berlin), 1983, 243 pp.

18. Zienkiewicz, O. C. Finite Element Methods in Engineering Science. 3rd ed., McGraw-Hill (London), 1977, 787 pp.

19. Brady, B. H. G., and A. Wassyng. A Coupled Finite Element-Boundary Element Method of Analysis. Int. J. Rock Mech. Min. Sci. and Geomech. Abstr., v. 18, 1981, 475-485 pp.

20. Berry, D. S. An Elastic Treatment of Ground Movement Due to Mining - Part I. Isotropic Ground. J. Mech. Phys. Solids, v. 8, 1960, pp. 280-292.

21. Berry, D. S., and T. W. Sales. An Elastic Treatment of Ground Movement Due to Mining - Part II. Transversely Isotropic Ground. J. Mech. Phys. Solids, v. 9, 1961, pp. 52-62.

22. Berry, D. S., and T. W. Sales. An Elastic Treatment of Ground Movement Due to Mining - Part III. Three-Dimensional Problem, Transversely Isotropic Ground. J. Mech. Phys. Solids, v. 10, 1962, pp. 73-83.

23. Salamon, M. D. G. Elastic Analysis of Displacements and Stresses Induced by the Mining of Seam or Reef Deposits. J. S. Afr. Inst. Min. Metall., v. 64, Nov. 1963, pp. 128-149.

24. ____. Elastic Analysis of Displacements and Stresses Induced by the Mining of Seam or Reef Deposits - Part II. Practical Methods of Determining Displacement, Strain and Stress Components from a Given Mining Geometry. J. S. Afr. Inst. Min. Metall., v. 64, Jan. 1964, pp. 197-218.

25. ____. Elastic Analysis of Displacements and Stresses Induced by the Mining of Seam or Reef Deposits - Part IV. Inclined Reef. J. S. Afr. Inst. Min. Metall., v. 65, Dec. 1964, pp. 319-338.

26. Plewman, R. P., F. H. Deist, and W. D. Ortlepp. The Development and Application of a Digital Computer Method for the Solution of Strata Control Problems. J. S. Afr. Inst. Min. Metall., v. 70, Sept. 1969, pp. 33-44.

27. Starfield, A. M., and S. L. Crouch. Elastic Analysis of Single Seam Extraction. Paper in Proceedings of 14th U.S. Symposium on Rock Mechanics, Penn. State Univ. ASCE (New York), 1973, pp. 421-439.

28. Crouch, S. L., and C. Fairhurst. The Mechanics of Coal Mine Bumps and the Interaction Between Coal Pillars, Mine Roof, and Floor (contract H0101778, Univ. MN). BuMines OFR 53-73, 1973, 88 pp.; NTIS PB 222 898.

29. Crouch, S. L. Two-Dimensional Analysis of a Near Surface, Single-Seam Extraction. Int. J. Rock Mech. Min. Sci. and Geomech. Abstr., v. 10, 1973, pp. 85-96.

30. ____. Analysis of Stresses and Displacements Around Underground Excavations: An Application of the Displacement Discontinuity Method. Univ. MN Geomech. Rep. Dept. of Civ. Miner. Eng., Univ. MN, Minneapolis, MN, 1976, 268 pp.

31. Kripakov, N. P., L. A. Beckett, D. A. Donato, and J. S. Durr. Computer-Assisted Mine Design Procedures for Longwall Mining. BuMines RI 9172, 1988, 38 pp.

32. Kripakov, N. P., and L. E. Rockwell. Application of Numerical Modeling Techniques for Gate Road Design in Bump Prone Mines. Paper in Proceedings of Longwall USA, Pittsburgh, PA, Industrial Presentations, Inc., Aurora, CO, 1989, pp. 87-99.

33. Dahlquist, G., and A. Bjork. Numerical Methods. Prentice-Hall, 1974, 571 pp.

34. Wang, F. D., W. A. Skelly, and J. Wolgamott. In Situ Coal Pillar Strength Study (contract H0242022, CO Sch. Mines). BuMines OFR 107-79, 1976, 243 pp.

35. Iannacchione, A. Behavior of a Coal Pillar Prone to Burst in the Southern Appalachian Basin of the United States. Paper in Proceedings of Second International Symposium of Rockbursts and Seismicity in Mines. Univ. MN, June 1988, pp. 427-439.

36. Heasley, K. A., and K. Barron. A Case Study of Gate Pillar Response to Longwall Mining in Bump-Prone Strata. Paper in Proceedings of Longwall USA, Pittsburgh, PA, 1988, Industrial Presentation, Inc., Aurora, CO, 1988, pp. 91-105.

37. Cook, N. G. W. The Basic Mechanics of Rockbursts. J. S. Afr. Inst. Min. Metall., v. 64, Oct. 1963, pp. 71-81.

38. ____. The Design of Underground Excavations. Paper in Proceedings of 8th Symposium on Rock Mechanics, Univ. MN, ed. by C. Fairhurst. AIME, 1967, pp. 167-193.

39. Brady, B. H. G., and E. T. Brown. Energy Changes and Stability in Underground Mining: Design Applications of Boundary Element Methods. Trans. Inst. Min. and Metall (London), Section A, v. 90, Apr. 1981, pp. A61-A68.

40. Salamon, M. D. G. Rockburst Hazard and the Fight for Its Alleviation in South African Gold Mines. Paper in Rockbursts: Prediction and Control. Inst. Min. and Metall. (London), 1983, pp. 11-36.

41. Jaeger, J. C., and N. G. W. Cook. Fundamentals of Rock Mechanics. Chapman and Hall (London), 1979, 593 pp.

42. Dahl, H. D., and H. S. Von Schonfeldt. Rock Mechanics Elements of Coal Mine Design. Paper in Proceedings 17th U.S. Symposium on Rock Mechanics, Univ. UT, Salt Lake City, UT, 1976, pp. 4A1-1 - 4A1-9.

43. Owili-Eger, A. S. C. Dynamic Fractured Flow Simulation Model. Min. Eng., AIME, 1989, pp. 110-114.

44. Singh, M. M., and F. S. Kendorski. Strata Disturbance Prediction for Mining Beneath Surface Water and Waste Impoundments. Paper in Proceedings 1st Conference on Ground Control in Mining, WV Univ., Morgantown, WV, 1981, pp. 76-89.

## APPENDIX A.—REDERIVATION OF SALAMON'S ENERGY RELEASE EQUATION

This appendix gives an abbreviated rederivation of Salamon's (*6*)[1] energy release equation presented as equation 41 in the text. The rederivation here uses a notation similar to Salamon's that is improved and, hopefully, easier to follow. The analysis begins with equation 39, which is the energy release relationship derived from basic energy conservation considerations.

$$W_R = U_M + (W\text{-}U_C\text{-}W_{SP}), \qquad \text{(A-1)}$$

where $W_R$ = total energy release for this step,

$U_M$ = strain energy release from the mined-out rock,

$W$ = work done on the system by boundary and body forces,

$U_C$ = change in strain energy in the rock mass,

and $W_{SP}$ = change in strain energy in the backfill (gob) and support systems.

The term in parentheses is called the kinetic energy release $W_K$.

Figure A-1 (same as figure 17) illustrates the basic problem and notation considered in this derivation. Mining proceeds in a small step from state I to state II during which a volume of rock $V_M$ with surface area $S_M$ is extracted. The open area and volume change from $S_{OI}$ and $V_{OI}$ to $S_{OII}$ and $V_{OII}$. The backfill (gob) area and volume change from $S_{GI}$ and $V_{GI}$ to $S_{GII}$ and $V_{GII}$. The volume of the rock mass and its outer boundary area remain unchanged at V and S, respectively. A summary of basic volume and surface area definitions follows.

$V$ = rock mass volume

$V_{OI}$ = volume open in state I

$V_{OII}$ = volume open in state II

$V_{GI}$ = volume gob in state I

$V_{GII}$ = volume gob in state II

$V_M$ = volume mined this step

$\Delta V_O = V_{OII} - V_{OI}$

$\Delta V_G = V_{GII} - V_{GI}$

$S$ = rock mass boundary

$S_{OI}$ = surface open in state I

$S_{OII}$ = surface open in state II

$S_{GI}$ = surface backfilled in state I

$S_{GII}$ = surface backfilled in state II

$S_M$ = surface mined this step

$\Delta S_O = S_{OII} - S_{OI}$

$\Delta S_G = S_{GII} - S_{GI}$.

In this notation, subscripts have the following meanings:

I - state I

II - state II

G - gob (backfill) area or volume

O - open area or volume

M - mined-out area or volume this step

none - rock mass area or volume.

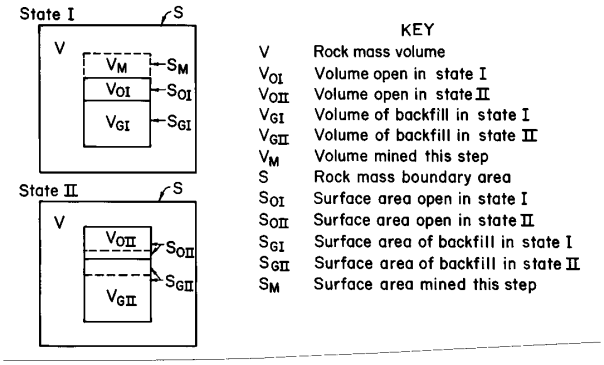


**Figure A-1.—Basic problem geometry for energy release derivations.**

[1]Italic numbers in parentheses refer to items in the list of references preceding the appendixes.

The following notations are used for displacements, stresses, surface tractions, and body forces:

$u$ = displacement

$\tau$ = stress

$T$ = surface traction over rock mass areas

$R$ = surface traction over backfilled areas

$X$ = body forces.

In going from state I to state II, these displacements, stresses, surface tractions and body forces must obey the following relations:

$$\begin{aligned} u_{II} &= u_I + \Delta u \\ \tau_{II} &= \tau_I + \Delta\tau \\ T_{II} &= T_I + \Delta T \\ R_{II} &= R_I + \Delta R \\ X_{II} &= X_I. \end{aligned} \tag{A-2}$$

Equilibrium of the rock mass in state I satisfies

$$\int_V X_I dv + \int_S T_I ds + \int_{S_M} T_I ds + \int_{S_{GI}} R_I ds = 0, \tag{A-3}$$

whereas in state II it satisfies

$$\int_V X_{II} dv + \int_S T_{II} ds + \int_{S_{GII}} R_{II} ds = 0. \tag{A-4}$$

The work W done on the system in going from state I to state II is found by considering the tractions on the bounding surface S and the body forces within the rock mass V and backfill (gob) $V_G$ as displacements undergo a change $\Delta u$. The work done on the system is

$$\begin{aligned} W = &- \int_S T_I \Delta u ds - \frac{1}{2}\int_S \Delta T \Delta u ds \\ &- \int_V X_I \Delta u dv - \int_{V_{GI}} X_G \Delta u dv \\ &- \frac{1}{2}\int_{\Delta V_G} X_G \Delta u dv. \end{aligned} \tag{A-5}$$

The negative signs arise from the sign convention discussed by Salamon (*6*).

As indicated in equation A-1, the work done on the system depicted in figure A-1 results in strain energy changes in the three components of that system: the rock mass mined-out during this step, the surrounding rock mass, and the backfill and/or gob. The strain energy changes in each of these areas are considered next.

In going from state I to state II, the strain energy change (or release) over the mined-out volume $V_M$ bounded by surface $S_M$ is found directly as

$$U_M = \frac{1}{2}\left[\int_{S_M} T_I u_I ds - \int_{V_M} X_I u_I dv\right]. \tag{A-6}$$

In state I, the <u>total</u> strain energy in the rock mass volume V bounded by surfaces S, $S_M$, and $S_{GI}$ is

$$\begin{aligned} U_{VI} = -\frac{1}{2}\Bigg[&\int_V X_I u_I dv + \int_S T_I u_I ds \\ &+ \int_{S_M} T_I u_I ds + \int_{S_{GI}} R_I u_I ds\Bigg]. \end{aligned} \tag{A-7}$$

Again, the negative sign arises due to the sign convention used. The strain energy in state I is one-half the product of the equilibrium forces in state I (equation A-3) multiplied by the displacements in state I $u_I$.

In state II, the total strain energy in the rock mass volume V bounded by surfaces S and $S_{GII}$ is

$$\begin{aligned} U_{VII} = -\frac{1}{2}\Bigg[&\int_V X_{II} u_{II} dv \\ &+ \int_S T_{II} u_{II} ds + \int_{S_{GII}} R_{II} u_{II} ds\Bigg]. \end{aligned} \tag{A-8}$$

Substituting equations A-2 into A-8, expanding the result, and subtracting A-7 results in the following expression for the change in strain energy in the rock mass volume V:

$$\begin{aligned} U_C = &-\frac{1}{2}\left[\int_S \Delta T u_I ds + \int_S T_I \Delta u ds + \int_S \Delta T \Delta u ds\right] \\ &-\frac{1}{2}\left[\int_{S_{GI}} \Delta R u_I ds + \int_{S_{GI}} R_I \Delta u ds + \int_{S_{GI}} \Delta R \Delta u ds\right] \\ &-\frac{1}{2}\left[\int_{\Delta S_G} \Delta R u_I ds + \int_{\Delta S_G} R_I \Delta u ds + \int_{\Delta S_G} \Delta R \Delta u ds\right] \\ &-\frac{1}{2}\int_V X_I \Delta u dv + \frac{1}{2}\int_{S_M} T_I u_I ds. \end{aligned} \tag{A-9}$$

The backfill and/or gob material may exhibit certain nonlinear stress-displacement behavior. Accordingly, the parameter $\alpha$ is introduced to account for this nonlinearity in the strain energy calculations. Figure A-2 (same as figure 19) illustrates the meaning of this parameter with linear elastic and strain-hardening materials. Most typically, backfill and/or gob materials exhibit a strain-hardening or linear elastic behavior; therefore, $\alpha$ has values in the ½ to 1 range.

Figure A-3 shows a typical stress-displacement relationship expected for backfill and/or gob. Based on this figure, the total strain energy in state I of the backfill and/or gob volume $V_{GI}$ bounded by surface $S_{GI}$ is

$$U_{GI} = \frac{1}{2}\left[\int_{S_{GI}} \alpha R_I u_I ds - \int_{V_{GI}} X_{GI} u_I dv\right]. \quad \text{(A-10)}$$

In state II, the total strain energy in the backfill and/or gob volume $V_{GII}$ bounded by surface $S_{GII}$ is

$$U_{GII} = \frac{1}{2}\left[\int_{S_{GII}} \alpha R_{II} u_{II} ds - \int_{V_{GII}} X_{GII} u_{II} dv\right]. \quad \text{(A-11)}$$

Substituting equations A-2 into A-11, expanding the result, and subtracting A-10 results in the following expression for the change in strain energy in the gob volume $V_{GII}$:

$$W_S = \int_{S_{GI}} \alpha R_I \Delta u ds - \int_{V_{GI}} X_{GI} \Delta u dv$$

$$+ \frac{1}{2}\int_{S_{GII}} \alpha \Delta R \Delta u ds - \frac{1}{2}\int_{\Delta V_G} X_{GI} \Delta u dv. \quad \text{(A-12)}$$

Equations A-5, A-6, A-9, and A-12 provide expressions for W, $U_M$, $U_C$, and $W_S$, respectively, necessary to evaluate the change in energy release given by equation A-1. However, to simplify the expression that results after substituting A-5, A-6, A-9, and A-12 into A-1 requires another relationship derived from the reciprocity theorem. This important theorem from elasticity theory states that the energy associated with the first equilibrium force system acting through the displacements of the second system is equal to the energy associated with the second equilibrium force system acting through the displacements of the first system. Stated mathematically, the reciprocity theorem is

$$F_I u_{II} = F_{II} u_I, \quad \text{(A-13)}$$

or alternatively,

$$F_I \Delta u = \Delta F u_I. \quad \text{(A-14)}$$

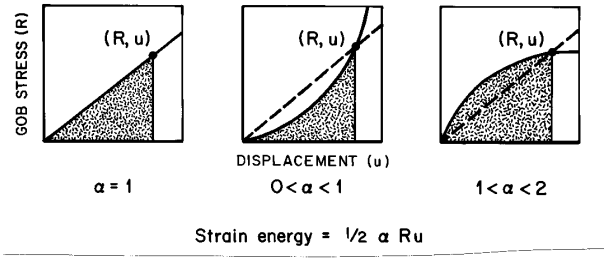


**Figure A-2.—Strain energy calculations for various linear and nonlinear material behaviors showing how parameter α accounts for degree of nonlinearity.**

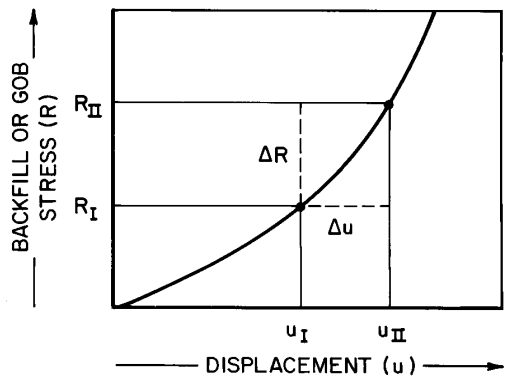


**Figure A-3.—Typical strain-hardening stress-displacement behavior for backfill or gob with basic notation.**

With the equilibrium force system given by equation A-3, the reciprocity theorem gives

$$\int_V X_I \Delta u dv + \int_S T_I \Delta u ds$$

$$+ \int_{S_M} T_I \Delta u ds + \int_{S_{GI}} R_I \Delta u ds$$

$$= \int_V \Delta X u_I dv + \int_S \Delta T u_I ds$$

$$+ \int_{S_M} \Delta T u_I ds + \int_{S_{GI}} \Delta R u_I ds. \quad \text{(A-15)}$$

This expression can be changed to

$$\frac{1}{2}\int_{S_M} T_I \Delta u\, ds = -\frac{1}{2}\int_S T_I \Delta u\, ds + \frac{1}{2}\int_S \Delta T u_I\, ds + \frac{1}{2}\int_{S_{GII}} \Delta R u_I\, ds - \frac{1}{2}\int_{S_{GI}} R_I \Delta u\, ds + \frac{1}{2}\int_{S_M} T_I u_I\, ds - \frac{1}{2}\int_V X_I \Delta u\, dv. \quad \text{(A-16)}$$

Finally, substituting A-5, A-6, A-9, and A-12 into A-1 and simplifying with A-16 results in the following expression for the total energy release:

$$W_R = \left[\frac{1}{2}\int_{S_M} T_I u_I ds - \frac{1}{2}\int_{V_M} X_I u_I dv\right] + \left[\frac{1}{2}\int_{S_M} T_I \Delta u\, ds + \frac{1}{2}\int_{S_{GII}} (1-\alpha)\Delta R \Delta u\, ds\right]. \quad \text{(A-17)}$$

The first term in brackets is called the strain energy release from the mined material ($U_M$), and the second term is called the kinetic energy release ($W_K$). In most practical circumstances, the body force term $X_I$ in the strain energy release is negligible compared with the surface traction term $T_I$. The energy subroutine in MULSIM/NL does neglect this body force term. In further notation, the first term of the kinetic energy release is referred to as the linear part of $W_K$ and basically represents a change in gravitational potential. The second term in $W_K$, referred to as the nonlinear part of $W_K$, arises from the nonlinear stress-displacement behavior of the backfill and/or gob material. In certain practical circumstances, it, too, is negligible compared with the linear part of $W_K$ (i.e., the change in gravitational potential). The energy subroutine in MULSIM/NL does retain this nonlinear term. In addition, the relative value of the first and third terms (i.e., the strain energy release $U_M$ and the kinetic energy release $W_K$) is step-size dependent. In many practical cases, the linear kinetic energy release may dominate the strain energy release from the mined material. Again, that is not always the case, hence MULSIM/NL retains the strain energy release term for completeness.

## APPENDIX B.—SUPPLEMENTAL DATA ON RIGID BOUNDARY EFFECT TESTS

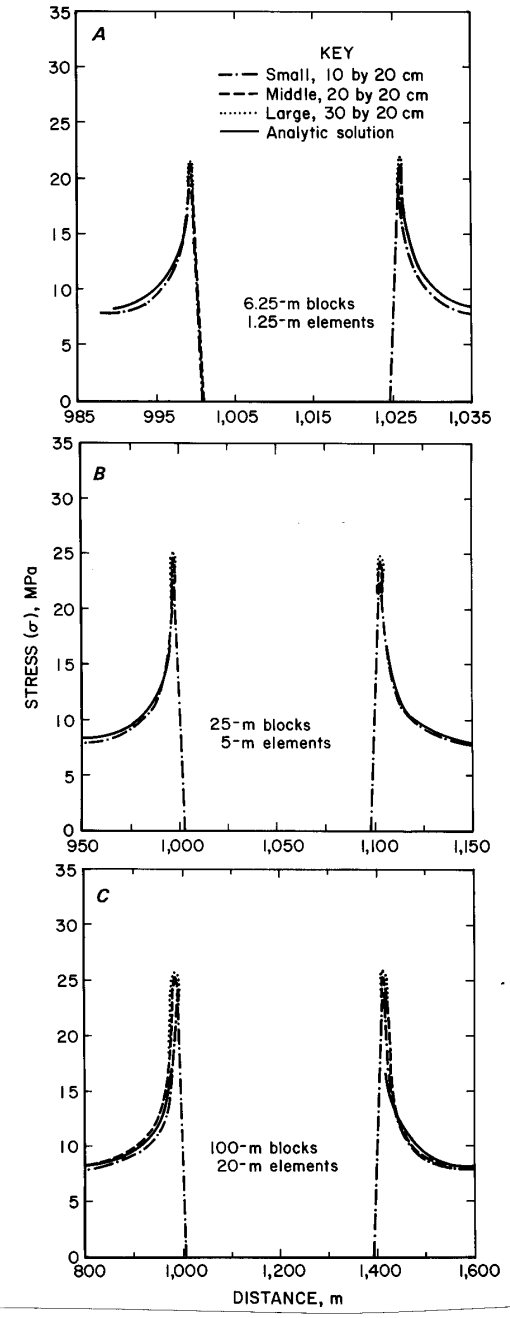


**Figure B-1.—Computed and analytic stresses at edge of opening with different coarse-mesh sizes. *A*, 25 m; *B*, 100 m; *C*, 400 m.**

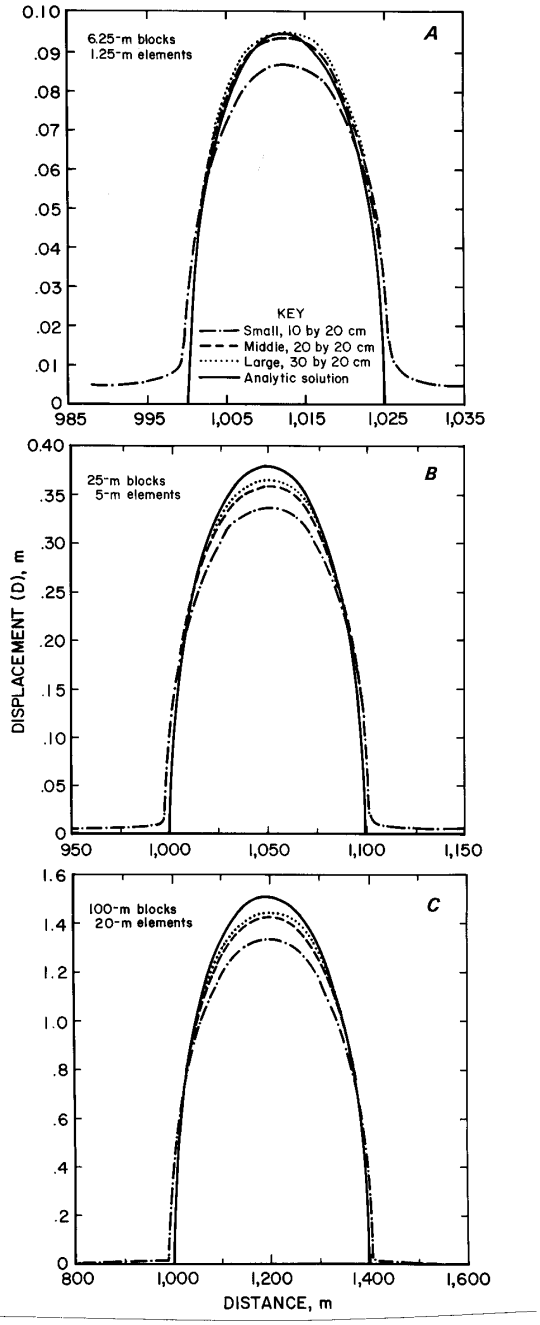


**Figure B-2.—Computed and analytic displacements across opening with different coarse-mesh sizes. *A*, 25 m; *B*, 100 m; *C*, 400 m.**

# APPENDIX C.—SUPPLEMENTAL DATA ON ELEMENT SIZE EFFECT TESTS

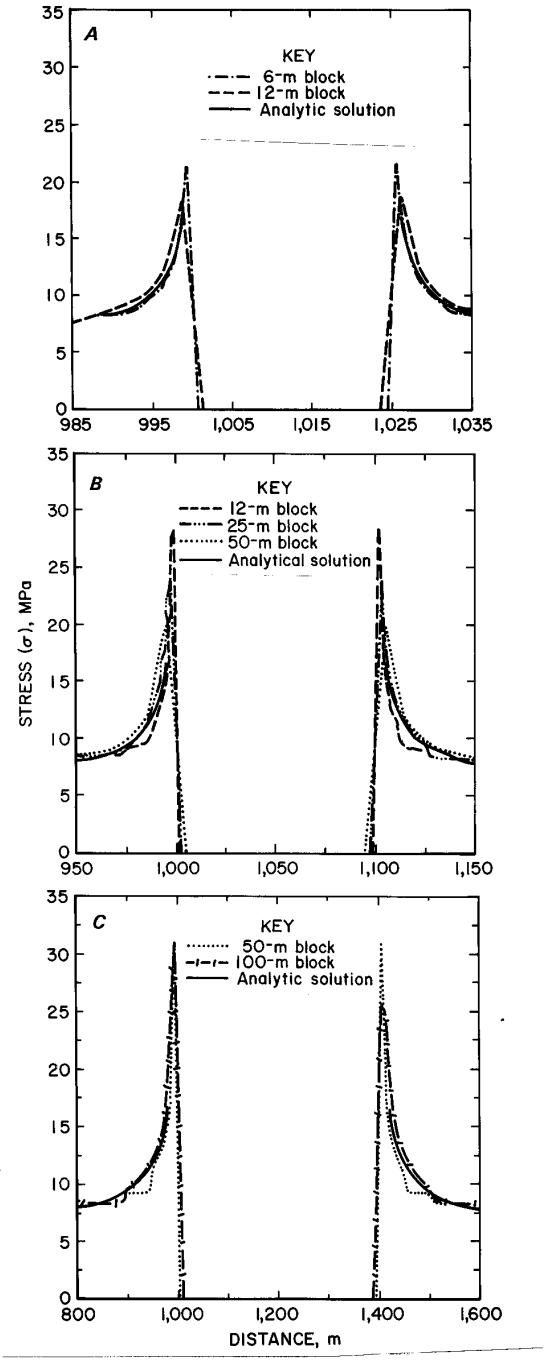


**Figure C-1.—Computed and analytic stresses at edge of opening with different block and element sizes. *A*, 25 m; *B*, 100 m; *C*, 400 m.**

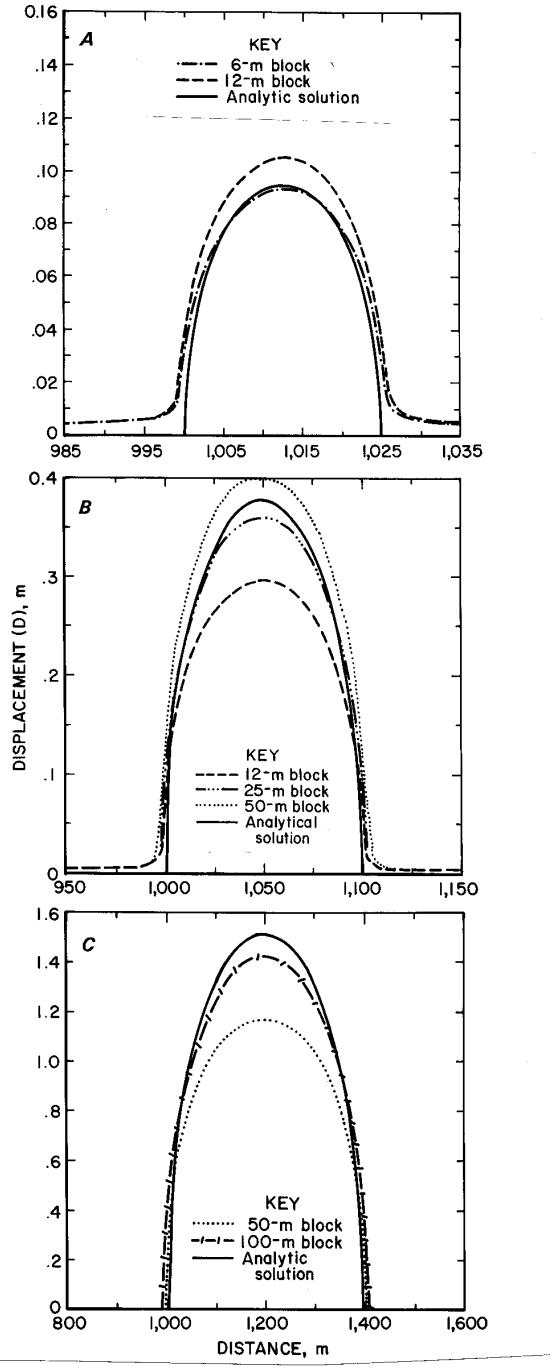


**Figure C-2.—Computed and analytic displacements across opening with different block and element sizes. *A*, 25 m; *B*, 100 m; *C*, 400 m.**

# APPENDIX D.—SUPPLEMENTAL DATA ON NONLINEAR EFFECT TESTS

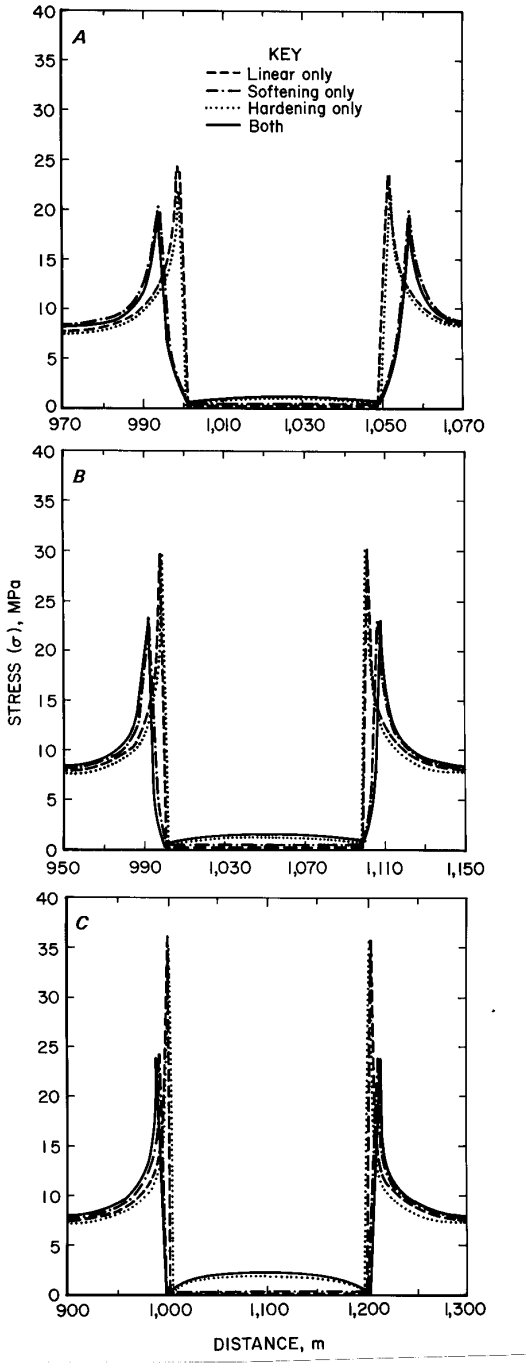


**Figure D-1.—Computed stresses at edge of opening using various linear and nonlinear material models. *A*, 50 m; *B*, 100 m; *C*, 200 m.**

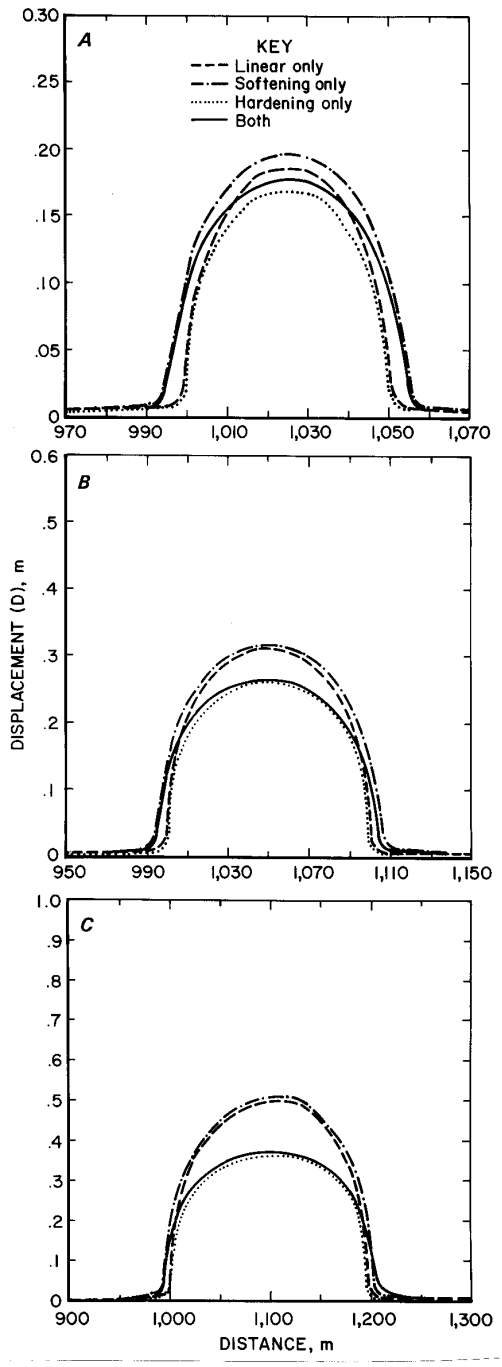


**Figure D-2.—Computed displacements across opening using various linear and nonlinear material models. *A*, 50 m; *B*, 100 m; *C*, 200 m.**

# APPENDIX E.—NONLINEAR STRESS-STRAIN RELATION FOR GOB

## INTRODUCTION

This appendix develops a nonlinear stress-strain relationship for gob material, which exhibits strain-hardening behavior, and discusses implementation of that model in MULSIM/NL. Gob formation occurs via a two step mechanism: first, the overburden rock behind a longwall face fractures, collapses, and swells to fill the newly created void, and second, the gob consolidates and follows a nonlinear, strain-hardening, constitutive relationship as vertical stress on the gob increases. Derivation of the model begins by assuming that the tangent modulus of the gob increases linearly with stress from some initial value to a final value. Based on this assumption, a nonlinear stress-strain relation for gob results is:

$$\sigma = \frac{E_I}{n}\left[\frac{n\sigma_v}{E_F - E_I}\right]\left[\exp\left[\left[\frac{E_F - E_I}{n\sigma_v}\right]\left[\frac{D}{t}\right]\right] - 1\right], \quad \text{(E-1)}$$

where $E_I$ = initial modulus,

$E_F$ = final modulus,

$\sigma_v$ = final stress,

$D$ = seam closure,

$t$ = seam thickness,

and $n$ = gob height factor.

## MECHANISM OF GOB FORMATION

Several geologic studies have examined rock movements in the overburden behind an advancing longwall face (*42-44*). Figure E-1 shows the three zones generally found as one progresses from the mined-out seam level up through the geologic column. First, a totally broken zone exists for a height ranging from two to six times the seam thickness. Rock within this zone exhibits considerable inelastic behavior, since it has first fractured, then moved downward, and then rotated randomly during its downward displacement. Above the totally broken zone is a fractured zone, whose top may lie 20 to 60 times above seam thickness. In this zone, considerable fracturing occurs with the downward displacement and mechanical properties such as modulus certainly decrease; however, gross rotation of the fragments does not occur and individual rock strata remain recognizable and correlatable. Finally, above the broken zone lies an elastic zone where no new fracturing has occurred and mechanical properties remain the same as the original rock mass.

Subsidence data also provide information on the delineation and behavior of these three zones. At risk of gross oversimplification, surface subsidence generally amounts to about 50% of seam thickness. Displacements at the base of the elastic zone shown in figure E-1 may equal 50% of the seam thickness as well. At the base of the fractured zone, displacements are approximately 60% of the seam thickness. Downward movement at the base of the totally broken zone is 100% of the seam thickness.

Mechanistically, the overburden rock first swells to fill the mined-out void, then consolidates to induce surface subsidence. During this swelling and consolidation, the totally broken zone sees a net vertical strain on the order of (1.0t - 0.6t)/(4t), which equals 0.100 or 10% strain. The fracture zone experiences a strain of (0.60t - 0.50t)/(40t) which equals 0.0025 or 0.25% strain. The elastic zone sees zero vertical strain. Since the strains in the broken zone are much larger than the strains in the fractured zone, then the mechanical behavior of the broken zone probably dominates overall gob behavior.

In this research, the fractured zone is effectively neglected by including it mechanistically with the elastic zone. Gob formation occurs via the two-step mechanism hypothesized in figure E-2. In the first step, the overburden rock behind the longwall face fractures, collapses, and swells to fill the newly created void. During this swelling phase, the broken material is essentially stress free and

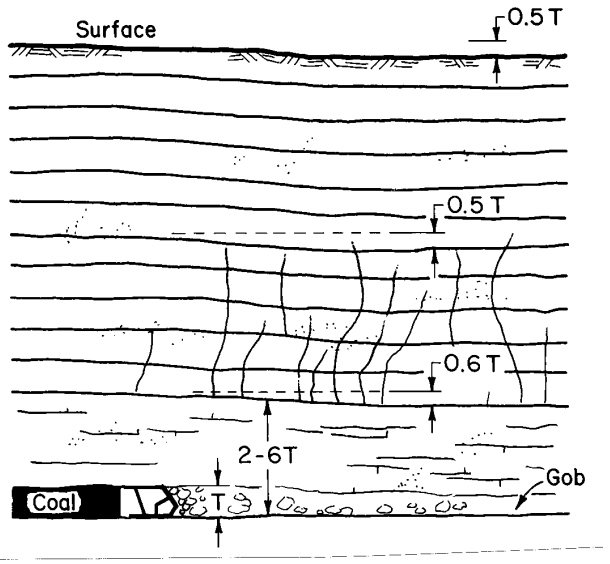


**Figure E-1.—Three mechanical zones found above mined-out coal seam. T is seam thickness. Lowest is totally fractured zone; middle is fractured zone; and top is elastic zone.**

does not transmit any significant vertical stresses to the floor rock. In the second step, as the longwall face moves farther away, the gob changes gradually from a swelling phase to a consolidation phase as it begins to experience higher vertical stresses. Ultimately, the vertical stress in the mined-out region may approach the virgin vertical stress and further vertical deformation or consolidation ceases.

## DERIVATION OF NONLINEAR STRESS-STRAIN RELATION FOR GOB

Two major assumptions underlie the gob model presented here. First, all the vertical strain that results in surface subsidence occurs within a broken zone whose height varies from two to six times the seam thickness. Justification for this assumption was presented earlier. The second assumption states that the elastic modulus of the gob material in the broken zone increases linearly from some initial value $E_I$ to some final value $E_F$. The initial modulus is that of the swelled gob material at zero vertical pressure, whereas the final modulus is that of the consolidated gob material at the virgin vertical stress $\sigma_v$. The assumed linear relationship between tangent modulus and vertical stress is shown in figure E-3.

The equation describing this linear relationship is

$$E = \left[\frac{E_F - E_I}{\sigma_v}\right]\sigma + E_I. \qquad \text{(E-2)}$$

The differential relation between stress and strain is

$$d\epsilon = \frac{1}{E}d\sigma. \qquad \text{(E-3)}$$

Substituting E-2 into E-3 and integrating between the limits 0 to $\epsilon$ and 0 to $\sigma$ yields

$$\epsilon = \frac{1}{\left[\frac{E_F - E_I}{\sigma_v}\right]} \ln\left[\left[\frac{E_F - E_I}{\sigma_v}\right]\frac{\sigma}{E_I} + 1\right]. \qquad \text{(E-4)}$$

Rearranging and exponentiating gives

$$\sigma = E_I\left[\frac{\sigma_v}{E_F - E_I}\right]\left[\exp\left[\left[\frac{E_F - E_I}{\sigma_v}\right]\epsilon\right] - 1\right]. \qquad \text{(E-5)}$$

From figure E-2, the strain in the broken zone is calculated as

$$\epsilon = \frac{D}{t} \qquad \text{(E-6)}$$

where D is the seam closure and t is the seam thickness.

## THE GOB HEIGHT FACTOR "n"

The above formulation utilizes effective modulus values and effective strain as opposed to true modulus values and

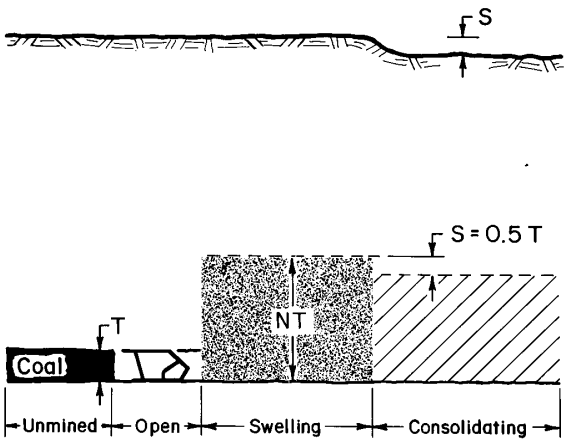


**Figure E-2.—Swelling and consolidation mechanism of gob formation. T is seam thickness; NT is totally fractured zone thickness where N is gob height factor; and S is surface subsidence assumed as 0.5 T.**

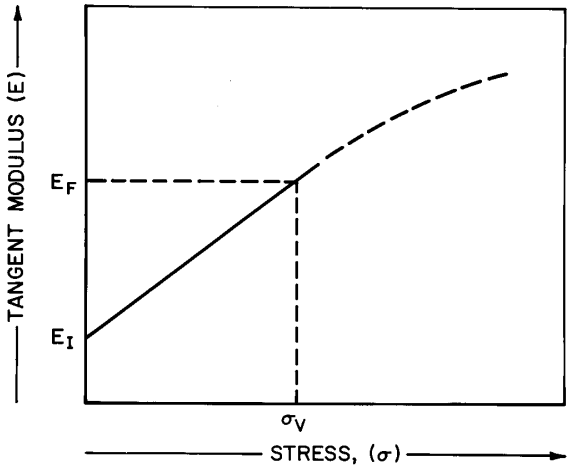


**Figure E-3.—Assumed linear relationship between tangent modulus (E) and stress ($\sigma$) over range 0 to $\sigma_v$. $E_I$ is initial modulus at zero vertical stress, and $E_F$ is final modulus at vertical stress $\sigma_v$.**

true strains. Derivation of the connection between true and effective moduli and strain follows.

Consider a zone with thickness t subject to a compressive displacement of 0.1t. Suppose the NT is the true thickness of the zone and it is subject to a vertical stress $\sigma_v$. The true strain is

$$\epsilon_T = \frac{\Delta L}{L} = \frac{0.1t}{nt} = \frac{1}{10n}. \qquad \text{(E-7)}$$

True stress is simply

$$\sigma_v = E_T \epsilon_T = E_T \left[\frac{1}{10n}\right] \qquad \text{(E-8)}$$

where $E_T$ = true modulus.

The effective strain is

$$\epsilon_E = \frac{\Delta L}{L} = \frac{0.1t}{t} = \frac{1}{10}. \qquad \text{(E-9)}$$

Effective stress is

$$\sigma_v = E_E \epsilon_E = E_E \left[\frac{1}{10}\right] \qquad \text{(E-10)}$$

where $E_E$ = effective modulus.

Equating stresses yields

$$E_T \left[\frac{1}{10n}\right] = E_E \left[\frac{1}{10}\right] \qquad \text{(E-11)}$$

or

$$E_E = E_T/n. \qquad \text{(E-12)}$$

Therefore, the true modulus values require modification by factor n which is equal to the broken zone height divided by the seam thickness.

In terms of true elastic moduli, the nonlinear stress-strain relation for gob is

$$\sigma = \frac{E_I}{n}\left[\frac{n\sigma_v}{E_F - E_I}\right]\left[\exp\left[\left[\frac{E_F - E_I}{n\sigma_v}\right]\left[\frac{D}{t}\right]\right] - 1\right] \qquad \text{(E-13)}$$

where $E_I$ = initial modulus,

$E_F$ = final modulus,

$\sigma_v$ = virgin vertical stress,

D = seam closure,

t = seam thickness,

and n = gob height factor.

## IMPLEMENTATION INTO MULSIM/NL

Subroutine MODHARD implements this nonlinear stress-strain model for gob in MULSIN/NL. An array called EPROP stores material property data for up to 26 different materials. EPROP has dimensions 26 by 10 so each material can have up to 10 descriptors in its material model. The first of the 10 material descriptors in EPROP acts as a flag identifying the material model to use, which is five for strain-hardening. For the strain-hardening case, the EPROP descriptors are as follows:

EPROP(*,1) = 5 – material type strain-hardening

EPROP(*,2) = – initial modulus

EPROP(*,3) = – final modulus at stress

EPROP(*,4) = – virgin vertical stress

EPROP(*,5) = – gob height factor

EPROP(*,6) = – Poisson's ratio

Descriptors 7 through 10 remain unused.

Subroutine MODHARD returns values for the Young's modulus perpendicular to the seam plane and the shear moduli parallel to the seam plane based on current estimates of the stresses. The user specifies material properties normal to the seam only. The associated shear moduli are calculated as

$$G = \frac{E}{2\,(1 + v)}. \qquad \text{(E-14)}$$

While the material property specifications for the normal and shear directions for an element are linked, the boundary conditions for these directions are decoupled and act independently. Coupling these boundary conditions may have certain intuitive appeal; however, it will overspecify the system (i.e., more equations would exist than unknowns). Such a procedure may lead to numerical difficulties of unknown proportions.